Organic Electrochemical Transistor: a tool for cell tissue monitoring

Relatore:
Prof.ssa Beatrice Fraboni

Correlatore: Presentata da:
Dott.ssa Marta Tessarolo   Vito Vurro

To my family.

ii

Abstract

Questa tesi si inserisce nel ramo di ricerca della Bioelettronica organica, in particolare l'obiettivo è quello di monitorare per via elettrica la formazione e la rottura di ricoprimenti e barriere cellulari. Queste sono di particolare importanza dal punto di vista biologico per il loro ruolo di protezione e per l'azione regolatrice nel passaggio di ioni e macromolecole necessarie al benessere dell'organo.

Per fare questo sono stati utilizzati gli Organic ElectroChemical Transistor (OECT) basati sul polimero organico biocompatibile PEDOT:PSS. Per poter portare a termine questo lavoro il primo passo è stato lo sviluppo di un apparato sperimentale, detto TE-OECT (Tissue Engineering-Organic ElectroChemical Transistor), che permettesse l'acquisizione delle misure a bassa intensità di segnale dall'interno di un incubatore oltre alla trasparenza necessaria all'acquisizione di misure ottiche utilizzate come riferimento. Oltre allo sviluppo, l'ottimizzazione e la calibrazione dei dispositivi e del TE-OECT, è stato sviluppato un programma per l'elaborazione dei dati.

Sono state misurate le risposte degli OECT in differenti fasi della crescita di due ricoprimenti cellulari (HeLa e NIH-3T3). Per validare le misure elettriche nelle varie fasi della crescita cellulare sono state acquisite immagini al microscopio dei ricoprimenti studiati. Come ulteriore conferma di quanto osservato è stata utilizzata la Tripsina per provocare il distacco dei ricoprimenti. Sono state eseguite misure elettriche durante il distacco per verificare se fosse possibile monitorare in tempo reale l'integrità dei layer cellulari. Questo tipo di analisi permette di ottenere utili informazioni aggiuntive sullo stato del ricoprimento cellulare e rende possibile svincolare l'efficacia di un agente patogeno o l'efficacia di un enzima utilizzato per il distacco cellulare dalle analisi di tipo ottico.

Contents

Introduction

The purpose of this thesis is the electrical monitoring of the formation and the detachment of cell covering and barrier performed by organic device. It is possible to insert this work in the research field of the Organic Bioelectronics. This is a multidisciplinary field that has the purpose of studying and developing electronic devices able to transduce ionic signals, typical of biology, into electronic signals and vice versa. In this work this interaction is possible by an organic polymer, the poly(3,4-ethylenedioxythiophene)-poly(styrenesulfonate) (or PEDOT:PSS) which is used as a sensitive element of a Organic ElectroChemical Transistor (OECT).

An OECT is a three terminal device (Drain, Source and Gate) composed by a stripe of conductive polymer that woks as a channel and by another electrode, usually a metal, that acts as a gate. The current in the channel is controlled by the injection of ions from an electrolyte into the polymeric channel. The growth of cell layer directly on the device should affect the ionic current entering into the channel, the evaluation of the drain current variations should be used as a marker to evaluate the cell coverage. The development of this electrical method could be an alternative to the common optical methods used in biology often influenced by subjective evaluation.

In this work to perform an evaluate this method, the Tissue Engineering - Organic ElectroChemical Transistor (TE-OECT) has been developed; this set-up, with its biocompatibility and its compactness, allows the growth of cell layer directly on the device, a high viability of the cell, electrical measurements into an incubator and to perform the classical optical evaluation. In the Chapter 1 first of all the Bioelectronics is introduced. Then there is a presentation of the conductive polymers and how this polymers lead to the Organic Bioelectronics. In the end of the Chapter the attention is focused on the PEDOT:PSS, the polymer used in this work.

The Chapter 2 is an overview of the biological features of the cell layers. The characteristics of the formation of cell layer, the method commonly used to evaluate its integrity and the methods used to cause the detachment or to compromise the integrity of the cell layer are treated.

The Chapter 3 is focused on the Organic ElectroChemical Transistor theory. After the explanation of the working principles of the device, it is presented a model for the OECT and are explained its steady state and transient behaviour such as the operating regimes

of the devices. The last section concerns the applications in the cell layer monitoring of the OECT, following the articles according to their time publishing.

In the Chapter 4 the materials and the methods used for the fabrication of the device and their characterization are discussed. Moreover the electrical measurements performed in this thesis are explained and the biological and optical analysis are introduced.

The Chapter 5 is a summary of the path followed for the realisation of the TE-OECT. Moreover the custom Matlab program, used to analyze the acquired data, is explained. In the end a series of measurements are presented, these are used to calibrate the system before the evaluation of the cell growth.

The Chapter 6 is centered on the presentation of the acquired data. In the first two sections the growth and the detachment of the coverage of HeLa cells and of the NIH-3T3 cells are presented. In the last section a comparison between the two cell-lines and an interpretation of the result are presented. Finally the conclusions and the future work are discussed.

Chapter 1

Organic Bioelectronics

1.1 Development of Bioelectronics

Bioelectronics is a field of study born with Luigi Galvani in the 18th century at the university of Bologna. Galvani performed some experiments in which he made twitched a detached leg of a frog by the application of a small voltage. For the first time he understood the possibility to translate the signals and function of biology in the language of human-made electronic processing system, inducing muscular activity by means an electrical impulsed.

This discovery led to a new interdisciplinary field that involves biology, electronic, electrochemical and medicine, that is called *Bioelectronics*. The biological world is ruled by different signal divided in two groups: intra- and extra-cellular; these signals control cell function, morphology and life cycles and they influence their interactions with tissues and other biological surfaces mediated by proteins and enzymatic complexes. This brief overview shows the complexity of this field. The aim of Bioelectronis is to detect and stimulate this large variety of signals in order to produced an improvement in healthcare and simplify the the prevention and treatment of diseases [2] [5].

The path started by Galvani led to new exciting horizons like implantable cardioverter-defibrillator (ICD), implantable device that interpret neural signals and help disabled to control prosthetic arms or also biosensor that allow sick people to get better control over an important marker, for example a sensor that is able to monitoring the health status of a diabetics by measuring the glucose level [4].

During the development of this emerging technologies a great effort has been made to exceed the limitation due to the materials, the solid state technologies doesn't match with biological system; in the '60s and '70s the scientific research, to overcame this limitation, focused on the study of new materials which were biocompatible and had good electronic property. This step was crucial to the transition to organic Bioelectronics.

1.2   Conducting Polymers

In order to make electronic devices able to transduce ionic signals, typical of biological system, to electronic signals the main problem is to overcome the limitation due to the Debye screening (Figure 1.1), peculiar of traditional inorganic semiconductors [6]. This physical effect limits the effectiveness of the conversion forming a double layer on the surface of the sensing material that reduce the distance over which a charge can be sensed in liquid media.
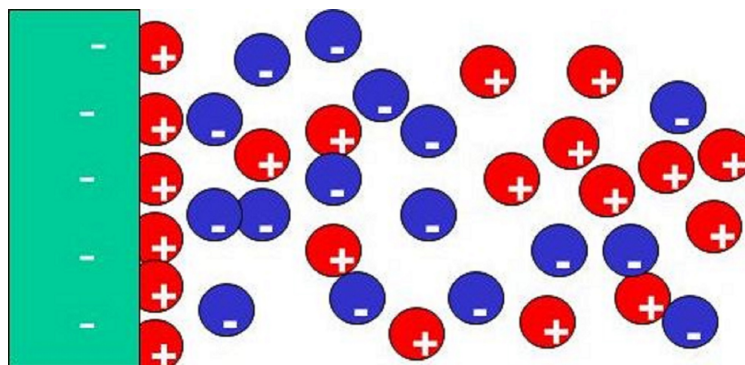
Figure 1.1: Debye screening is the formation of an electrical double layer on the surface of a sensing material. This reduces the distance over which a charge can be sensed in liquid media.

A wide range of new electronic materials and technologies, such as graphene [8] [9], carbon nanotubes [10] [11], nanostructure [12] [13] and organic semiconductors, show interesting results that solve the problem previously explained. A very promising class of materials, used in this context, are the conducting polymers. These are organic semi-conductors developed in the '70s by A.J. Heeger, A.G. MacDiarmind and H. Shirakawa [14] [15] who won the Nobel Prize in Chemistry in 2000 [16].

A polymer is a macromolecule obtained by the repetition of an elementary unit called monomer; a polymer is said *organic* if its monomers are hydrocarbon or carbon compounds. Among them if the monomers are alternately linked by a single or a double carbon-carbon bond, the polymer is called *conjugated polymer* [1]; in conjugated polymers the carbon orbitals are in $sp_2 p_z$ configuration, this means that, for each carbon atom, there is one unpaired electron in a π-bonding [18]. This bonding, for two successive carbon, overlaps and this allows the delocalizing of the unpaired electrons along the entire polymer backbone. The electronic structure in this kind of polymers is determined by chain symmetry, this leads the conjugated polymers to exhibit semiconducting or even metallic properties [17]. Over the last 40 years the developed polymers of greatest interest are those based on polyaniline, polypyrrole, polythiophenes, polyphenylene and poly (p-phenylene vileni); these polymers are shown in Figure 1.2. A second class of

organic polymers are the *saturated polymers*, in this all valence electrons are used in σ covalent bond. The saturated polymers are inert, resistant and flexible organic plastics. One last distinction is made between *extrinsically conductive polymers* and *intrinsically conductive polymers*; the first are obtained by mixing electrically non conducting polymers with conductive additives, the latter are developed by introducing electric charges in conjugated polymer by chemical or electrochemical methods [18].
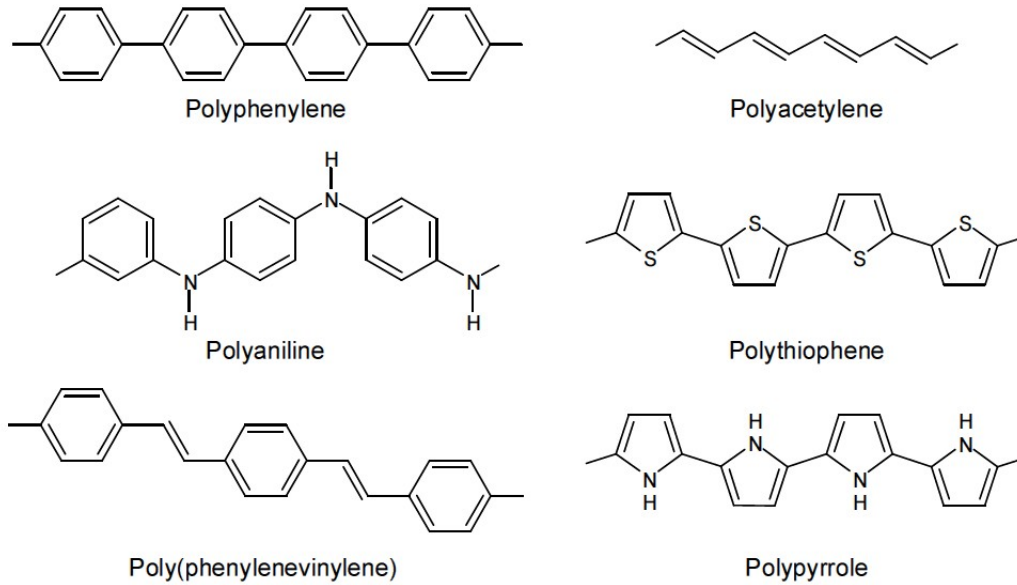
Figure 1.2: Chemical structure of the main conductive polymers.

1.2.1 Electrical conductivity in Conjugated Polymers

In this Section, using a simple free electron molecular orbital model, will be given a basic quantitative description of a conductor, semiconductor or insulator made of a linear chain of atoms [19]. As a reference to explain this model is used the simplest conjugated polymer, the polyacetylene (PAc, molecular formula $[-CH]_n$) which is shown in Figure 1.2. This polymer is built up with three σ-bonds, two between neighbour carbon atoms and one with an hydrogen atom; the fourth valence electron is a π electron. Assuming that the total length of the chain is Nd, where N is the number of the atoms in the row and d is the distance between two neighbour, it is possible, according to the quantum-mechanical model for a free particle in a one dimensional box, to write the eigenvalues of the wave function [20] :

$$E_n = \frac{n^2 h^2}{8 m_e (Nd)^2} \tag{1.1}$$

where h is the Planck's constant, m the electron mass and n the quantum number (equal to 1,2,3...).

Assuming that the π-electrons from the N p-orbitals are in this energetic level, with two electron per molecular orbital, it is possible to obtain the *Highest Occupied Molecular Orbital* (or HOMO) and *Lowest Unoccupied Molecular Orbital* (or LUMO) energy level:

$$E_{HOMO} = \frac{(N/2)^2 h^2}{8m_e(Nd)^2} \qquad E_{LUMO} = \frac{(N/2+1)^2 h^2}{8m_e(Nd)^2} \qquad (1.2)$$

In this way it is possible to determine the required energy to excite an electron from HOMO to LUMO (in the approximation of large N):

$$\Delta E = E_{LUMO} - E_{HOMO} = \frac{(N+1)h^2}{8m_e(Nd)^2} \approx \frac{h^2}{8m_e N d^2} \qquad (1.3)$$

Theoretically the *band gap* is predicted to decrease as $1/N$ (Equation 1.3) so longer is the polymer, lower should be the gap until it disappears for macroscopic dimensions. Then a macroscopic polymer should behave like a conductors but this is refuted experimentally [21]. It seems to be an upper limit beyond which the conjugation doesn't cause change in an infinite linear chain. The discrepancy between theory and experiments was solved assuming a one-dimensional distortion which state that a one-dimensional and evenly spaced chain is unstable, called *Peierls distortion* [22]. This distortion causes an instability of the polymer chain which reorganizes itself at the expense of its symmetry, and then the result is a rearrangement of the orbital's levels. In the case of PAc the distortion leads to a repeat unit made of two carbon atoms closer together than the next two, it is possible to write the repeat unit as $[-CH = CH-]$ instead of $[-CH-]$. In the new geometry the π-electrons wouldn't be spaced out along the entire chain and consequently they wouldn't be found in a half-filled continuous band but they would be in a new energy gap between a completely filled π band and an π^* empty band caused by the alternatively short and long bonds [18]. The new energy gap E_g is obtained by the difference between the HOMO in the π band and the LUMO in π^* band ($E_g = \pi - \pi^*$). The described bond-alternating structure is common to all conjugated polymers, this caused the typical low conductivities of the intrinsically conducting polymers, whereas their non distorted structure would have a metallic behaviour. Considering again the PAc its intrinsic conductivity is low ($< 10^{-5} \quad Scm^{-1}$) but exposing it to oxidizing or reducing agent it can be raised ($\sim 10^3 \quad Scm^{-1}$), this process is called *doping*.

1.2.2   Doping and Charge transport

In solid state the term *doping* is used to describe the introduction, in a crystal lattice, of an external atom that modify its electronic structure [23] while, as explained in Section 1.2.1, doping a polymer is intended as a charge transfer reaction resulting in the partial

oxidation (or reduction) of the polymer [18]. The doping is outline considering the neutral polymer as a ionic complex consisting of a polymeric charged ion and a counterion. In the case of p-type doping the charge of the polymer is positive (polymeric cation) and the counterion consist of the reduced form of the oxidizing agent. For n-type doping, conversely, the counterion is the oxidized form of the reducing agent and the polymer is negatively charged (polymeric anion). Thanks to the reversibility of doping and its ease of execution it is possible to define a polymer as a potentially *conducting polymer* [24]. The easy removal or addition to the polymer of charge carriers, made by the dopant, changes the electrical conductivity with small effects on the σ-bonds which hold the polymer together, furthermore the ability of these carriers to move along different π-system increase considerably the conduction. It is possible to summarize two reasons why doped conjugated polymers are good conductors [17]:

- A relatively large number of charge carriers can be introduced into electronic structure by doping, in fact each monomer is a potential redox site so conjugated polymers can reach high charge carriers density.

- The electrons are able to move according to two main routes. The primary charge transport takes place along the polymer chain and it is called *intrachiain transport*. But the electrons are also delocalized along the polymer chain due to the attraction of the neighboring repeat units; for this they have a certain mobility into 3-D which leads to a interchain electron transfer. This ability of the electrons to move from one polymer chain to another is the *interchain hopping* and it is a secondary transport.

Charges introduced by a low doping are stored in novel states called *polarons*, *bipolarons* and *solitons* while a high doping produce a degenerate Fermi sea that give a metallic behaviour to the polymer [25]. A description of the three non linear state is given below (Figure 1.3).
A *polaron* is the response of the polymer chain to the addition/removal of an electron, the variation of the number of electrons causes a deformation of the chain and a change of the electronic structure levels. Two electronic levels are shifted in the band gap once from the valence and once from the conduction band, if an electron is added in the new level shifted from the conducting band the polaron is called *electronic polaron*. On the other hand it is named *hole polaron* if a hole is removed from the new level shifted from the valence band. Both cases provide for the formation of a half-full level with spin equal to 1/2 and its distance from the band edge depends on the band gap and on the chain length [18]. The polaron is achieved by electrical attraction towards the counterion, which generally has a low mobility, and due to the local variations in the equilibrium geometry of the cation. Because the polaron can move in the field of the neighboring counterions, its mobility is greater if there is a high concentration of counterions. Therefore to obtain high mobility along the chain it is necessary a high doping level.
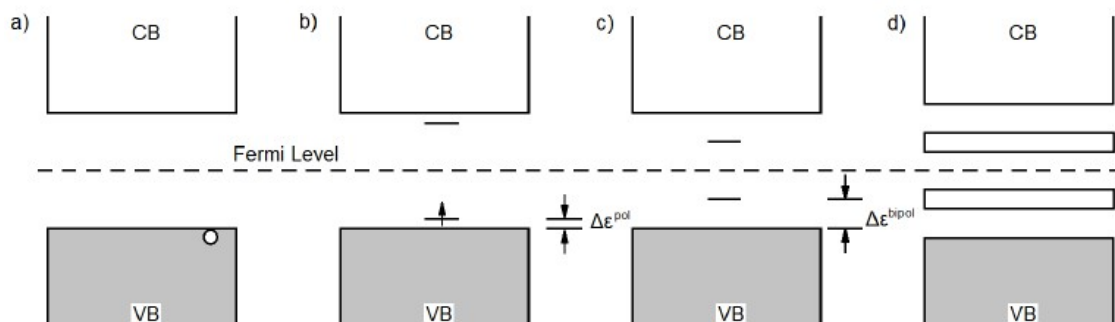
Figure 1.3: Alteration of the band structure of a polymeric chain in case of formation of: (a) delocalized hole, (b) a polaron, (c) a bipolaron and (d) a bipolaron bands in high doping condition.

The combination of two polaron with the same charge creates a *bipolaron*, this has two levels in the energy gap. If the bipolaron levels are fully occupied it is called *negative bipolaron*, if the levels are both empty it is called *positive bipolaron*; in either case, having the polaron spin equal to $1/2$, the spins of bipolarons is zero. Generally, because of their charge, the bipolarons are localized close to their counterions.

The last excited state is formed only in degenerate polymer, that are polymers in which despite a single bond is exchanged for a double along the chain, there are no change in the structure. This new level is the *soliton*, it is a new level located in the center of the gap; if the level is occupied by of one electron, it is named *neutral soliton* with spin equal to $1/2$; if it is full of two electrons, it is called *negative soliton* with spin equal to 0; if it is empty, it is defined *positive soliton* with spin equal to 0. The presence of solitons contributes to the charge transfer with the *intersoliton hopping* that describe a soliton jump between localized states or adjacent polymer chains [26].

1.3   Organic Bioelectronics

The organic Bioelectronics, a term coined by Berggren and Richter-Dahlfors [2], is the application of the conducting polymers to electronics, optoelectronics and their interfaces with biology. The great development of organic Bioelectronics is due to the properties of devices based on organic materials that are more suited than traditional silicon semiconductors. A comparison between p-doped silicon and poly(3,4-ethylenedioxythiophene) polystyrene sulfonate (PEDOT:PSS), the most important organic semiconductor, is shown in Figure 1.4. The main difference lies in the semiconductor structure, the silicon has a regular lattice firmly held together by covalent bonds in which each atom shares electrons with four neighbors, instead the molecular chains, held together by covalent bonds, feel a weak mutual interaction due to the van der Waals force and to the

electrostatic interaction, if the semiconductor is doped. This weak interaction, that characterizes the organic semiconductor, defines their "soft" nature which offers flexibility and ease of processing making them highly biocompatibile; in contrast the "hard" silicon nature complicates the use of inorganic semicondutors in biology. The free spaces in the semiconductor, which are much larger compared to the ions, allow the passage of the ions from biological medium into the electronic material; this makes the volume of the organic bulk sensitive to biological variation and it allows the organic semiconductor to trasduce ionic signals into electronic and viceversa. Furthermore the interaction of a silicon crystal with the air forms an oxide layer at the interface, because of which there is the formation of dangling bonds while organic semiconductors allows direct contact with biological environments with no problem. All these difference are summarized in Figure 1.4.
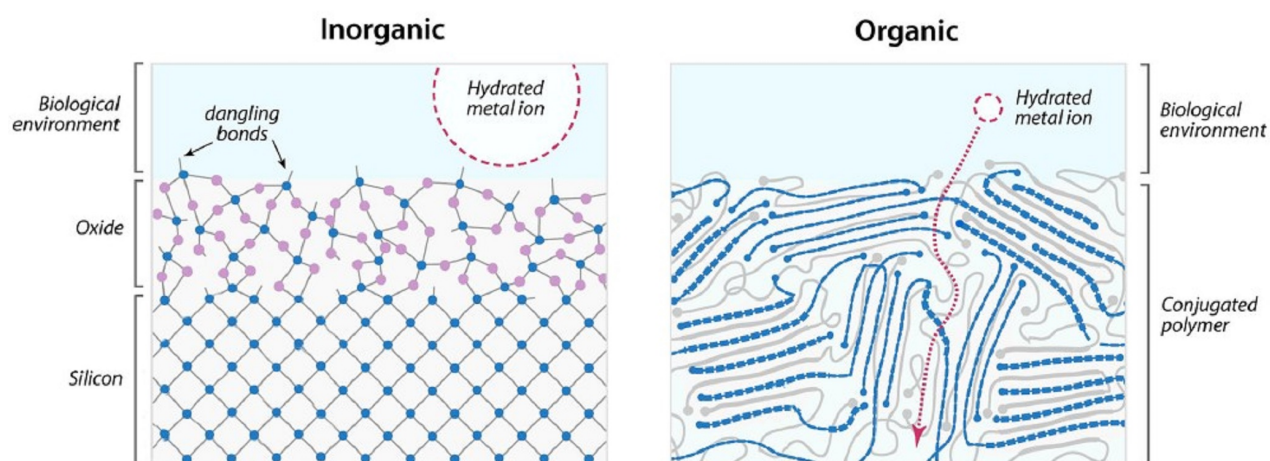
Figure 1.4: Schematics of an inorganic semiconductor (Silicon) and an organic semiconductor (PEDOT) at the interface with an electrolyte. The hydrated metal ion is meant to be the same in both schematics, defining the relative scale [5].

Another important property concerns the organic semiconductor thin film, is that they are often transparent allowing optical transmission imaging, which are really important for biological analysis. At last this organic semiconductors can be functionalized, to simplify their use in biological fields and it is possible to modify their optical and electronic properties working on the molecular structure. All this properties make the organic Bioelectronics a promising research field [2] [3] [5] [7] and the use of organic polymers allows to realize different devices with different geometries applicable in many situation. In Figure 1.5 are shown different type of device, the simplest one is a thin organic film contacted by two electrodes. In this devices the charge conduction varies depending on

chemical reactions occurring on the surface or within the organic film, a such device is used as a chemical resistors. Another possible device is a classical field-effect transistor, this structure can be achieved combining a vertical electrode configuration with a lateral one and also including a gate insulator.
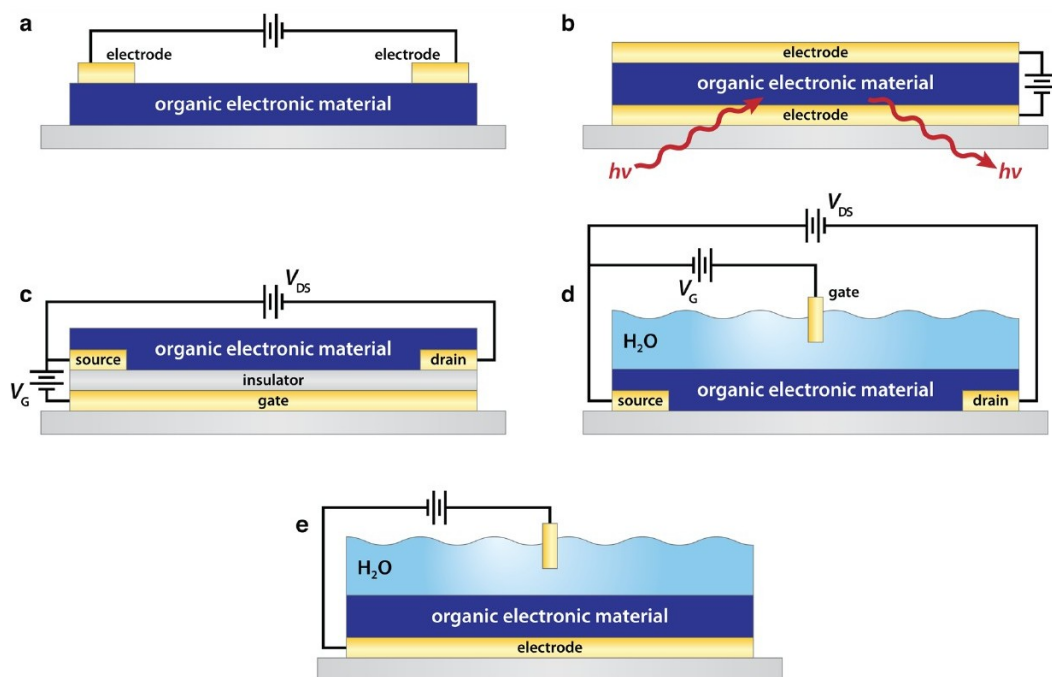
Figure 1.5: Device structure of (a) an organic chemical resistor, (b) a diode, (c) a field-effect transistor, (d) a water gated transistor and (e) an electrode operated in aqueous medium [7].

1.4 PEDOT:PSS

1.4.1 PEDOT and its properties

In the second half of the '80s at the Bayer AG laboratories in Germany was sintetized a new polymer, derived from the polythiophene: the poly(3,4-ethilenedioxythiophene) or PEDOT [18]. The monomeric unit of the PEDOT is the 3,4-ethilenedioxythiophene (or EDOT) that is shown in Figure 1.6, the PEDOT is prepared using standard oxidative chemical or electrochemical polymerization methods.

PEDOT is an insoluble conductive conjugated polymer exhibiting some very interesting properties [27]:

Reversible doping state: It is possible to change repeatedly the doping state of the PEDOT, moreover it is easy to identify the doped state of this polymer by the shift
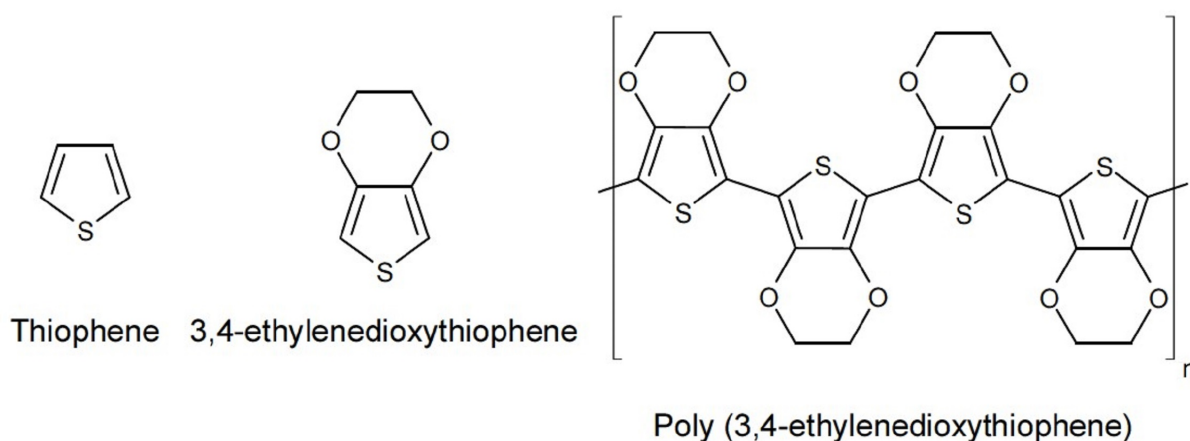
Figure 1.6: From left to right are shown th chemical structure of Thiophene, 3,4-ethilenedioxythiophene (or EDOT) and poly(3,4-ethilenedioxythiophene) (or PEDOT)

of the absorption peak. This property makes it widely used in optical applications such as electrochemical display [28].

Great stability: PEDOT high stability is caused by the circle geometry and by the stabilization due to the offsetting of positive charges present along the polymer chain with electrons donated by oxygen atoms. Studies about the thermal and electrical stability show a degradation above 150°C and a complete decomposition above 390°C [29], the electrical conducting properties are almost unchanged in time under environmental conditions.

High conductivity: PEDOT has a low energy gap of about $1.5 - 1.6\,eV$ [30], moreover in its doping state this polymer reduces its gap below $1\,eV$ in the metallic state which implies a very high electrical conductivity equal to $550\,S/cm$ [31].

Electrochemical properties: Electrochemically synthesized PEDOT films, compared to other conducting polymers, show an excellent stability in the doped state and has a low redox potential.

1.4.2 PEDOT:PSS Dispersion and Deposition

The main problem of doped PEDOT is its absolute insolubility, this was overcome by the synthesis PEDOT:PSS. It is possible to prepare a polyelectrolyte complex combining the PEDOT, as a polycation, and the poly(styrenesulfonic acid), as counterion; this process forms a stable dispersion composed by a mix of polycation(PEDOT) and polianion(PSS) as it is shown in Figure 1.7. The PSS choice has historical reasons because it was the

first polyanion used in this context [18], its combination with the PEDOT gives two main effect:

- The PSS balances the positive charge of the PEDOT polymer chain by acting as a counterion;

- The PSS maintains the PEDOT segment dispersed in an aqueous microdispersion;
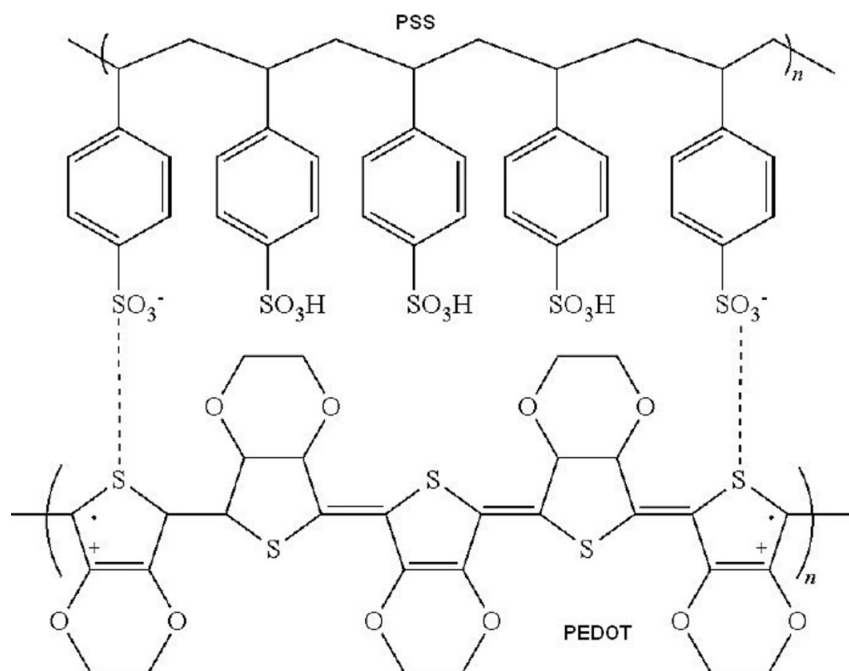
Figure 1.7: Chemical structure of PEDOT:PSS [32]

The ratio of tiophene groups to sulfonic acid groups is between 1 : 1.9 and 1 : 15.2 for the molecular ratio and between 1 : 2.5 and 1 : 20 for the weight ratio, this implies that the charge of PSS in excess, of that of the PEDOT, is from 6 to 46-fold [18]. The PEDOT:PSS structure is based on random interactions between polymer chains, this happens because of the delocalization of positive charges in PEDOT and the different spacing of charges in PEDOT and in PSS, this model is named *scrambled-egg arrangement* [18]. As a result of this interaction it is obtained a gel polymer network composed of aqueous gel particles and a solid content depends on the ratio between the amount of PEDOT and PSS. The PEDOT:PSS, in addition to being soluble in water, has now excellent *film-forming* properties [33]. The ratio between PEDOT and PSS changes the physical properties of the film such as the conductivity, the *sheet-resistance*, the solute content and the surface roughness; in particular the increase of PSS concentration

Trade Name	Solids Content in Water (w/w)(%)^a	PEDOT:PSS Ratio (w/w)	Viscosity at 20°C (mPas)	Particle Size $d_{50}(nm)$	Conductivity (S/cm)
Clevios P	1.3	1:2.5	80	80	<10
Clevios PH	1.3	1:2.5	20	30	<10
Clevios P VP AI 4083	1.5	1:6	10	40	10^{-3}
Clevios P VP CH 8000	2.8	1:20	15	25	10^{-5}
Clevios PH 500	1.1	1:2.5	25	30	500^b
Clevios PH 750	1.1	1:2.5	25	30	750^b
Clevios PH 1000	1.1	1:2.5	30	30	1000^b

^{a} Typical values for solids content, viscosity, particle size, and conductivity are given; no spesification.
^{b} Conductivity for Clevios PH500, PH750, PH1000 are mesured for dispersions containing 5% dimethyl sulfoxide.

Table 1.1: Commercial PEDOT:PSS Dispersions in Water and Their Properties [36].

produces thinner and less conductive films.
The PEDOT:PSS is produced in industrial scale and is readly commercially (by Heraeus GmbH [36]) and its commercial standards are summarized in Table 1.1.

The PEDOT:PSS in aqueous dispersion can be deposited using most of all standard techniques for deposition of films, but the dispersion is dependent on the specific deposition technique because it can required specific characteristic. This can be done using different formulation of PEDOT:PSS or by the addition of water soluble or dispersible additives such as surfactants, stabilizers or crosslinking agents. The viscosity, the surface tension and the adhesion to the substrate are the main properties which determine the quality of the film [18].
It is now discussed the main deposition techniques of PEDOT:PSS, these can be divided into three families: *coating*, *printing* and *electrodeposition*. The first family of methods have the characteristic to completely covers all the available surface with the solution while the second family is able to control the shape and the size of the coating. The best known deposition methods are *sping coating*, *spray coating*, *painting*, *slit coating*, *bar coating*, *screen printing*, *pad printing*, *ink-jet printing* and *nozzle printing* [34]. The electrodeposition instead is an electrochemical *in situ* technique in which two electrode drive a monomer and a dopant on a substrate where the polymerization takes place; in the case of PEDOT:PSS the monomer is the EDOT and the dopant is the PSS. This technique requires a conductive substrate and allows a fine control of the amount of de-

posited material. The Spin Coating, among these methodologies, is of great importance for the purpose of this work and it is described in Section 4.1.3.

1.4.3   PEDOT:PSS Thin Film

This Section presents the main characteristics of PEDOT:PSS thin films. PEDOT:PSS thin films are subjected to a process to remove residual water that could affect the optoelectronic characteristic; this process can be performed in several ways: by heating (temperature below 150°C), by infrared illumination, by applying a vacuum or by combining the previous techniques. Thin films are typically dry after a heating of a few seconds on a hot plate set to 100°C [18]. In general it is possible to find a relation between PEDOT:PSS film degradation and temperature, ultraviolet (UV)-light exposure and oxygen exposition but it is possible to limit this effect blending the PEDOT:PSS with additives as stabilizers [36] or encapsulating the device (as it is shown in Figure 1.8).
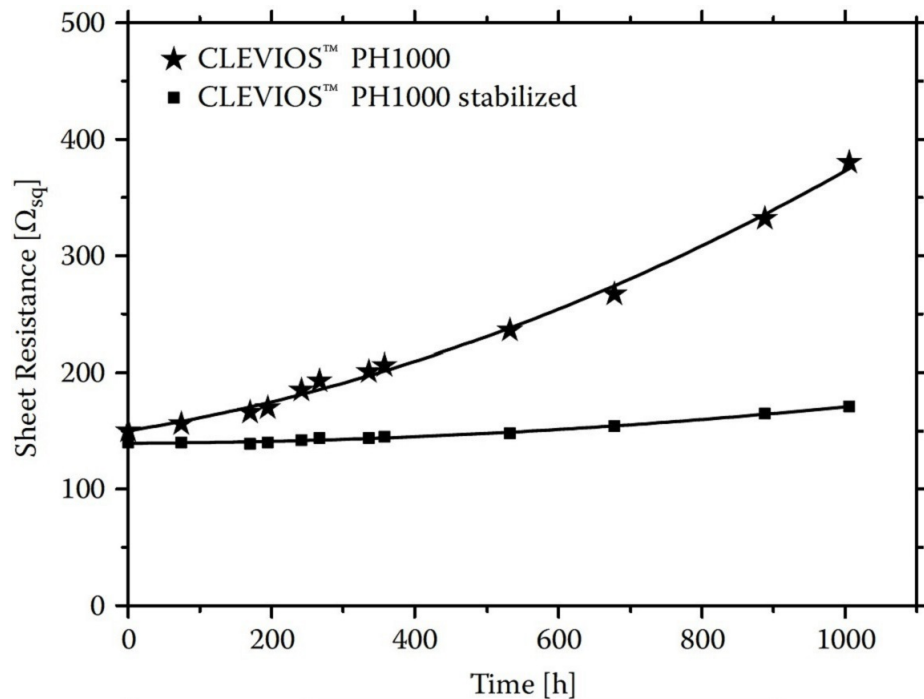
Figure 1.8: Sheet resistance as function of time of PEDOT:PSS film including 5% ethylene-glycole stored at 85 °C and 85% relative humidity (Data from [36]) adapted image from [18].

Termal Stability

The thermal stability is studied by the thermogravimetrical analysis (TGA) and returns the weight loss with increasing temperature in a controlled environment [18]. PEDOT:PSS shows a good thermal stability, it is possible to observe in Figure 1.9 that up to 100 °C there is a slight loss of weight due to evaporation of remained water while about 250 °C it is observed a significant weight loss of the sample. This is explained by the fragmentation of the PSS sulfonate group; at higher temperature (> 350 °C) other fragments due to carbon oxidation are detected. Accordingly PEDOT:PSS can be considered stable up to temperature of 200 °C.
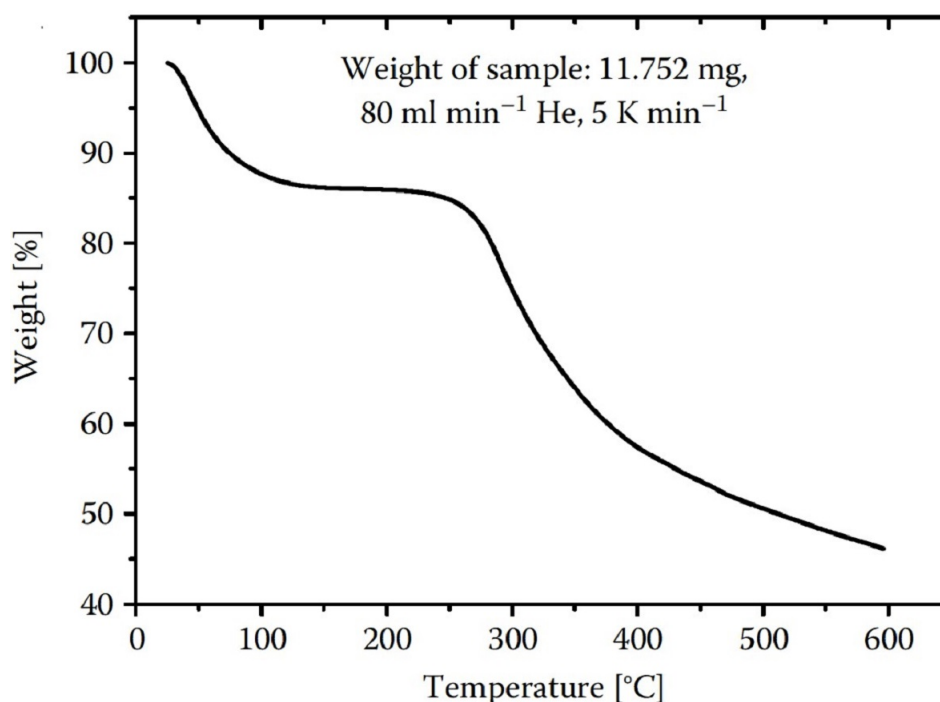
Figure 1.9: Thermogravimetric analysis (TGA) of PEDOT:PSS with a ratio 1 : 20 by weight of PEDOT to PSS. The measurement is performed heating the sample with a constant reat of 5 K/min [18].

Light Stability

Several studies have investigated the light stability of PEDOT:PSS and its derivatives and the decay mechanism seems to be oxidation by oxygen enhanced by light (Figure 1.10) which produce a decrease of conductivity [18].
Figure 1.11 shows the increasing resistivity of a thin film of pristine PEDOT:PSS (with PEDOT:PSS ratio equal to 1 : 2.5 and 5 % of DMSO) caused by lighting continues.
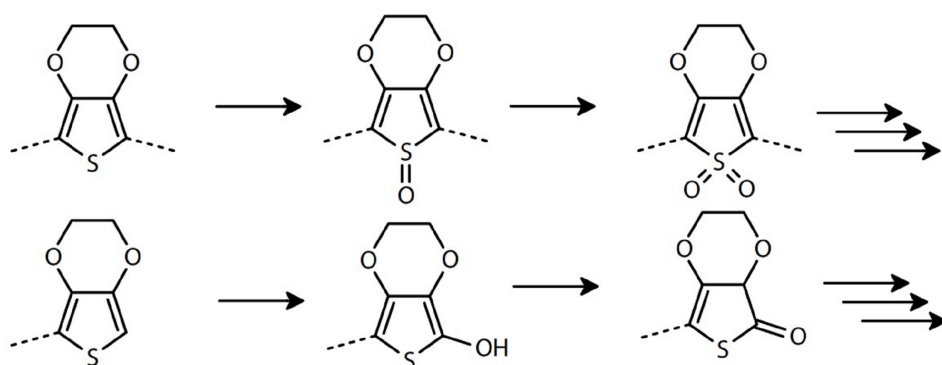
Figure 1.10: Possible degradation reaction of PEDOT[18].

The interesting observation, which confirms the role played by the oxygen in PE-DOT:PSS degradation, concerns the different worsening obtained encapsulating the film (by a thin glass plate to avoid the contact with ambient air). The UV light increases the degradation of PEDOT due to the oxidation. In particular certain wavelengths influence the kinetics of degradation [18]. PEDOT:PSS films have an increased degradation for absorbed UV photons in the spectral range of $\lambda < 320\,nm$.

Water Uptake

PEDOT:PSS is strongly hygroscopic. The water absorption of a pre-dried PEDOT:PSS sample of $1.5\,g$ and a thickness of several ten microns is shown in Figure 1.12; within three minutes the sample has increased the weight by $10\,\%$ when brought in contact with ambient air. The geometry of the sample and the humidity rate influence the water uptake. PEDOT:PSS thin films up to a thickness of about $100\,nm$ absorb instantaneously water from the environment. The layer thickness increases as the absorbed water is incorporated in the film, this swelling depends not only on the level of relative humidity but also by the PEDOT to PSS ratio, indeed layer with greater amount of PSS increase their thickness in a more pronunced way (up to $30\,\%$). [18].

Electrical Conductivity

PEDOT:PSS is an intrinsically conducting polymer with metal-like properties in which the charge transported stems from free charge carriers. The strong doped thiophene ring form a conjugated π system and every three-four ring, due to the oxidative reaction polymerization ruled by radicals, is created a free positive charge. The PSS doesn't play a direct role in charge transport, indeed its part is to keep PEDOT in dispersed states and to provide film-forming properties. The macroscopic way to determine PEDOT:PSS conductivity is via four-point or two-point measures, this gives the *sheet resistance R_{sq}*
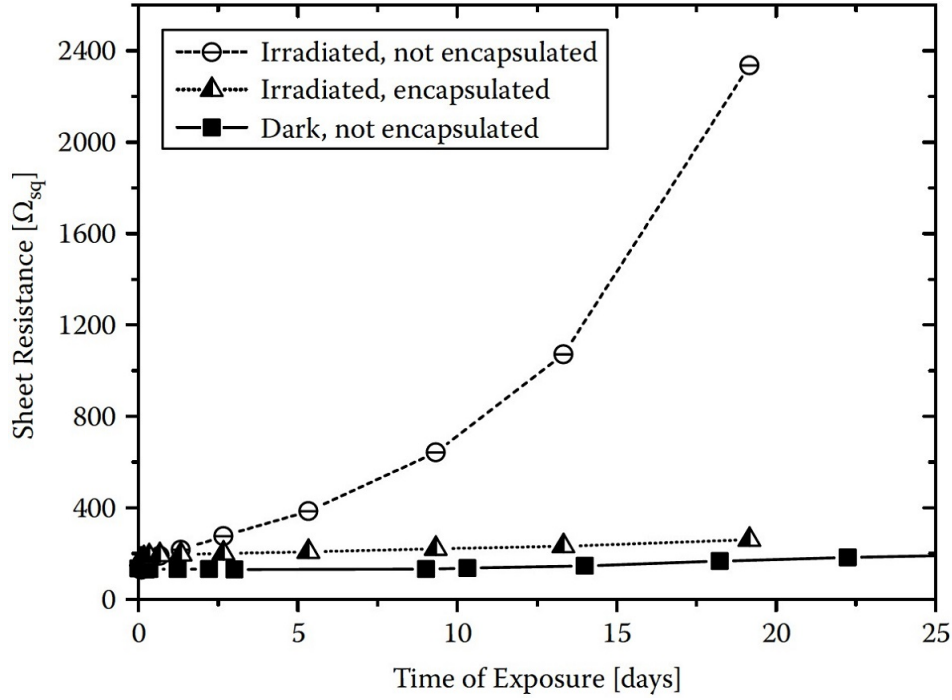
Figure 1.11: Sheet Resistance of pristine PEDOT:PSS films monitored over time while the sample is exposed to the radiation of an Xe lamp. [18].

related to conductivity σ according to:

$$\sigma^{-1} = \rho = R_{sd} \cdot d \tag{1.4}$$

where d is the layer thickness and ρ is the resistivity [37].
Microscopically PEDOT:PSS conductivity can be altered by various ways, as outlined in Table 1.1. The ratio of PEDOT to PSS has a direct impact on the conductivity because it defines the density of charge transporting PEDOT sites. The addition of solvent (like ethylene glycol, dimethyl sulfoxide or polyvinylalcohol) and the alteration of pH can modify the conductivity of thin films. A comprehensive transport model for the conjugated amorphous polymers, especially for strong doping, is missing; the conduction mechanism of conjugated polymers is explained through charge hopping between adjacent sites(following the concept of transport in amorphous inorganic semiconductor). In this theory segments of polymers are forming electrically active sites due to their oxidized and reduced ability. The energetic position, the distance and the relative orientation among two adjacent sites affect the frequency of charge transport [38]. Aleshin *et al* [39] have studied the conductivity and magnetoresistance of PEDOT:PSS as function of temperature finding that they increase with the temperature; this dependence of conductivity from temperature was discussed using the model of variable range hopping
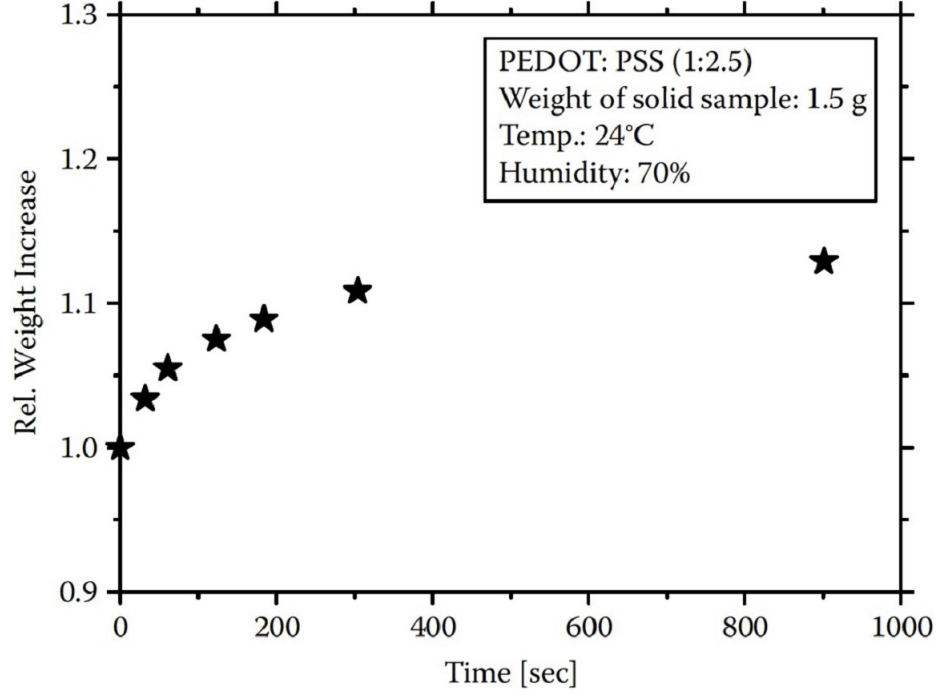
Figure 1.12: PEDOT:PSS (whit a weight ratio of 1:2.5 of PEDOT:PSS) thick layer weight increasing as a function of time in a air with a relative humidity of 70 % [18].

(VRH) [40]:

$$\sigma(T) = \sigma(0) \cdot exp\left(- \left(\frac{T_0}{T} \right)^{\alpha} \right) \tag{1.5}$$

where σ_0 is the conductivity for an infinite temperature, $T_0 = 16/k_b N(E_f)\xi^3$ for $\alpha = 1/4$ in a 3D case, $N(E_f)$ is the density states at the Fermi energy and ξ is the distance from a site for the electron wave function to decay to $1/e$. The temperature dependence of the conductivity has been widely studied [39] [41] [32] [42] within the framework of the VRH model, the Table 1.2 summarizes the main results obtained as a function of the ratio PEDOT:PSS and the experimental condition used.

It must be observed that all data acquired show that pristine material has a 2-3 orders of magnitude lower conductivity compared to films treated with enhancing agents (as discussed in the next Section); that pH value affects the conductivity which is higher for pH value between 0 and 3. There is a proportionality between temperature and conductivity (in the range 0-300 K) and a decrease of T_0 with increasing of σ, in agreement with the VRH model. Furthermore reading the Table it's obvious that all data are best modeled with $\alpha = 0.5$, this parameter is connected to dimensionality of the system and it assumes a value equal to $1/4$ for a 3D system and a value equal to $1/2$

PEDOT: PSS Ratio[a]	Layer Thickness	pH	Conductivity Enhancing Agent	σ (@RT) (S/cm)	T_0/K	α
1:2.5	25-40 μm	1.23	None	20.6	610	0.52
1:2.5	25-40 μm	5.2	None	0.077	3400	0.43
1:2.5	10-30 μm	$\sim 2^b$	None	0.8	1700	~ 0.5
1:2.5	10-30 μm	$\sim 2^b$	DMSO^c (25%)	80	$\sigma(\text{DC}) \propto T^{0.54}$	
1:2.5	n.d.	$\sim 2^b$	None	0.4	2927	~ 0.5
1:2.5	n.d.	$\sim 2^b$	EG^d (purge)	200	903	~ 0.5
1:2.5	28 nm	$\sim 2^b$	None	0.015	4200	~ 0.5
1:2.5	24 nm	$\sim 2^b$	EG^d (20%)	3.0	360	~ 0.5
1:6	90-100 nm	$\sim 1.8^b$	None	0.0011	3200000	0.25±0.1
1:6	90-100 nm	$\sim 1.8^b$	Sorbitol	4.18	2720	0.53±0.02

[a] Ratio of PEDOT to PSS by weight, following material producer specifications.
[b] pH-value following material producers specifications, not determined explicitly.
[c] Dimethyl sulfoxide.
[d] Ethylene glycole.

Table 1.2: Temperature Dependence of PEDOT:PSS Films, Discussed in terms of the Variable Range Hopping Model [40] [18]

for a 1D system [43]. One of the assumption made, in the work of Nardes *et al.* [42], connects the 1D type conductivity with low conductive and the 3D type with the high conductive.

The definition of conductivity is the product of elemental charge (e), carrier density (n) and carrier mobility (μ); the more general formulation considers negative (subscript n) and positive (subscript p) carriers that contribute to the conductivity according to:

$$\sigma = e \cdot \mu_n \cdot n_n + e \cdot \mu_p \cdot n_p \tag{1.6}$$

In PEDOT:PSS free electrons will immediately recombine at oxidized sites thus they don't contribute to conduction to which contribute only the hole. By geometrical consideration, for highly conductive films, it is possible to calculate the hole density that is approximately equal to $n_p = 3 \times 10^{20}\,cm^{-3}$ by which is obtained a conductivity value of about $1000\,S/cm$. From these quantity it is possible to estimate a value of mobility hole which is approximately equal to $\mu_p = 20\,cm^2/Vs$ [18].

Conductivity enhancing agents

There is a second way to increase the conductivity, different from the previously discussed addition of oxidizing (p-type doping) or reducing (n-type doping) agents, that is called

secondary doping. This refers to the addition of another solvent which further enhances the conductivity of an already doped polymer by several orders of magnitude [44]. These solvents produce an irreversible effect, unlike reversible primary doping, and as these do not change the doping level [45] are often called *conductivity enhancing agents* (CEA) [46]. The most effective substances, used as CEA, are dimethyl sulfoxide (DMSO), copper(II) chloride and ethylene glycol (EG); these are usually added to the PEDOT:PSS dispersion before the deposition. Two important observation were made during the study of CEA [47] [48]:

- In a narrow concentration range, the additive proportionally increases the conductivity up to reach a plateau. In this second area an increase of the additive concentration do not change the electrical properties.

- The presence of the secondary dopant, after the deposition of the film, can be removed sithout decreasing the conductivity which retains its increased value.

As shown in Figure 1.13 the conductivity does not change by added too small or exceeding a limit concentration
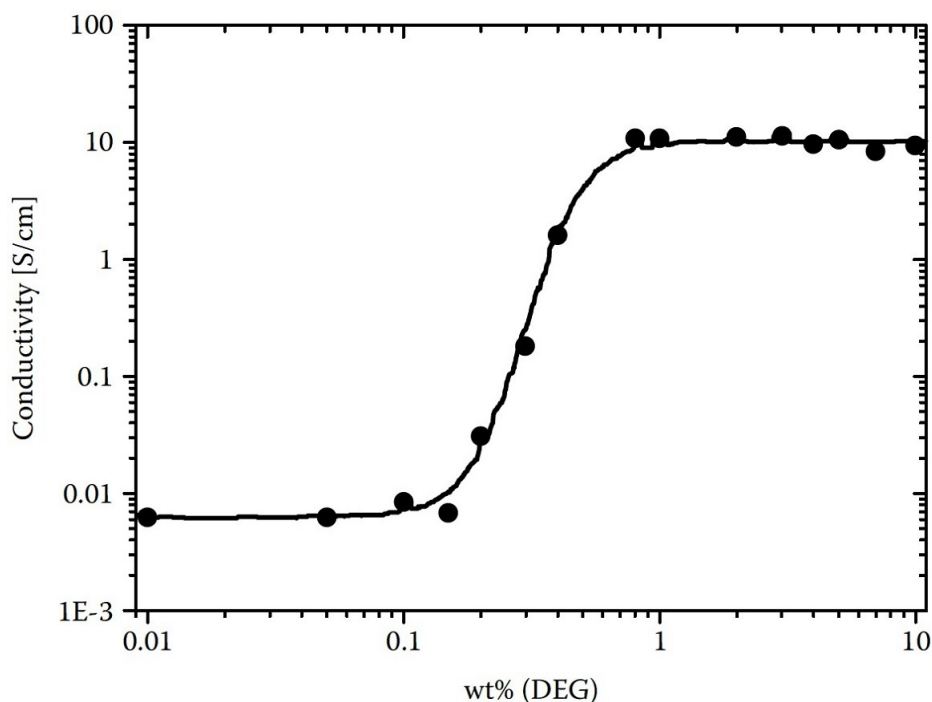
Figure 1.13: Plot of the conductivity of PEDOT:PSS film as function of amount of DEG (diethylene glycol) in the suspension [47].

There is another class of additives known as *crosslinker* which promotes the formation of covalent bonds between the polymer chains changing their physical properties.

For example the 3-glycidoxypropyltrimethoxysilane (GOPS) is able to reduce the delamination of the PEDOT:PSS film caused by water exposure. It is possible to observe in Figure 1.14 that GOPS addition produces an electrical and mechanical stability but it produces a worsening of the thickness and of the conductivity [18].
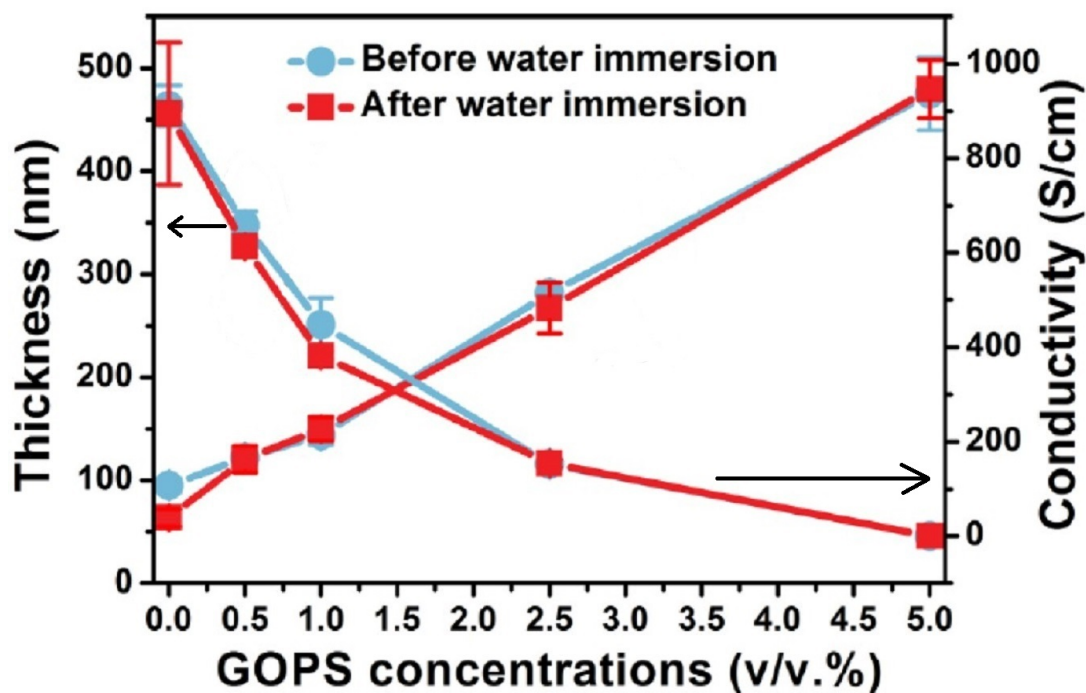
Figure 1.14: Influence of GOPS concentration on thickness (left y scale) and conductivity (right y scale) of PEDOT:PSS films before and after water immersion [48].

Another process which increase the conductivity is the *annealing*. The PEDOT:PSS thin films are heated for a long time (about 1 hours at temperatures) in order to allow the electron to achieve a energetically favorite state, this results into and increase of the conductivity (as it is shown in Figure 1.15). Moreover the annealing allows to improve the removal of water and solvents in excess which evaporate during this process.

From a microscopic point of view, the deposition from a aqueous dispersion leaves the polymer chains in the film in a state of non-equilibrium [42]. The presence of additives enables the dispersion to re-organize itself in order to find the chain in a new termodinamically favorite position. The CEA interacts with ion charge of the polyanion and polycation changing the spatial position that these would take in its absence. The PEDOT and the PSS retain their mutual organization even after the removal of the CEA. The electric charge in this condition can hop between two areas full PEDOT overcoming the areas with low conductivity which are full of PSS. Additives allow the ordering of the PEDOT segments improving the conductivity along the film.
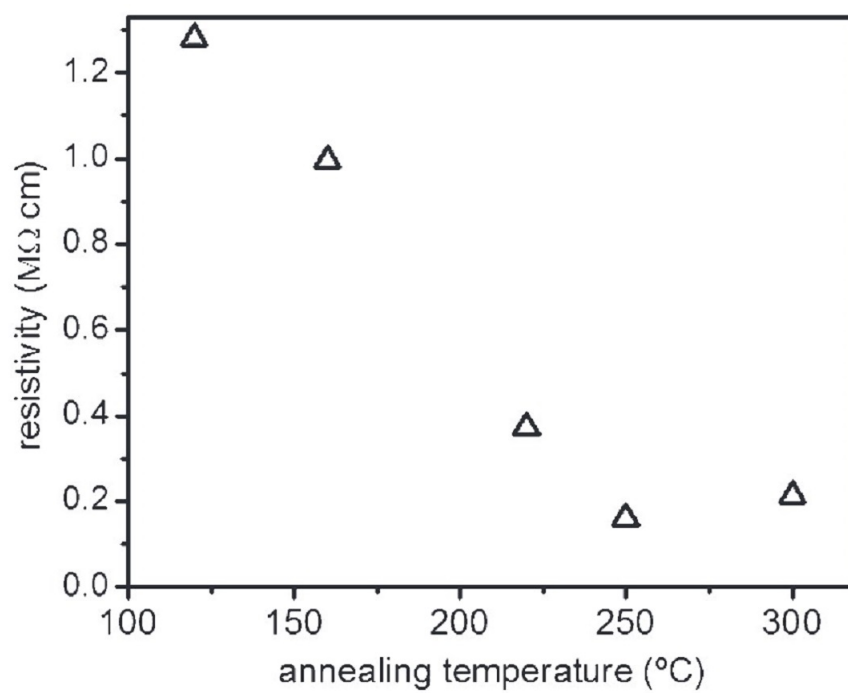
Figure 1.15: Resistivity if PEDOT:PSS films as a function of annealing temperature [49].

Chapter 2

Cell Junctions in Tissue Forming

Different kind of cell developed this ability to interact with external environment. Human epithelial and endothelial cells have this peculiar skill of forming barrier tissue that generally consists of a single layer of cells. This layer acts as a physical barrier able to stop motion of ions, macromolecule, immune cells and phatogens and to adjust the absorption of the major nutrients, electrolytes and water that sustain the host. Compartmentalization, protection, selective absorption and transport are just a few roles played by the barrier that are essential to develop multicellular organisms [50]. A lot of study are carried out on these processes in order to investigate and to understand the disruption or malfunction of the tissue fro toxicology and drug development. The goal is to improve and make more efficient the treatment of diseases that depends on these malfunction. In order to do this several methods, that observe the layer functionality, have been developed. Most of these are based on optical observations, for this the research is developing methods based on different physical quantities which can improve the sensibility of this observation. In this thesis a method based on electrical parameters is developed in the following. Moreover this type of study is relevant to improve the knowledge of the working principle of the barrier. This allows to understand the operation of various phenomena such as the nutrient exchange and led to cure various disease. Conditions such as Crohn's disease, Coeliac disease and irritable bowel syndrome are linked to disruption of tissue of gastrointestinal tract [54]. In the same way this study can led to new understanding of the *Blood Brain Barrier* and a great number of disease linked to it rather than the drug deliver and absorption in the brain [51] [52] [53]. All the analysis presented in this chapter are *in vitro*. This type of study is the important first step before the *in vivo* experimentation. It is used to maximize the information and optimize the initial condition of *in vivo* test.

2.1   Cell Layer Features: Coverage and Barrier

The formation of cell layer is mediated by two types of junctions: *Anchoring junctions* (Aj) and *Thight junctions* (Tj); that provide important adhesive contacts [55]. The membrane of these cells present two different polar region: the apical and baso-lateral domains; the polarity is defined by the polarity complex that define the anchorage points. Aj and Tj complex is referred to as the apical junction, where the apical domains is a region of the cell membrane. Aj and Tj are multiprotein complexes with the specialized role of forming extracellular and intracellular bound. The extracellular links regulate the contact between cells and intracellular bounds are the connection to the actin cytoskeleton. It is possible to differentiated two kind of Aj: the *Aderhens junction* and the *Desmosome*. The first type is located in the apical domains just below the Tj, the second is located even lower and is responsable of binding secondary intermediate filaments. The initial intercellular contact is stabilized by the Aj (through trans-pairing between proteins, in particular the cadherins, on opposing cells); furthermore a lot of cytoplasmatic proteins, which locally regulate the organization of the actin cytoskeleton and intracellular signaling pathways, are directly and indirectly bound to the cadherins. The second type of Aj are the cell-substrate junction that are named *Focal Adhesion*. All this junction are schematically represented in Figure 2.1. In general the presence of Aj is the first step to assembly of the Tj.

Tj are the most apical junctions, they are linked to the cytoskeleton by intracellular proteins [56] and to other cells by the transmembrane proteins occludin [57] and claudin [58]. Intercellular spaces between adjacent cells are sealed by Tj, this form a physical barrier that regulate the passage of ions and macromolecules across the barrier. Tj, in response to various internal or external stimuli, can selectively open or close the barrier space. This junction maintain highly regulated fluid compartments in multi-cellular organisms and are of various tightness depending on tissue type [54]. For the purpose of this work it is possible to distinguish two different types of cell layers. It will be define *Coverage* and *Barrier*. The *Coverage* represent a cell layer in which Focal Adhesion and Aj are present, while the *Barrier* is a cell layer connected by Tj forming cells addition to Aj and Focal Adhesion. The main difference between the two cell layers is the ability to reduce the flow of ions or macromolecules between two adjacent cells; this flux is known as *Paracellular flow*. Coverage and Barrier screen effect is shown in Figure 2.2.

2.2   Coverage or Barrier Forming Cell-line

In this Section various cell-lines, with Coverage or Barrier properties, are presented. This lines will be named or used in following Section.

Among Coverage forming cell-lines are reported three examples from the lowest to the higher ability of screening the paracellular flow:
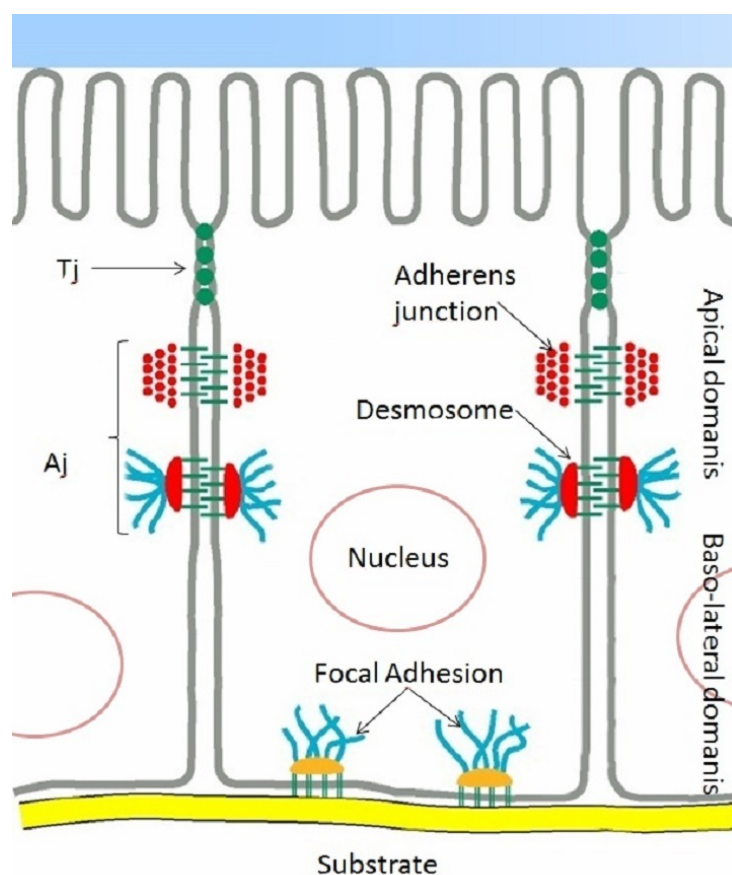
Figure 2.1: Schematic representation of the cellular junction. It possible to see the physical barrier made by the Tj that close the intracellular space.

HeLa: is a cell-line of immortalized human epithelial tumor cells [59]. This cells are isolated from a cervical cancer of *Henrietta Lacks*, from who comes the name HeLa. This line were isolated and commercialized by George O. Gey in 1951. This cells are very resistant and can survive in adverse conditions. They also have undergone a mutation for which they are able to reproduce most of the normal cells. This cells are shown in Figure 2.3.a.

HEK293: is a cell-line of human embryonic kidney cells, generated in 1973 by A. van der Eb's in Leiden [60]. This cells are shown in Figure 2.3.b.

NIH3T3: is a cell-line of mouse embryonic fibroblasts cells that come from a cell line isolated in 1962 and established from a NIH Swiss mouse embryo [61]. This cells are shown in Figure 2.3.c.

On the other side are reported two barrier forming cell lines with different barrier
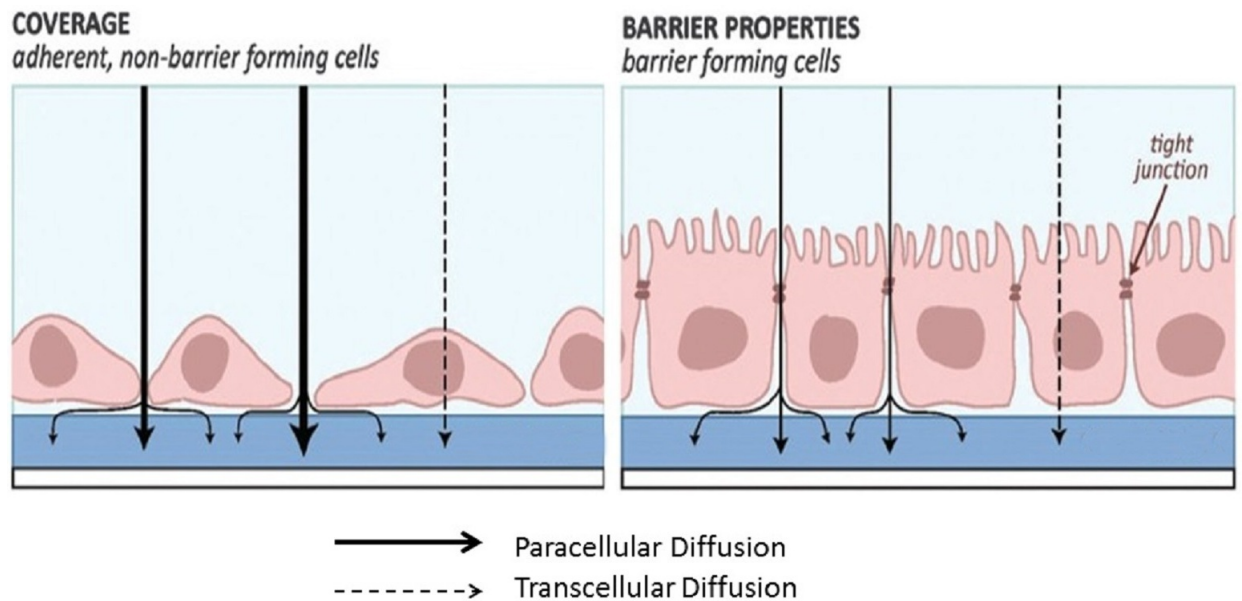
Figure 2.2: Schematic representation of the ion flow through a Coverage (o the left) and a Barrier (in the right) [87]. The width of the continues line is the intensity of the paracellular flow.

properties. Also in this case the lines are ordered in the same way:

Caco-2: is a cell-line of heterogeneous human epithelial colorectal adenocarcinoma cells. This line, developed by J. Fogh in the 1975 [63], has an intermediate barrier tightness [87]. This cells are shown in Figure 2.3.d.

MDCK-I: is a cell-line of canis familiaris epithelial kidney cells, this cells derive from a normal adult female cocker spaniel. The name comes from Madin-Darby Canine Kidney and the line was derived by S.H. Madin and N.B. Darby in the 1958 [62]. This cells are considered the tight barrier tissue cells [87]. This cells are shown in Figure 2.3.e.

2.3 Biological Analysis for Layer Integrity

The integrity of a cell layer can be assessed by different methods, the most common are the immunofluorescence, the permeability assay and the evaluation of the so-called Trans-Epithelial/Endothelial Electric Resistance (TEER or TER).

The immunofluorescence is a common assay in biological field, it is based on the labeling of the object of study with fluorescent dyes. In tissue context the idea is to
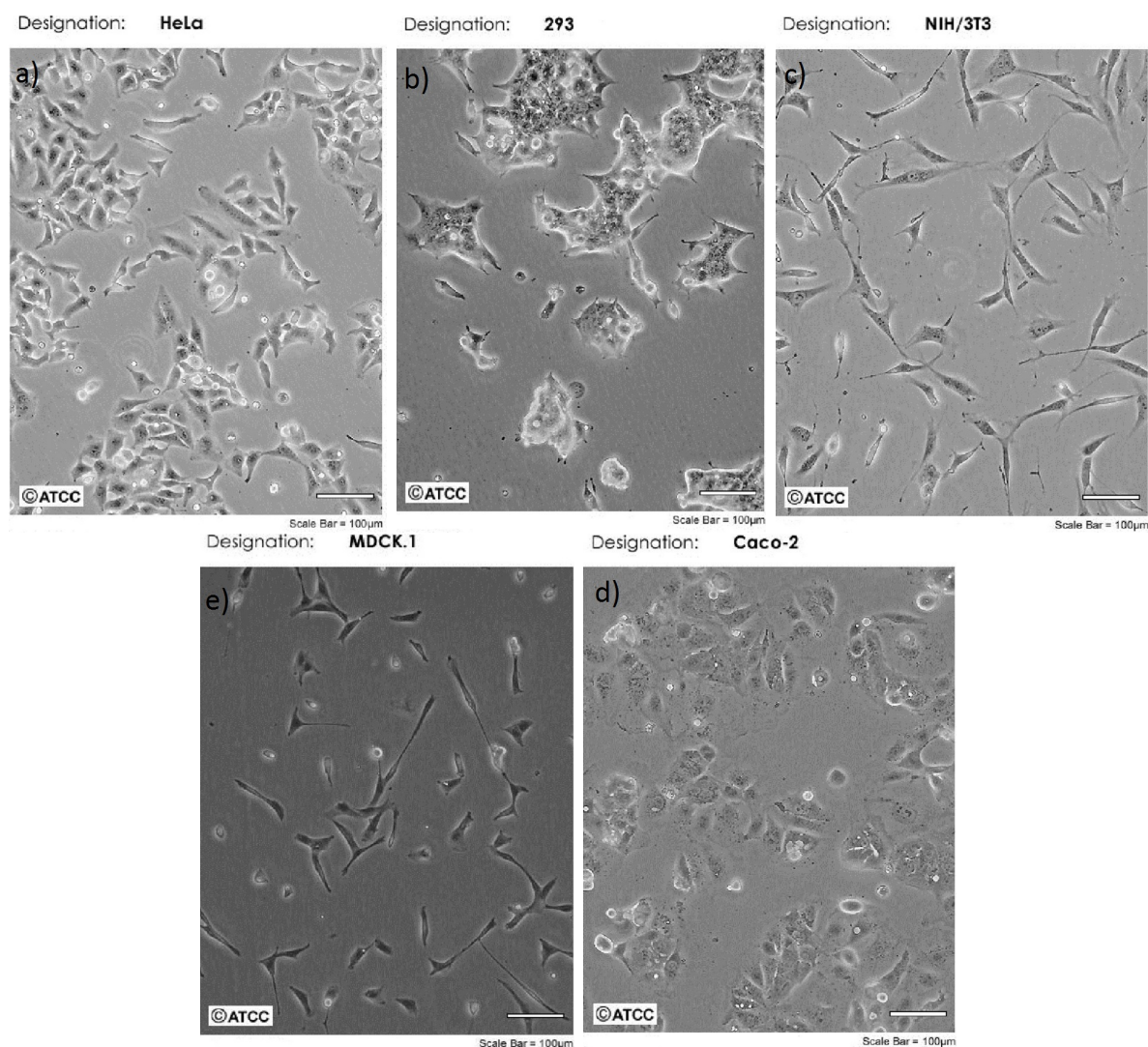
Figure 2.3: This are microscope images of a) HeLa cells [59], b) HEK cells [60], c) NIH-3T3 cells [61], d) MDCK-I cells [62] and e) Caco-2 cells [63].

display the presence of the junction before and after a disruption, in order to assess the damage of the layer. Both TER and permeability are parameter related to the flux that pass through the cell layer and they are directly correlated to each other. The permeability is a measure of solute flux performed by the use of a Transwell device (Figure 2.5.a) combined with a tracer molecule. The cells are seed on a porous membrane and when these reach the confluence some radio-labeled or dyes are add in the top side of the device. Depending on the quantity of the added compounds founded in the lower chamber, it is possible to obtain the degree of permeability of the cell layer. However
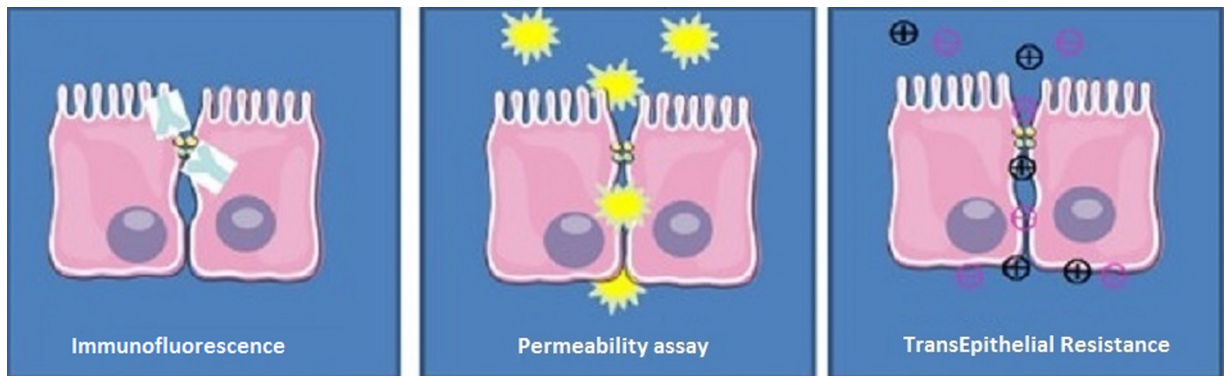
Figure 2.4: Three different kind of integrity analysis, from left to right it is shown the immunofluorescence, the permeability assay and the TER measure. The immage is adapted from [54].

this measure is strongly dependent on the charge and on the size of the radio-labeled molecules used, because the dependency of the flow from these features.

TER is a measure of the resistance opposed by a cell monolayer to a ionic current and it is performed by a hand-held epithelial voltohmmeter (EVOM) or by an Electric Cell-substrate Impedance Sensing (ECIS) System.

In the EVOM the resistance is calculated based on Ohm's law as the ratio of the voltage and current. The voltage is applied by two electrode (Figure 2.5.b) while the current is measured, in order to not damage the cell-layer an alternating current voltage signal is used. Instead the ECIS is performed by applying a frequency sweep of a small amplitude AC signal and measuring amplitude and phase response of the resulting current. The TER value is obtained by a fitting algorithm of the available data [65].
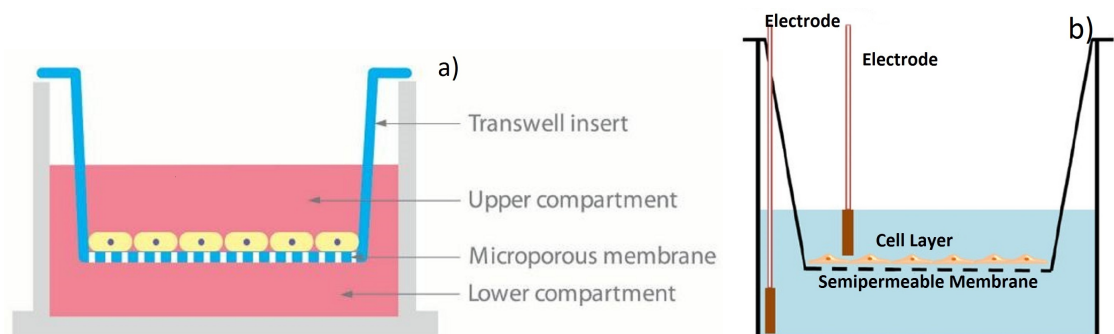
Figure 2.5: (a) A schematic representation of a transwell [64]. (b) A EVOM-EICS set up used to measure the TER [65].

2.4 Layer Detachment and Disruption

Another useful topic for this work concerns how to cause a damage to cell layer. There are several way to compromise the layer integrity and the used agent can cause different kind of damages to the cell layer. It is possible to detach the layer, compromise the junction or obtain a cytotoxic effect.
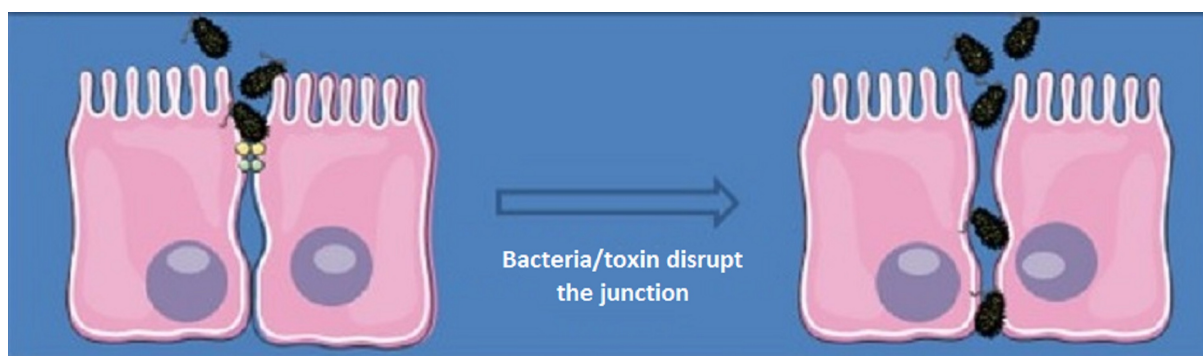
Figure 2.6: Disruption of the junction by a pathogens, the attacking element have the objective to penetrate the layer. The image is adapted from [54].

Here are reported four agent which will be used in the following chapter.

Trypsin-Ethylenediaminetetraacetic acid(EDTA) Trypsin is a protease able to detach cell from substrate, while EDTA is able to chelate metal ions such Ca^{2+} and Mg^{2+}. They can be used to detach cells from the substrate because the integrine, the major cell-substrate binding proteins, is Mg^{2+} dependent and it can be removed by the EDTA while the Trypsine is a non-specific protein cutter and it is used routinely to detach cells from surfaces [85].

Ethanol (EtOH) is know to cause functional damage to barrier tissue by producing a progressive disruption of Tj [67]. Different dose of EtOH produce different effects, a high dose of EtOH (40%) have a cytotoxic effect while lower dose just disrupt the Tj in a reversible way [83].

Hydrogen Peroxide: (H_2O_2) is used to induce a change in tissue integrity, H_2O_2 is a reactive molecules that disrupt the Tjs [66]. Different concentration of H_2O_2 produce disruption at different rate [83].

Ethylene Glycol Tetraacetic Acid (EGTA) is a specific Ca^{2+} chelator and it is know to compromise the Tj functionality. Its action can be revealed by a rapid decrease in the resistance of epithelia to ion flow [85] [68].

Chapter 3

Theory of Organic Electrochemical Transistor

A transistor is a semiconductor-based device with three terminal: the gate (G), the drain (D) and the source (S). It is possible to modulate the current I_{DS} that flows between drain and source, by a second current or a voltage applied on the gate (I_G or V_G). Generally high gain is a requirement for transistors in a great range of application, for example a sensor must amplify a small input signal to make it easily detectable [70]. The idea to realize and optimize an organic transistor is the center of a lot of studies in the past 30 years, the realization of soft device with interesting properties (like flexibility, light weight, low cost, ease of processing and biocompatibility) supports the idea of using organic electronics to substitute the actual inorganic technologies. Among organic semiconductor devices, organic thin film transistor (OTFT) have attracted considerable interest [71] and the organic electrochemical transistors (OECTs), a type of OTFT, have distinguished in recent years. OECT was demonstrated by White *et al.* in the 1984 with polypyrrole [69], but in the years several conducting polymers, like poly (3-metiltiophene), polyaniline and PEDOT, were used in OECT [72].

3.1 Working Principles

An OECT is made by three electrodes which are usually metallic; two of them (drain and source) are connected by thin film of doped polymer channel, that is in its doped state. The third electrode (the gate) is in contact with the channel by an electrolyte medium, this geometry is shown in Figure 3.1. As the channel is reversible doped/dedoped, it is possible to control the conductivity of the channel by the application of a gate voltage (V_g). This voltage induces a definite effect, the device switches between an "on" (or conductive) state to an "off" (non conductive) state of the polymer due to the high difference in conductivity between doped and undoped state [74]. Applying a voltage

31

V_d between drain and grounded source, it is possible to measure this switch observing the modulation of the current I_d. OECT can work both in depletion or accumulation mode, generally, as also in this work, it is used in depletion mode. This means that the conduction is mainly due to the hole so all the analysis are referred to p-type doping, neglecting the electrons contribution. In the depletion mode the polymer pass from doped to de-doped state due to the application of V_g which must be a positive voltage that pushes the cations from electrolyte into the organic film. This decreases the source-drain current I_d because of the de-doping that occurs in the channel. For the gate effect the OECT may be used as ion to electron trasducer, the devices is able to bridge the gap between biomolecular environment and electronic devices [75].
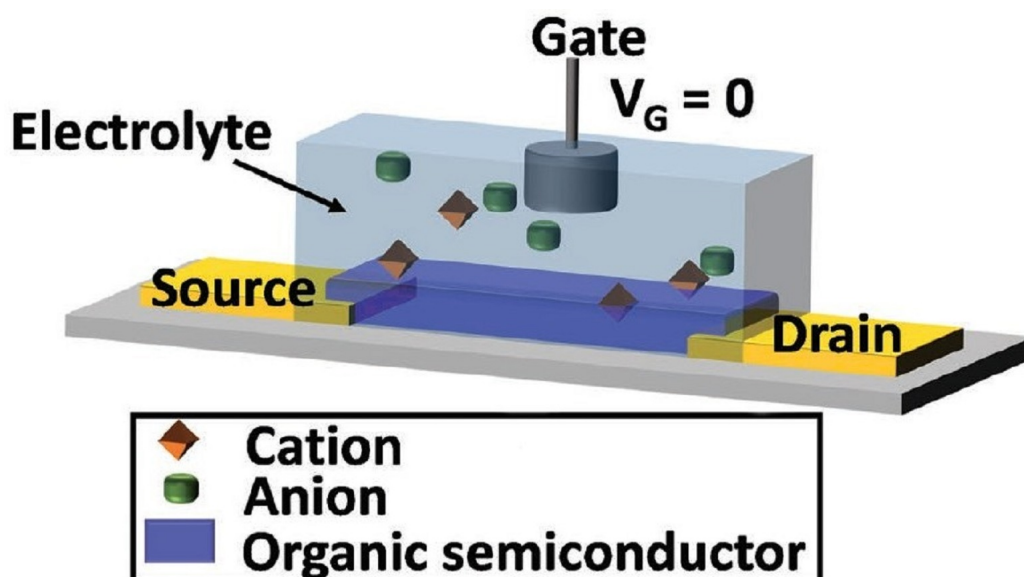
Figure 3.1: Schematic representation of an OECT. It is possible to see the three electrodes (Gate, Source and Drain) and the polymeric channel. The gate electrode controls a ionic current that modulates th drain-source current [76].

3.2   Device Model

A complete model to describe the behaviuor of the OECT was introduced by Bernards and Malliaras in 2007 [77]. They split up the behaviour of the OECT in two equivalent electronic circuit:

- The first describes the hole transport between the source and drain in a p-type organic semiconductor film. This transport is described by the Ohm's law therefore

it is ruled by the hole density and mobility. This is called *Electronic Circuit* and it is explained in Section 3.2.1.

- The second accounts for transport of ionic charge in the electrolyte. This is named *Ionic Circuit* and it is presented in Section 3.2.2. This is modeled as a series of resistor and capacitors which describe the behaviour of the charge at the interface gate-electrolyte and channel-electrolyte.

The interaction of this elements, that are shown in Figure 3.2, describes the injection of ions into polymer channel and is fundamental to describe the behaviour of OECTs.
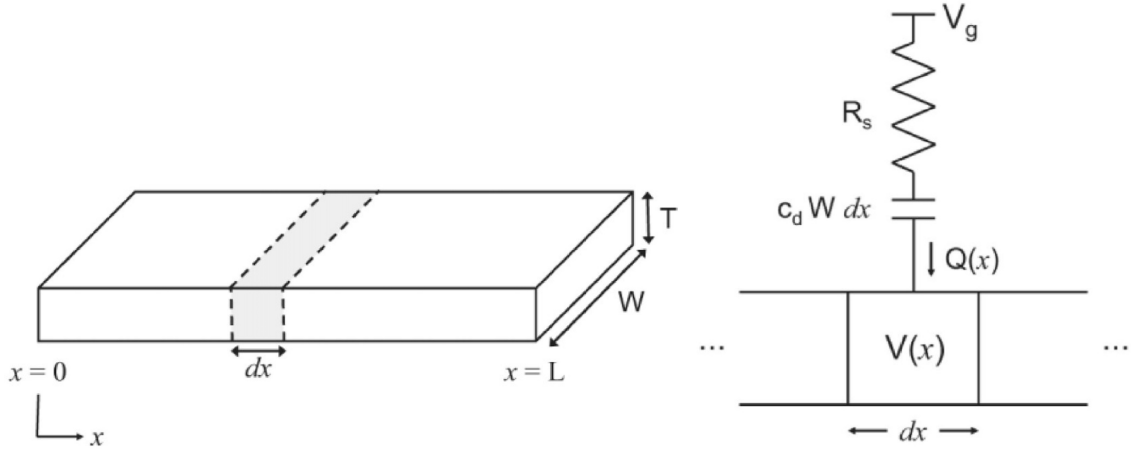
Figure 3.2: On the left is shown an OECT channel and its characteristic size: length (L), width (W) and thickness (T). Generally the source electrode is located at $x = 0$ and the drain at $x = L$. On the right Electronic and Ionic Circuit.

3.2.1 Electronic Circuit

Using the Ohm's law and referring to the Figure 3.2 it is possible to describe the electronic circuit as:

$$J(x) = q\mu p(x)\frac{dV(x)}{dx} \tag{3.1}$$

where J is the current flux, q is the elementary charge, μ is the hole mobility, p is the hole density and dV/dx is the electric field. In order to obtain the calculation of the analytical solution, the mobility μ is treated as constant. This is valid in a first approximation, although in a more detailed and accurate description, the mobility depends on the field and on the carrier concentration. However in this case the analytical solution may not be derived and a numerical solution is required. The dedoping, due

to the application of a positive gate voltage, is the process that describe the carrier concentrations into the organic semiconductor (Section 3.1). The cations are injected from electrolyte into the channel and each one compensates one acceptor. The de-doping takes place and the charge neutrality of the organic semiconductor is maintained: for each ion that enters the organic film, a hole extracted at the source isn't replaced by injection at the drain (working with $V_d > 0$). Neglecting the conductivity of the un-doped channel it is possible to give an expression of the effective dopant density of the semiconductor material:

$$p = p_0 \left(1 - \frac{Q}{q p_0 v} \right) \tag{3.2}$$

where v is the volume of the semiconductor channel, p_0 is the initial hole density in the organic semiconductor before the application of the gate voltage and Q is the total charge of the cations entered in the film from the electrolyte. Because of the approximation of uniformity of all the charge density across the thickness of the film, this model is limited to thin film. This approximation is used in order to simplify the calculation.

3.2.2   Ionic Circuit

The ionic circuit describes the ionic motion through the electrolyte and the accumulation of charge at the interfaces gate-electrolyte and channel-electrolyte therefore it is possible to outline this circuit as a series of a resistor (R_s) and a capacitors (C_d) [78].

The first element represents the electrolyte conductivity and it is an indication of its ionic strength. Instead regarding the capacitance, the semiconductor-electrolyte interface is generally greater than gate-electrolyte interface due to the high capacitance of PEDOT:PSS [79]. As a result the device properties (like extent of gating and transient response time) depend by the characteristic of the gate such as the material, the size and the geometry.

It is important to restrict this model, if oxidation or reduction significantly takes place at the gate electrode the model may not be accurate. This condition is the Faradaic regime and it is not the ideal operate condition of the OECT because the effective drop potential of the gate result on the channel bigger than the applied potential. Instead in the non Faradaic regimes there is no reaction at the gate electrode and the applied drop potential is equal to the effective drop. This model retains its accuracy in non Faradaic regime [80]. Treating the interface channel-electrolyte as a capacitor with parallel flat faces, it is possible to write the total charge that pass through the ionic circuit as $Q_{ss} = C_d \Delta V$ where ΔV is the applied voltage. The application of this voltage produce the transient behaviour, due to the RC circuit:

$$Q(t) = Q_{ss} \left[1 - exp\left(- \frac{t}{\tau_i} \right) \right] \tag{3.3}$$

where $\tau_i = C_d R_s$ is the *ionic transit time* [77]. Theoretically this time depends on the area of the channel A and on the capacitance per unit area c_d, related together by the equation $C_d = c_d A$. Furthermore, to treated c_d as a constant, the dependence of the capacitance, due to the ionic double layer, by carrier concentration and potential is neglected. Recently, in a successive paper of Rivany *et al.* [81], it has be reported a different experimental evidence, indeed τ_i results to be dependent by the channel volume. Extracting from the experimental data the value of c_d, they found a value of capacitance per unit area 100 times greater than the expected theoretical value. The capacitance is dependent on the volume of the channel and it is expressed by $C^* = C_d/v$, where v is the volume of the channel (equivalently it is possible to write the relationship between c_d e C^* as $C^* = c_d/T$, where T is the thickness of the channel). In the light of what was found, they propose a new equivalent circuit for describing the system, that is shown in Figure 3.3, where it is introduced a parallel resistor R_p which describes the electrochemical effects to the interface. Furthermore this circuit can return to the previous theoretical case for $R_p \to \infty$.
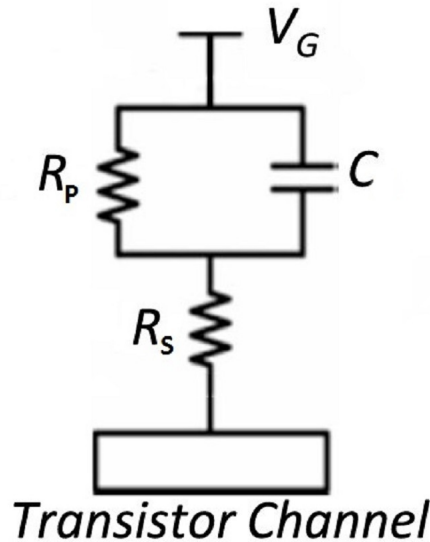
Figure 3.3: Ionic Circuit modified in order to consider the dependence of the capacity from the volume.

3.3 Steady State Behaviour

The behaviour of an OECT is linked to the effective dopant density (Equation 3.2) into the organic film; knowing its spatial distribution it is possible to calculate the charge in

a slice of organic semiconductor. Considering a slice of the channel located between x and $x + \Delta x$ (Figure 3.2) it is possible to calculate the charge in it at steady state as:

$$Q(x) = C^* \cdot T \cdot W \cdot dx (V_g - V_x) \tag{3.4}$$

where V_g is the gate tension, $V(x)$ is the spatial voltage profile into the organic film and W is the width of the film (referring to Figure 3.2). This charge expression is linked with Q_{ss} in the Equation 3.3. As the density of electronic charge within the organic semiconductor is high, it works as source of electronic charge that results from electrochemical de-doping; for this reason the de-doping can occur throughout the organic channel. To obtain the equation which ruled the OECT behaviour at steady state, the Equation 3.4 and Equation 3.1 must be combined in:

$$J(x) = q\mu p_0 \left[1 - \frac{V_g - V(x)}{V_p} \right] \frac{dV(x)}{dx} \tag{3.5}$$

The parameter V_p is the *pinch off* voltage and it is equal to $q \cdot p_0 / C^*$. To solve the Equation 3.5 in steady state the source drain current is assumed to be constant along the channel; in this condition the equation can be solved explicitly. The result is discussed in four different regimes dependent on the value of V_d and its relation with V_g (that is always $V_g > 0$). The first regime occurs when $V_g > V_d > 0$, in this case the de-doping involves the entire channel. Being the source placed a $x = 0$ and the drain at $x = L$, as explained above, it is possible to solve Equation 3.5 explicitly and in this condition it becomes:

$$I_{ds} = G \left[1 - \frac{V_g - 1/2V_d}{V_p} \right] V_d \tag{3.6}$$

where the parameter $G = q\mu p \frac{WT}{L}$ is the conductance of the organic semiconductor film.

In the second case, where $V_d > V_g > 0$, the equation that describe the regime is:

$$I_{ds} = G \left[V_d - \frac{V_g^2}{2V_p} \right] \tag{3.7}$$

In this regime the de-doping takes place only in the region of the channel where $V(x) < V_g$, the current increases with drain voltage and it is possible to observe a linear behaviour when $V_d = V_g$. The last case, which is defined for $V_d < 0$, provides for the possibility to completely de-dope portion of the organic channel, this happens when the the local density of injected cations becomes equal to intrinsic dopant density of the organic semiconductor. Defining the current saturation $V_d^{sat} = V_g - V_p$, this regime can be mathematically summed by the following equation:

$$V_g - V_d \geq V_p \Leftrightarrow V_d \geq V_d^{sat} \tag{3.8}$$
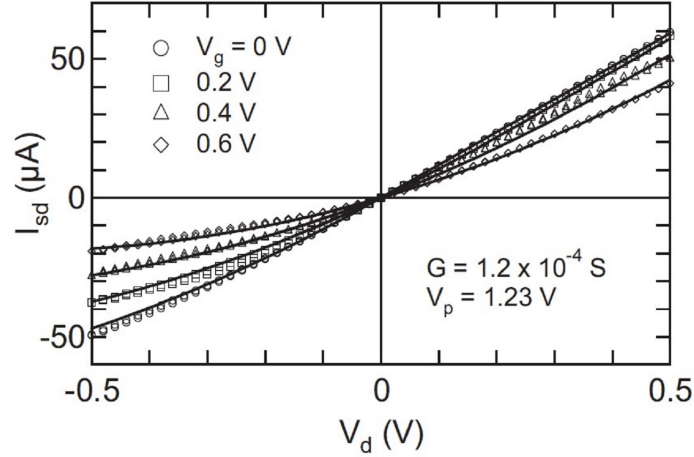
Figure 3.4: Experimental steady state I-V graphic (data point) obtain for an OECT with channel dimension $L = 5\,mm$ and $W = 6\,mm$. 10mmol NaCl solution is used as the electrolyte. Solid lines are the fit obtain with the model with $G = 1.2\cdot10^{-4}\,S$ and $V_p = 1.23\,V$ [77].

In this regime the depletion region il located near the drain electrode but, despite this region, the holes still be transported to the drain. The current achieves the saturation value, which is:

$$I_{ds}^{sat} = -\frac{G \cdot V_d^{sat}}{2V_p} \tag{3.9}$$

This expression is true for sufficiently long film, indeed in this approximations, when V_d rises beyond V_d^{sat}, the depletion region slightly moves towards the source but it still be localized near the drain electrode; therefore the current can achieved its saturation value. If the channel length is small, the displacement of the depletion region is significative with the drain potential variation; in this situation the current will not saturate but will continue to increase. In the end there is a last method to completely de-doped the channel, it is possible to apply a potential $V_d > 0$ and $V_g = V_p$. This last case is not of great interest because the high gate voltage requires.
In a realistic situation, it is possible that not all the channel is involved in the process. In this case a significant drop voltage takes place across regions of channel that aren't gated and the system is described with an additional resistance in the electronic circuit. For example in Figure 3.5 a deviations from the theoretical behaviour is introduced due to two symmetrical not gated regions, that are shown in the inset of the same Figure. As a consequence the onset of the saturation is achieved for more negative voltage.
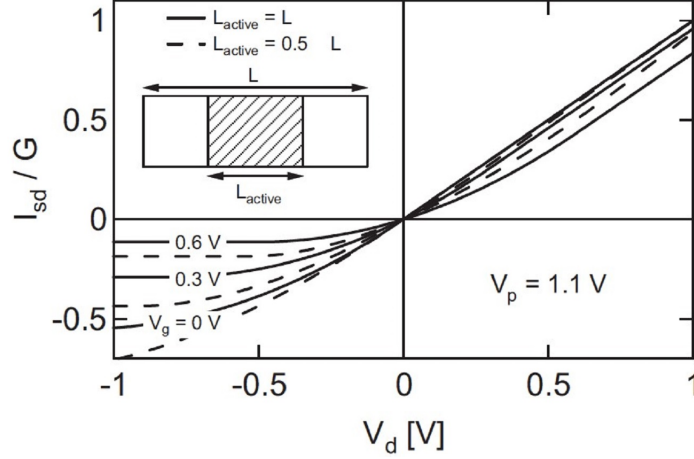
Figure 3.5: Simulated steady state I-V behaviour for an ideal device geometry (solid line) and for a device with additional series resistance (dashed lines) with $V_p = 1.1\,V$ [77].

3.4   Transient Behaviour

The injection of cations and the removal of hole at the source ($V_d > 0$) are the effect that ruled the transient behaviour. To describe this behaviour in a first approximation the hole density and ionic current are treated as constants within the channel and they are equal to their average value. A simplified behaviour is obtained adding the current associated to the removal of holes due to the de-doping and the one from the Ohm's law of the electronic circuit:

$$J(t) \approx q\mu p(t)\frac{V_d}{L} + qfL\frac{dp(t)}{dt} \tag{3.10}$$

The proportionality constant f takes into account for the spatial non-uniformity of the de-doping process. It assume different value in relation to relative magnitude of V_d and V_g, the characteristic range for f go from 0 (for instance $V_d \gg V_g$ with positive drain tension) to $1/2$ (if for instance $V_g \gg V_d$). This constant depends on gate and drain voltages and it is related to the time characteristic response. Combining the last equation (Equation 3.10) with the Equation 3.2 it is obtained:

$$I(t) \approx G\left(1 - \frac{Q(t)}{qp_0v}\right)V_d - f\frac{dQ(t)}{dt} \tag{3.11}$$

where the ionic circuit is expressed by its the transient response time $Q(t)$. To verify this response it is possible to set two different regimes, one is obtained fixing the gate current (I_g) and the other fixing the gate voltage (V_g). The first is preferable to better understand the physics of the device but is not a typical operating regime. Setting the

gate current is equal to fix the kinetics of ionic circuit and in this condition is possible to focus on the electronic circuit characteristic irrespective of the ionic circuit. This first regime is described by:

$$I(t, I_g) = I_0 - I_g\left(f + \frac{t}{\tau_e}\right) \tag{3.12}$$

with $\tau_e = L^2/\mu V_d$ is the electronic transit time and I_0 is the current fluxing between source and drain in the absence of gate current. An interesting use of this regime is the extraction of an effective value of the mobility μ in the organic film. In Figure 3.6 is shown a typical response to a constant I_g transient; in this is possible to note the recovery of the source-drain current upon the removal of the gate one, this is due to the diffusion of the ion which tend to go back in the electrolyte from the organic film.
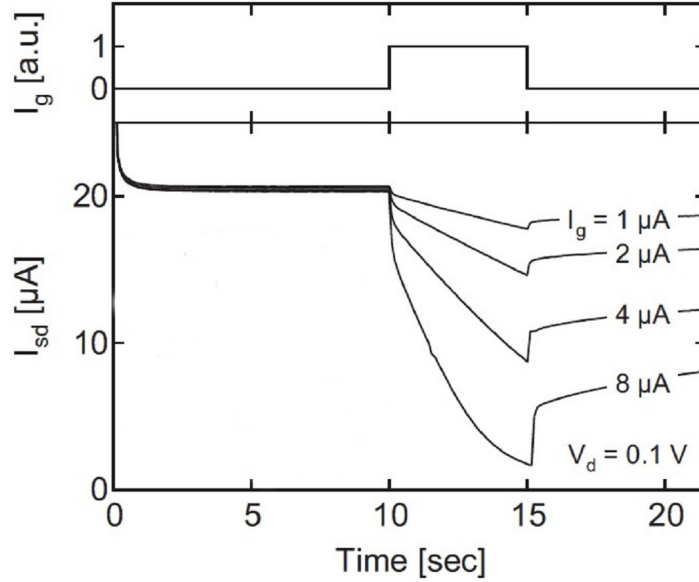
Figure 3.6: Costant I_g response of an OECT with electrolyte $1mol$ NaCl solution and dimension of the organic channel $L = 0.5\,mm$ and $W = 6\,mm$ [77].

The attention is now focused on the transient response to a constant gate voltage, in this regime the Equation 3.3 is used to model the electrolyte. In order to simplify the description, it is assumed that the de-doping equally occurs within the organic film without saturation effects and the drop voltage between gate electrode and organic channel is equal to an average value $\Delta V = V_g - 1/2V_d$; this ensures a good consistent between transient behaviour and steady state. In this approximation it is possible to describe the

transient behaviour for a simplify OECT as:

$$I(t, V_g) = I_{ss}(V_g) + \Delta I_{ss}\left(1 - f\frac{\tau_e}{\tau_i}\right) \cdot exp\left(-\frac{t}{\tau_i}\right) \tag{3.13}$$

where I_{ss} is the source-drain current for a fixed gate voltage (V_g) at the steady state and $\Delta I_{ss} = I_{ss}(V_g = 0) - I_{ss}(V_g)$. This behaviour is particular, indeed the response approach to the steady state in two possible way, depending on the relation between τ_e and τ_i (Figure 3.7).

- if $\tau_i > f\tau_e$ the response is a *monotonic decay*, in this condition the electronic response can be ignored because is faster than the ionic one, the hole extraction is a very fast process and is negligible compared to the transient response. This is the case of large V_d and/or small channel length.

- if $\tau_i < f\tau_e$ a *spike and recovery* response is shown. In this case the hole extraction is the dominant process which occurs with a relatively slow time.
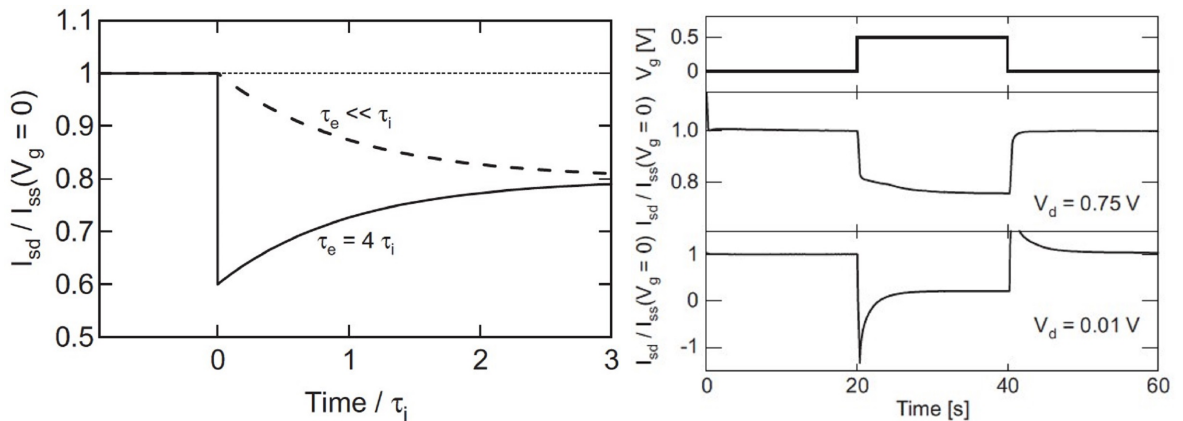
Figure 3.7: On the left are shown two different possible response of the source-drain current transient for a constant V_g (with fixed $f = 1/2$ and arbitrary ΔI. On the right two different response of the source-drain current transient, obtained for two different value of V_d keeping constant the electrolyte $10\,mmol$ NaCl solution and dimension of the organic channel $L = 0.5\,mm$ and $W = 6\,mm$. The current is normalized to its value before the application of gate voltage [77].

The two parameter τ_e and τ_i characterize the response time of the OECT as outline by the Equation 3.13. The solution resistance and capacitance of the ionic double layer define the time constant τ_i for ionic transport in the electrolyte; this time constant can be linked with the physical quantities of the device, using the Gouy-Chapman theory, $\tau_i \sim l/C^{1/2}$ where C is the ionic concentration and l is the distance between the gate

electrode and the organic film. The device response can be tuned by changing them, for example decreasing the distance l or increasing the electrolyte concentration led to an improvement of the response time of the device. The Equation 3.13 is also influenced by the electronic time constant, indeed the time response of the device is define by the ratio τ_e/τ_i. Knowing the ratio expression (that is $\tau_e/\tau_i \sim lL^2/\mu V_d$) it is possible to understand how the transient response can be modulated by varying the electrode position, the channel length or the drain voltage. In Figure 3.7 there is an example of this change of behaviour after a variation of the voltage V_d.

3.5 Sensing with OECT

This Section will introduced different OECT-based techniques used to monitoring cell growth and to evaluate cell layer integrity. Conceptually all this methods are based on one idea, the evaluation of how ion current (fluxing from electrolyte to organic semiconductor) is altered by the presence of a cell layer.
A first attempt to evaluate the presence of cell by an OECT is reported in the work of Peng Lin et $al.$ [72]. They observe a change in the steady state behaviour of OECT (Figure 3.9), which is dependent on the presence of the cell (directly grown on the channel of the device, Figure 3.8).
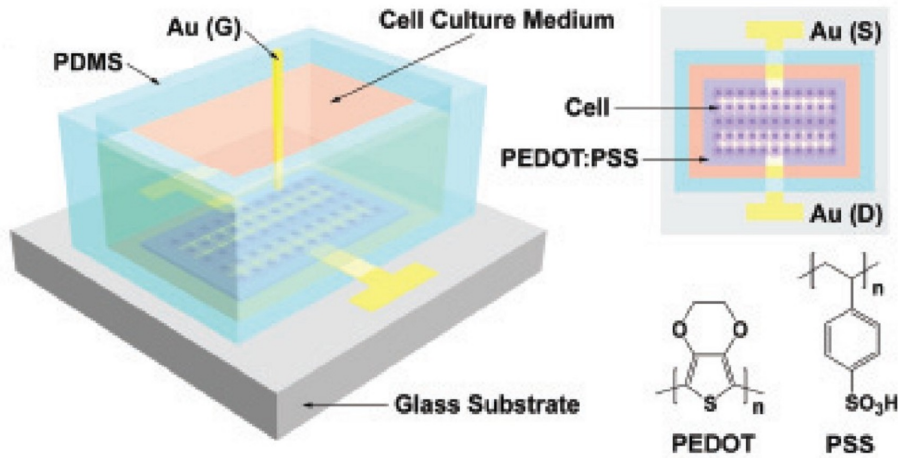
Figure 3.8: Schematic of the device based on PEDOT:PSS used by Lin et $al.$. The cell are seed on the channel of the OECT [72].

In this work they propose to modify Equation 3.6, replacing V_g with :

$$V_g^{eff} = V_g + V_{offset} \qquad (3.14)$$

where V_{offset} is an offset voltage dependent by potential drop at the two interfaces, gate/electrolyte (whose capacitance is C_g) and electrolyte/PEDOT:PSS (whose capacitance is C_d). They measure the capacitance C_d before and after the cell growth at zero bias voltage and they find a difference of less than 2% for capacitance value while in the steady state measurement the difference is more significant. Therefore this shift is caused by a change of the offset value V_{offset} in Equation 3.14, particularly considering the electrolyte/(PEDOT:PSS+Cell) interface, the change is given by:

$$\Delta V_{offset} = \left(1 + \frac{C_d}{C_g}\right)\Delta\Psi \qquad (3.15)$$

where $\Delta\Psi$ is the potential charge since the cell are cultivated on organic film.
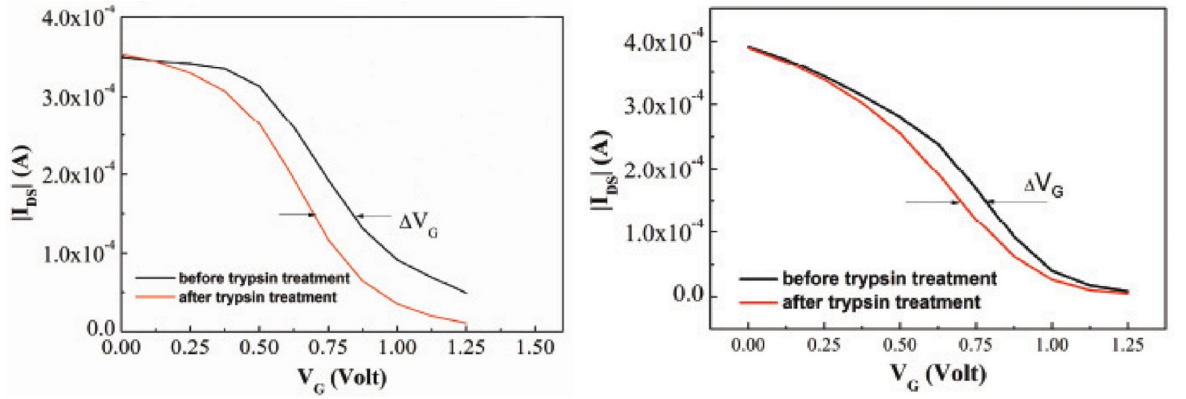
Figure 3.9: I_d vs. V_g graphics of the OECT before and after the detachment of two different cells (cancer cell on the left and fibroblasts on the right). The images are adapted from [72].

Ling *et al.* assume that the electrostatic interaction between the cell layer and PEDOT:PSS film produce this shift, furthermore the cell acts like an additional double layer and this electrostatic screening is described by the *Zeta potential*. The average of the Zeta potential of the cell is expected to be the modulating agent of the potential drop at the interface between electrolyte and the organic channel. Zeta potential of a cell is given by [82]:

$$\zeta = \frac{\rho}{\varepsilon De} \cdot \frac{1}{k} \qquad where \qquad k = \left(\frac{e^2 n_i^0 z_i^2}{\varepsilon k T}\right)^2 \qquad (3.16)$$

where ρ is the cell surface charge density, ε is the dielectric permittivity of the electrolyte, e is the elementary charge, n_i^0 is the concentration of ions of type i in the electrolyte, z_i is the valence of z ion, k is the Boltzmann constant and T is the measurement temperature.

This potential depends on the surface charge density of cells and on the concentration and type of ions in the electrolyte. Normally the Zeta potential of a cell is negative of
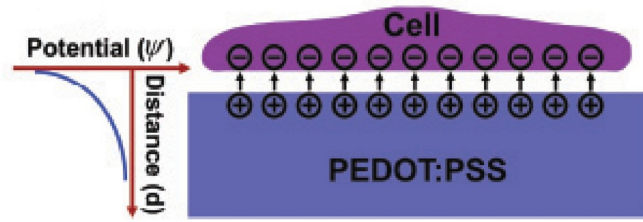
Figure 3.10: Schematic representation of the electrostatic interaction between an attached cell and PEDOT:PSS film [72].

tens of millivolts and due to its small value is difficult to accurately simulate the effect of the attached cells on the performance of OECTs. A cell attached on the channel surface applies an additional negative voltage on the OECT (Figure 3.10), thus the gate electrode have to compensate the difference by the application of a higher voltage. Even if it is difficult to measure this, in the paper a drop voltage is measured which is consistent with the potential change $\Delta\Psi$.
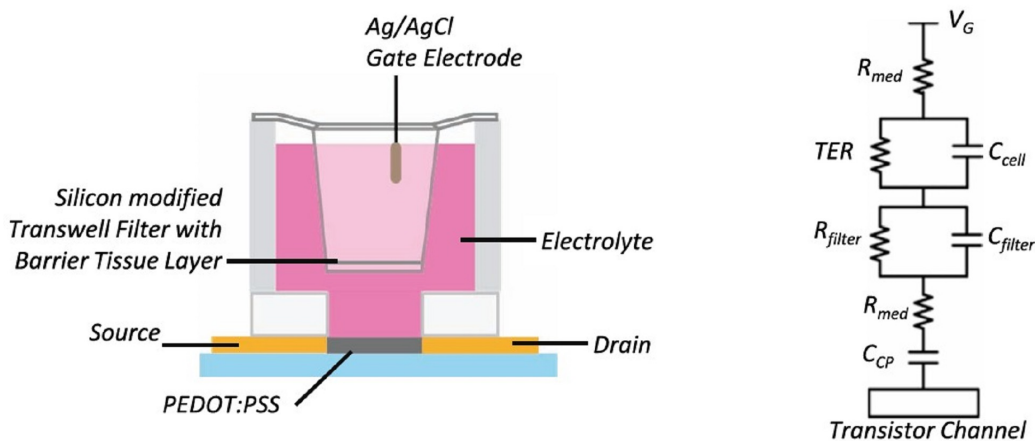
Figure 3.11: On the left A schematic representation of the device architecture. On the right the equivalent circuit that describes the ionic transport between gate electrode and the channel. TER refers to transepithelial resistance, C_{cell} is the capacitance of the cell layer, R_{med} is the resistance of the media, C_{CP} is the capacitance at the interface channel-electrolyte and th parallel R_{filter} and C_{filter} are the porous filter equivalent circuit. The images are adapted from [83].

Starting from 2012 the group of Róisín M. Owens is focusing its work on the monitoring of cell tissue via OECT. In the work of L.H. Jimison *et al.* [83], they propose an alternative method for monitoring in vitro barrier tissue integrity; the most common

techniques are based on permeability assay or on the measurement of the TER (see Section 2.3) but this kind of analysis are poorly reproducible, incompatible with high throughput methods and they require long time. They develop a set up composed by a transwell rest on the channel of an OECT (that is shown in Figure 3.11). Their idea is to substitute the generally used dyes or radio-labeled molecules with and OECT, in this way the OECT acts like a transducer of ionic signals in electronic current and is able to evaluate variation in ionic flow and consequently is able to evaluate formation and integrity of a cell layer. A great advantage of this geometry is to exploit the amplification of the transistor, it is possible to sense small variation in ionic flux from the changes of the amplified current, easier to sense. The ionic circuit, that is shown in Figure 3.11, is modified in order to consider the cell layer and the transwell filter, both are represented as a resistor and capacitor in parallel.
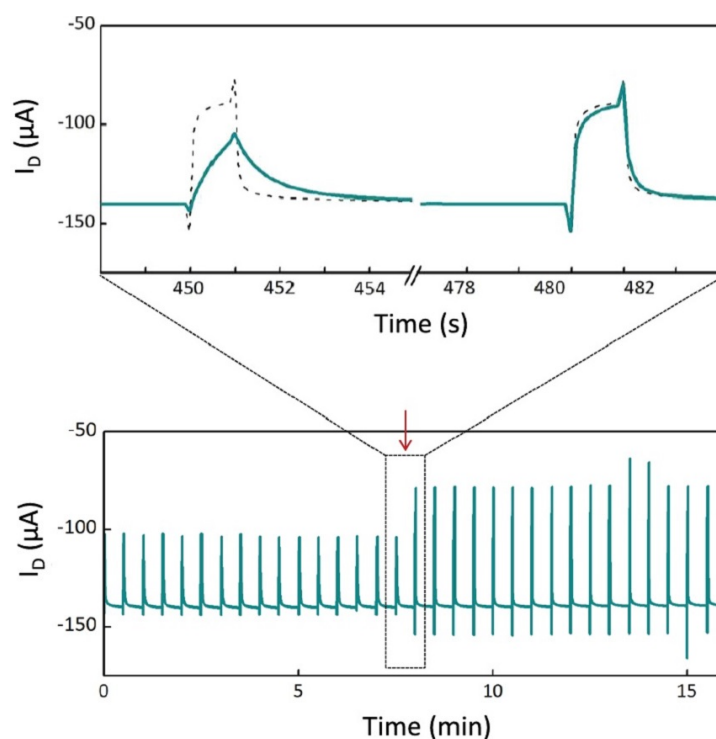
Figure 3.12: OECT response to a periodic squared V_g pulses. In the expanded scale it is show the point of H_2O_2 introduction labeled with the red arrow. The images are adapted from [83].

The aim of this experiment is to find an electrical parameter that is easy to measure and which allows a *dynamic measurements* of the barrier, where dynamic means acquired during the growth and not only at the end of this. The test of this set up is carried out with Caco-2 cell line (that form TJ); this choose is due to the well know model of the

cell and to the great impact of the barrier effect on the ionic flux. To better assess the sensitivity of the system, after the cells have reached the confluence, the barrier integrity is broken by the use of H_2O_2 (see Section 2.4). In Figure a 3.12 is show the response of the device during the rupture of the Tj caused by H_2O_2. L.H. Jimson *et al.* identify the drain-source current modulation as the figure of merit of this method; this modulation is defined as $\Delta I_d = I_d(V_g \neq 0) - I_d(V_g = 0)$ A great advantage of this set up is the compatibility with the existing barrier tissue characterization and toxicology techniques, however the transwell doesn't make possible optical analysis. In the paper of Tria *et al.* [84] the system is optimized further, indeed they observe that a measure of τ (which is the OECT transient time, see Section 3.4) is a more direct and less noisy. This parameter is normalized between 0 and 1, it assigns the value 0 to the response time of the device without cells and the value 1 to the response time with cells. The Figure 3.13 shows the variation of the response time of the OECT as function of the barrier tissue and the stability over time of the normalized response time of the device with and without cells.
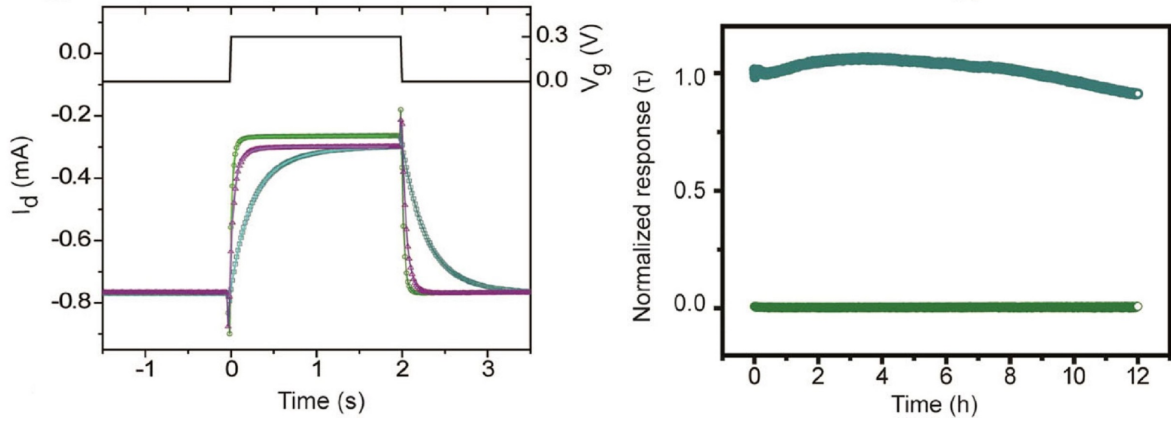
Figure 3.13: On the left the OECT response before (green line) and after (blue line) the cell growth while the purple line is the OECT response after the cells detachment. On the right the normalized response of the OECT as a function of time. The green line refers to an OECT without cells while the blue line to an OECT with cell [84].

Another optimization of this paper concerns the parameter extraction, unlike the theory that provided an exponential trend (Section 3.4), the time constant is extracted by a fit of the data to a bi-exponential equation:

$$I_d = \alpha \left\{ \left[1 - e^{\frac{-(t-t_0)}{\tau}} \right] + \left[1 - e^{\frac{-(t-t)}{\tau'}} \right] \right\} \tag{3.17}$$

where τ is the time constant, t_0 is the time which the pulse starts and α is a constant scaling term describing the magnitude of the current response. The second exponential term is a long time evolution of the drain current, likely associated with the OECT,

described by a time constant and time offset τ' and t'.

In the work, published in 2014 [85], the incompatibility of optical and electrical measurement is overcome by a new planar all-polymer transistor whose geometry is schematically shown in Figure 3.14. Taking advantages from the optical transparency of PEDOT:PSS, this set up make possible the simultaneous optical and electrical monitoring of growing cells in vitro. The complementary of these techniques demonstrates definitively the higher sensibility of electrical measurements compared to the optical one. In the new geometry the gate is under the cell layer so the gate current is assumed to cross two time the layer (from gate into the electrolyte and than into the channel), rather laterally between gate and channel.
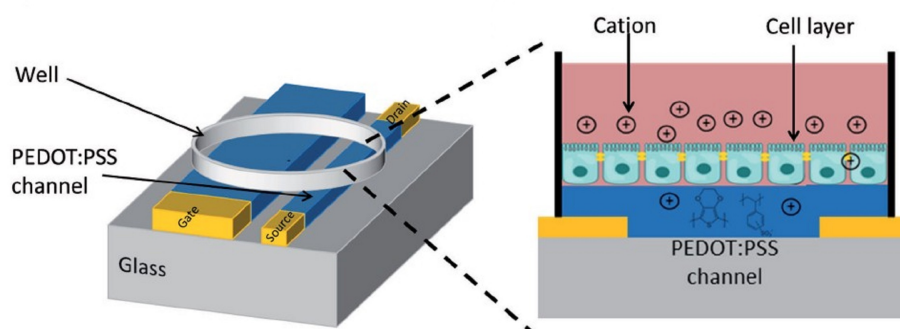
Figure 3.14: Schematic of the device. It is possible to see the polymer channel and gate patterned on a glass slide. The cell a the buffer are contained in a PDMS well [85].
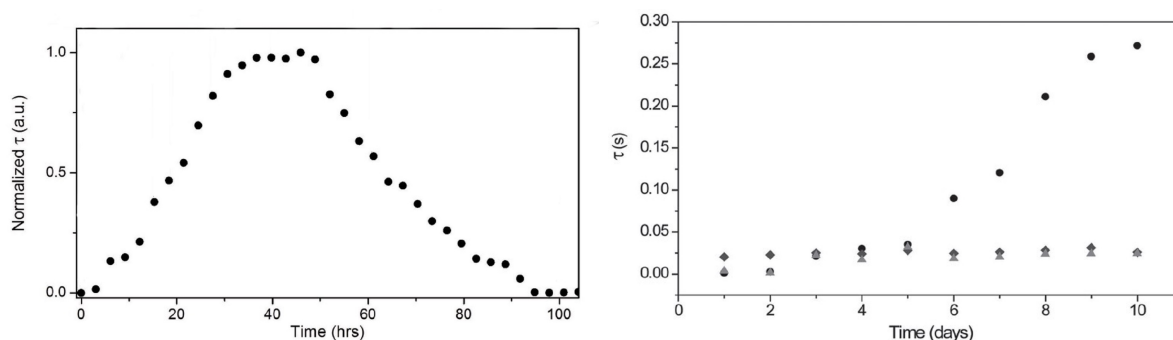
Figure 3.15: On the left the trend of the transient time measured every 3h for a MDCK-I cell culture. On the right the same measurement performed with Caco-2 cells (dark round markers), HEK-293 cells (dark-grey diamonds markers) and HeLa cells (grey triangle markers) [85].

The Figure 3.15 shows the monitoring, which is lasted four days, of τ after seeding of MDCK-I cells. It is possible to observe the achievement of confluence and the subsequent

detachment due to the contact inhibition. Furthermore to investigate if the τ variation is dependent on the barrier function of the cells or simply to a coverage effect, the changes in time response for different cell lines are evaluated. The trends are monitored for Caco-2, HEK-293 and HeLa cell lines and are shown in Figure 3.15. Lastly the disruption and the detachment of cell layer is studied. For the first kind of damage the EGTA is used while Trypsin-EDTA is used for the detachment. Figure 3.16 shows the effect for different concentration of the two previously named agent on a cell barrier, made by MDCK-I cells.
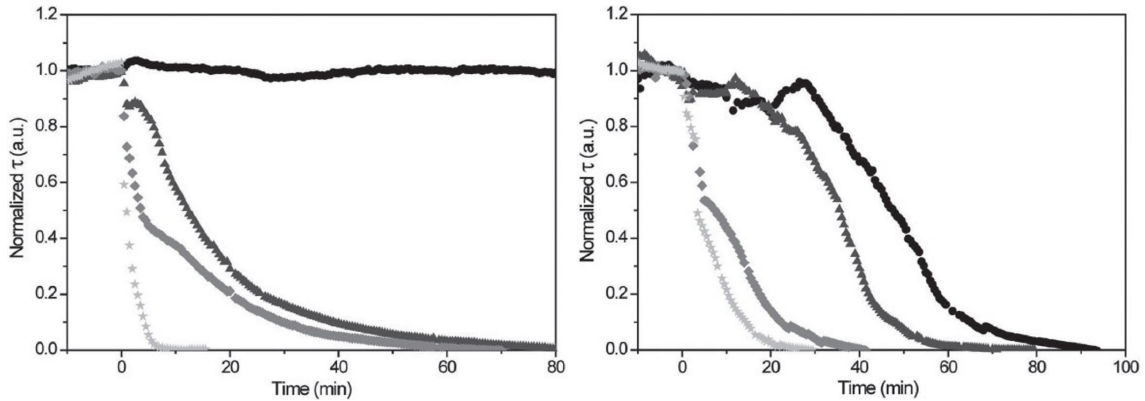
Figure 3.16: Effect of EGTA and Trypsin-EDTA on MDCK-I barrier both added a t=0. On the left the change of the transient response after the adding of EGTA. The different lines correspond to different concentration of EGTA: $1\ mM$ for dark round markers, $5\ mM$ for dark grey markers, $10\ mM$ for grey diamond markers and $100\ mM$ for light grey markers. The same graphic, obtained for the adding of Trypsin, is shown on the right. The different colors correspond to different concentration of Trypsin: $0.25X$ for the dark round markers, $0.5X$ for dark grey markers, $0.75X$ for grey diamonds markers and $1X$ for light grey markers [85].

A last work, made by the same research group (M. Ramuz *et al.* [87]), introduce a different type of data analysis: a normalized frequency dependent transconductance is monitored during nine days for the cell lines, previously appointed. This data sets are then appropriately fit to obtain a cell resistance (R_C). In Figure 3.17 are show transconductance and cell resistance trend. The EGTA test is repeated for MDCK-I cell line with this new figure of merit, the result are shown in 3.17 and confirm what occurred in previous experiments.
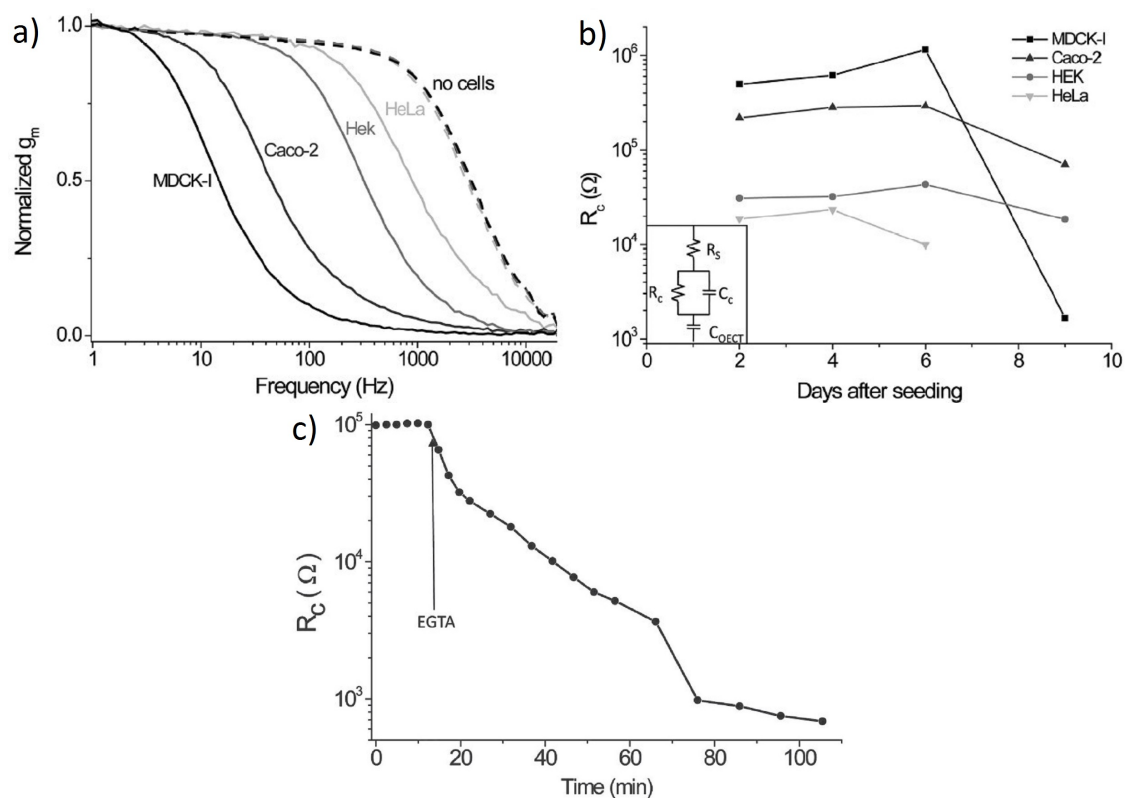
Figure 3.17: (a) Normalized g_m all day 6 obtained using OECT with different cell-lines. The full lines are the transconductance measured with cell while the dashed line is the transconductance without cells. (b) Time course of the cell resistance (R_c) extracted form a fit (circuit in the inset) for different cell-lines. (c) Extracted resistance as a function of the time monitored after the addition of the EGTA [87].

Chapter 4

Materials and Methods

This chapter explain the techniques, the working principles and the details of the instrument and the step followed to produce the OECT, to test the OECT, to grown the cells and to test the cell viability. It is important to emphasize that all processes performed to fabricate the OECT are performed by low coast processes.

4.1 OECT Fabrication Process

4.1.1 Evaporation Process

The Evaporation process have the objective to transfer atoms or molecules from a heated source to a substrate target. The first step of the evaporation is the creation of the high vacuum in a suitable chamber, then the source is heated until the evaporation temperature is reached. The atoms start to leave the source and travel towards the substrate. The atoms transfer their energy to the substrate target and condense because it is at lower temperatures. Since the vapor pressure at the new temperature is much higher, they not evaporate again. The thickness of the evaporated layer depends on the evaporation rate, the time of the evaporation and on geometrical relation between the source and the substrate. To obtain pure films there are several condition to keep, first of all the high purity of the evaporating material (at least 99.9%). A second important aspect is linked to the heater, this must be made of a material with low diffusion to not contaminate the process. Another condition concerns the vacuum level to avoid the contamination of residual gas. The high vacuum level ($[10^{-3}; 10^{-6}]$ $mbar$) is obtained by a two stage vacuum system. A rotary pump realizes the pre-vacuum then a turbo molecular pump allow to achieve the vacuum level required. Furthermore this is important to make possible the evaporation of the metal. The Figure 4.1 shows an operation diagram of an evaporator and the one used to realize the OECT.
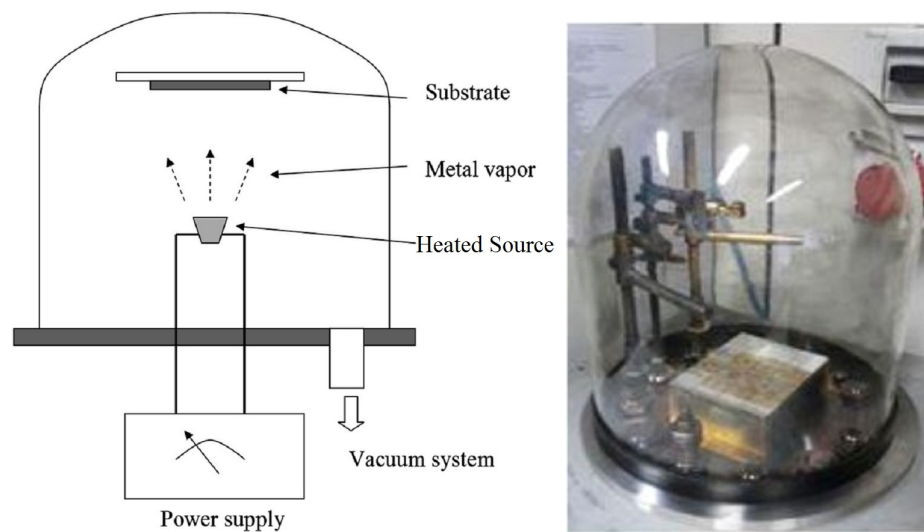
Figure 4.1: On the left a schematic representation of an evaporation chamber. In this picture all the component of the system are summarized, it is possible to see the heated source and its generator, the input of the vacuum system and the position for the target substrate. On the right the evaporation chamber used in this work.

4.1.2   Plasma Treatment

Plasma is a state of matter made of a mixture of charged particles. It is obtained providing energy to a gas and it is used in various treatment like cleaning, activation and etching of surfaces. In this work it is used to increase the wettability of materials helping the spread of liquid material. A schematic of the working principles of a plasma treatment is shown in Figure 4.2. This treatment is performed in a low vacuum chamber in which a known percentage of a gas (oxigen in the case of this thesis) is excited by a high voltage; this results in energetic gas ions which constitute the plasma. The high energy atoms are transported to the surface of the sample and remove impurities and radicals on the surface of the sample. The result is a surface without impurities and with a nanometer layer of free radicals which gives a high hydrofilicity to the sample. The plasma effect is not a permanent effect, in fact after several minutes the wettability returns to its standard value, if the sample is stored in air. The effect of plasma changes by varying the process parameter such as pressure, power, process time, gas flow and composition.

4.1.3   Spin Coating

The Spin Coating is a technique used to fabricate thin film from solution processable materials. it can be summarized in two steps: deposition of the solution on the sub-
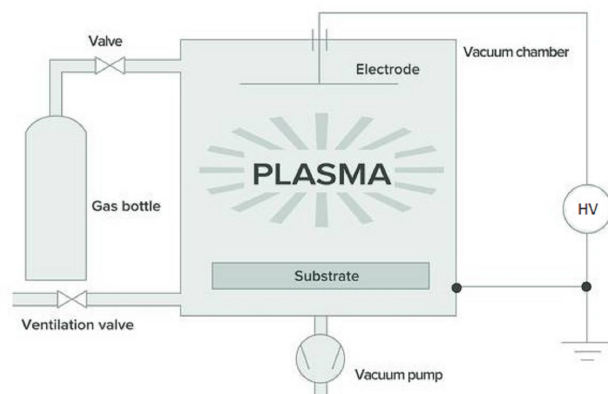
Figure 4.2: A schematic representation of an plasma treatment chamber

strate and rotation of the sample to spread evenly the solution. The obtained film is homogeneous and reproducible, in fact its characteristics (thickness and morphology) depend on the rotation speed, rotation time and on the solution ($d = k\omega^\alpha$ where d is the thickness, ω is the spin speed and k and α are parameters dependent on the solution). PEDOT:PSS, the semiconductor used in this thesis, can be spin coated with different thickness ranged from 40 nm to 800 nm. In Figure 4.3 is shown a deposition obtained with this techniques.
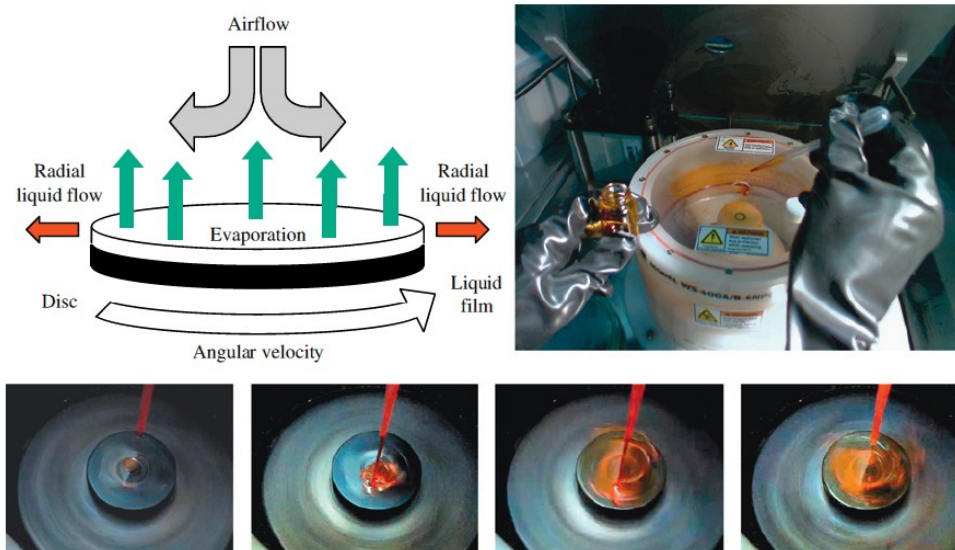
Figure 4.3: The two images on the top of the Figure are: on the left a schematic representation of the spin coating and on the right an images of the spin coating used in this work. On the bottom a sequence of images that show the operation of the spin coating process [35].

4.1.4 Preparing and Cleaning the Substrate

In the first step microscope glasses are cut with a diamond tip in order to obtain a rectangle substrate of 25×26 mm. The second step involves the cleaning of this substrate, this consist of four phases, lasting 15 minutes each one, within a sonicator. This four steps are successive baths of a mixture of water and soap (in a volumetric ratio 1 to 10), distilled water, acetone and lastly isopropanol. All glass substrates were fluxed with nitrogen after the washing, this procedure allows to avoid the formation of halos. The last step of the preparation is the application of a mask for metal evaporation with a specific pattern, reported in Figure 4.4, on the substrate.
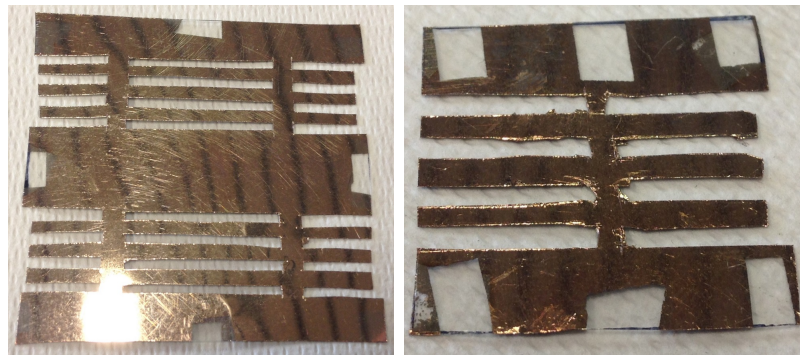
Figure 4.4: Two masks used for the evaporation, on the left it is shown a 4 device mask, on the right a 1 device mask.

4.1.5 Drain and Source Electrodes Evaporation

The metal electrodes are obtain by a sequentially deposition of chrome (Cr) and gold (Au), the first is used to improve the adhesion of the gold on the glass substrate, without the Cr the Au undergoes delamination and detachment when it is in contact with the electrolyte. To deposit the two metal it is used an evaporation chamber and two metal pure fibre with a purity equal to 99.9 %. The fiber are weigh in order to obtain about the electrode thickness, 25 mg is equivalent to 10 nm of Cr and 150 mg is equivalent to 50 nm of Au. This are cleaning with three sequential utrasonic bath in acetone, isopropanol and distilled water lasting 15 minutes each one. The vacuum is obtain by two stage, the first is achieved with a rotary pump and the second is achieved using a turbomolecular pump. When the pressure inside the chamber reaches value of about $2 \cdot 10^{-6}$ $torr$ it is possible to start the evaporation process.After evaporation, once removed the mask, the sample appears as reported in Figure 4.5.
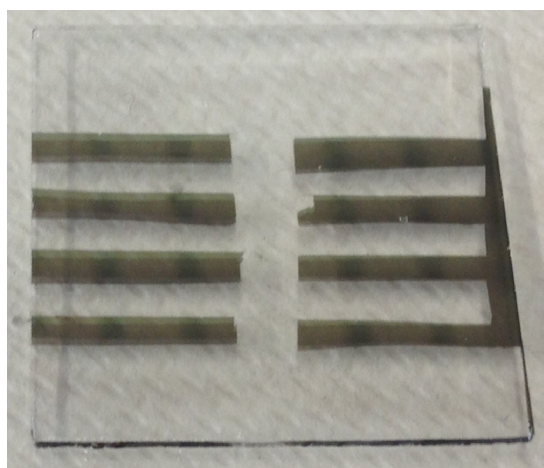
Figure 4.5: The second step of the fabrication, in this Figure are shown the electrode deposited on the glass substrate.

4.1.6 PEDOT:PSS Deposition

After the evaporation the substrate is treated with plasma (Section 4.2) to improve the hydrophilicity of the substrate. The plasma treatment is performed with oxygen at a pressure of 0.5 *torr*, with a power of 100 W and it lasts 300 s. The next step is the coating of the electrode with a teflon tape to keep the PEDOT:PSS contained in the central region of the substrate.

PEDOT:PSS is commercially available with several formulation [36], in this work it is used the $Clevios^{TM}$ *PH1000* which is a stable aqueous dispersion. Before the deposition the next additives are added to the dispersion:

- Ethylene Glycol (EG) used as conductivity enhancing agent to improve the conductivity. It is added a quantity equal to 10% by volume of the solution.

- Dodecylbenzene sulfonate (DBSA) to decrease the surface tension of the PEDOT:PSS, it facilitates the spreading out of the PEDOT:PSS on the glass and it improves the adhesion. it is added a quantity equal to 3% by weight.

- Glycidoxypropyl-trimetossilano (GOPS) is added a quantity of 1% by volume, it increases the bond between polymer chains of the PEDOT:PSS. This reduce the delamination of the film immerse in aqueous solution.

The obtained solution is stirred for about 15 minutes and it is filtered with a 1.2 μm cellulose acetate filter before the spin coating deposition (Section 4.1.3). The thin film, whose thickness is approximately 170 nm, is obtained setting on the spin coating a speed of 3000 RPM and a time of 10 s. The sample is dried on an *hot plate* for one

hour at a temperature of 120 °C and it is patterned to give the desired shape and size
to the channels. The last step is the deposition of a drop of silver paste on the edge of
the electrode to make the electrical connection more effective. The Device is shown in
Figure 4.6.

Figure 4.6: On the left the geometry of the produced device. On the right a comparison
photo of the fabricated device.

4.2   Electrical Measurement

4.2.1   Transient Response

All the electrical transient response measurements are performed by a source meter;
two different models, whit the same features, are used: the *Keysight B2912A* and the
Keithley 2612A controlled by a custom program for the acquisition. The two instrument
are shown in Figure 4.7.

Figure 4.7: Picture of the two source meter used in this work: the Keysight B2912A on the
left and the Keithley 2612A on the right.

This electrical measurement concerns the time transient response of the OECT (Equation 3.13). While the potential V_d is kept constant, on the gate electrode a repeated
sequence of squared wave pulse is applied. The drain current decreases each time the

pulse is applied with and exponential relaxation. All the measurements are performed setting the $V_d = -0.1\ V$, while the gate signal is in the low value (Off), equal to $0\ V$, for a time three time greater than the high value (On), equal to $0.3\ V$; we define the *On/Off Ratio* as the ratio between the time in which the gate applies the highest value and the time in which the gate applies the lowest value $R_{On/Off} = \frac{t_{On}}{t_{Off}}$ in a single repeat. Moreover a single pulse lasts $4\ s$ and all the process is repeated 5 times. The pulsed potential applied on the gate and the current response to this pulsed process are shown in Figure 4.8, it is a five time repeat of the exponential decay of the current.
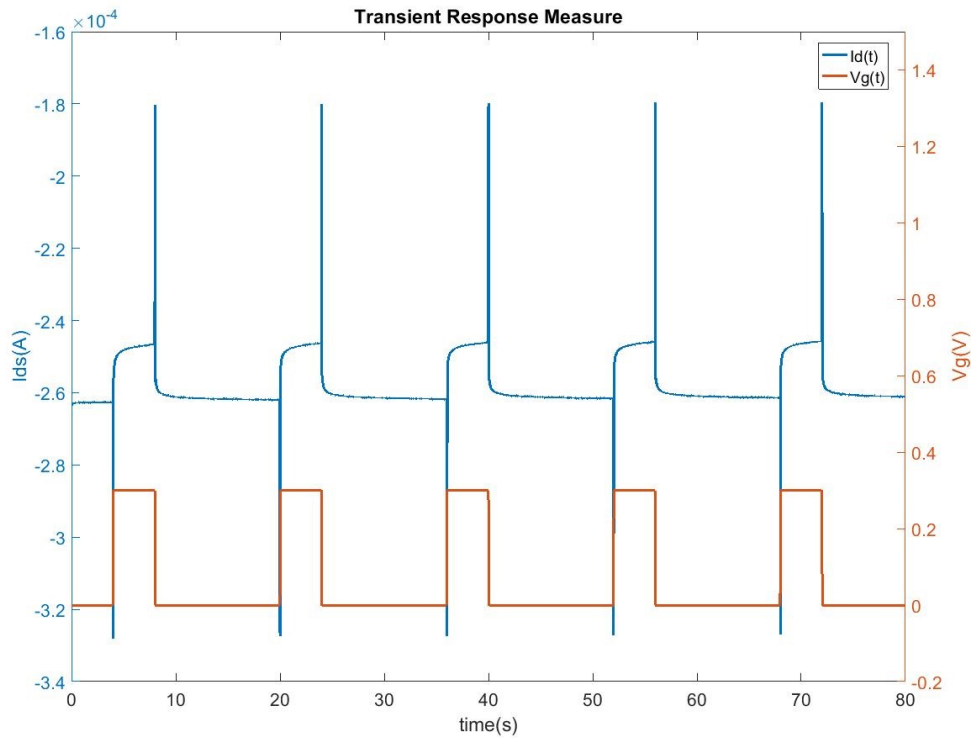
Figure 4.8: In blue the I(t) acquired measurement obtained with $V_d = -0.1\ V$, $V_g = [0.0; 0.3]\ V$, $DeltaT = 4\ s$ and $R_{On/Off} = 1/4$ while in orange the gate pulsed voltage.

The acquired data are then processed with a custom Matlab program, described in Section 5.2, to obtain the characteristic time of the decay.

4.2.2 Impedance Spectroscopy

The impedance analysis is an important tool to investigate the interfaces, in this work it is used to evaluate the equivalent circuit of the electrolyte-channel interface. Knowing

the value of the equivalent circuit it is possible to obtain an estimate of the transient time of the device. The measurement works by applying a voltage $V_{AC}(\omega) = \Delta V sin(\omega t)$ and by measuring a current $I(\omega) = \Delta I sin(\omega t + \phi)$. The ratio of this two physical quantities is the *impedance response* $Z(\omega)$. The equation that express the $Z(\omega)$ is:

$$Z(\omega) = \frac{V(\omega)}{I(\omega)} = Z_0 e^{i\Phi(\omega)} = Z_0[cos(\Phi) - isin(\omega)] = Z_{Re} - iZ_{Im} \qquad (4.1)$$

The working principle of the measure is summarized in Figure 4.9.
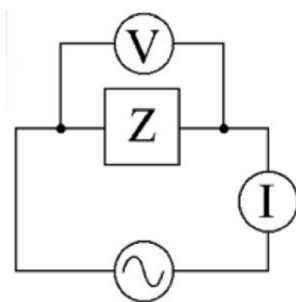
Figure 4.9: Schematic of the working principle of an impedance measure.

A correct measurement of $Z(\omega)$ has to satisfy three condition: a linear proportionality between the voltage and the current, a good stability along the used frequency and a good isolation from the noise. The data can be represented with the Nynquist and the Bode plot. The first shows the imaginary part of $Z(\omega)$ as a function of its real part while the second is a plot of the module of the impedance $|Z|$ and of the phase Φ as function of the frequency. Using a suitable program is possible to fit this data and to interpret them as an equivalent circuit. To performed this measurement an *Autolab PGSTAT204* (that is shown in Figure 4.10) is used. This instrument is used in combination with the software *NOVA* [93] which is able to set and control the potentiostat. Moreover NOVA is a tool to fit the data and to elaborate the equivalent circuit.

4.3   Biological Material and Measurement

4.3.1   Cell Culture

Both the used cell lines (Hela and NIH-3T3), that are described in Section 2.2, are cultured in a buffer composed of:

- *Dulbecco's modified Eagle Medium* (or DMEM), a modified version of the *Basal Medium Eagle* (BME), characterized by a higher concentration of vitamins, ammino acids, glucose and sodiumo bicarbonate;

Figure 4.10: Image of the Autolab PGSTAT204 used in this thesis.

- 10 % of *Fetal Bovine Serume* (FBS);

- 0.1 mM Non Essential Amino Acids (NEAA);

- 2 mM L-glutamine;

- Antibiotics (1 % streptomycin and 10 $\mu g/ml$ Blasticidin).

All cell lines are grown in standard physiological condition (37 °C, 5 % CO_2 and 95 % relative humidity).

4.3.2 MTT Assays

The MTT is a colorimetric Assay used to evaluate the cells viability, cells proliferation and the cytotoxicity of drugs. It is based on the conversion of a yellow-colored Terazolium salt (the 3-(4,5-dimethylthiazol-2yl)-2,5 diphenyltetrazoliumbromide) in a blue-colored formazan crystal by a mitochondrial enzyme. Because this reaction takes place only in metabolically active cells, this test is often used to evaluate their viability. MTT is dissolved at concentration of $2\,mg/ml$ in PBS $1X$ and it is filtered. MTT solution is added to each samples after two hours of incubation then the MTT solution is removed and DMSO is added to each samples. After the execution of the MTT protocol the well is plug in a plate reader and the reaction is evaluated by a spectrophotometric measurement of the sample at a wavelenght of 550 nm. A Spectrophotometry is a method to measure

the absorbance of a sample (Figure 4.11). A Beam of light of a specific wavelength passes through the sample that abosorbs or transmits light over a certain range of wavelength.
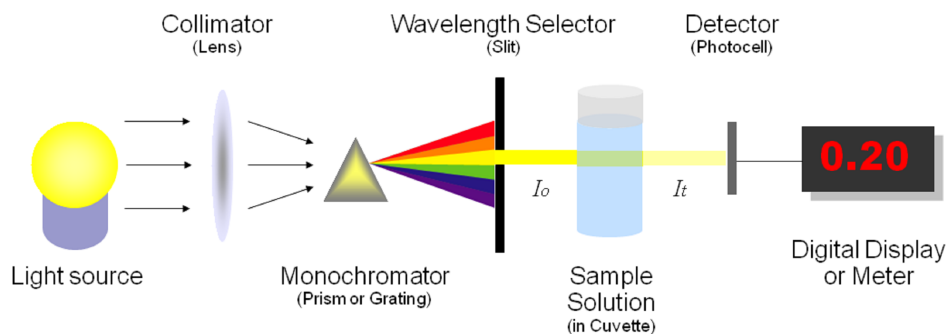
Figure 4.11: The basic principle of a spectrometer [88].

The figure of merit obtained is the absorbance, the common logarithm of the ratio between the incident and the transmitted radiant power through a material. An example of an absorbance spectrum, obtained by a spectrophotometer, is shown in Figure 4.12.
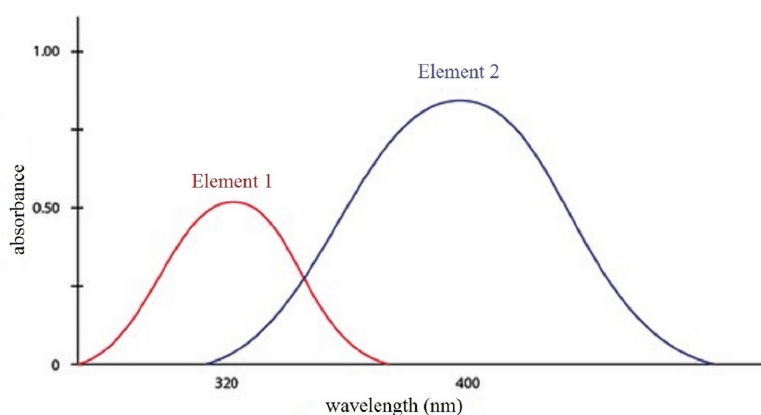
Figure 4.12: An example of acquired absorbance spectrum.

4.3.3   Optical Measurement

OpticalMicroscope

In this work it is done two types of optical measurements: an optical transmission measurements and an optical fluorescence measurements.

The transmission measurement is performed by the Nikon TS100 Eclipse (that is shown in Figure 4.13). In this technique the light crosses the sample, therefore it can

Figure 4.13: Inverted optical microscope Nikon TS100 Eclipse.

be used only with transparent sample. In this particular case, the Nikon TS100 is an inverted microscope, this means that the light source is placed over the sample, while the objectives are below. The microscope has four possible magnification (4x, 10x, 20x and 40x) and it is often linked to a camera in order to acquire digital images of the sample. The inverted microscopes are often used to observe living cells of organisms because they allow to obtain images in a more natural conditions.

Fluorescence Microscope

The second technique is the fluorescence microscopy, this is a very used technique based on the absorption and subsequent re-radiation of light by a sample. The technique of fluorescence microscopy is a very useful tool in biology and biomedical sciences because it makes possible to identify biological cellular components otherwise invisible with optical microscopy. The sample can exhibit autofluorescence or can be treated with additives fluorochromes that are excited by a specific wavelengths. The fluorochromes are attach to visible or sub-visible structures and makes this element easy to detect. The Figure 4.14 shows a diagram of the epi-fluorescence microscope used in this work, the Nikon Eclipse 80i. The vertical illuminator, in the center of the image, support the filter cube turret at one end and the light source at the other end. In this vertical illuminator a multispectral light is produced by an arch-discharge lamp, then this is filtered passing through a

wavelength selective excitation filter. The filtered light is deflected by a dichroic or a beamsplitter and reach the sample with an intense light through the microscope objective. If the sample fluoresces, an emission light is produced and is gathered by the objective. This light cross again the dichroic and is filtered by a barrier (or emission) filter, which selects the excitation wavelenghts.
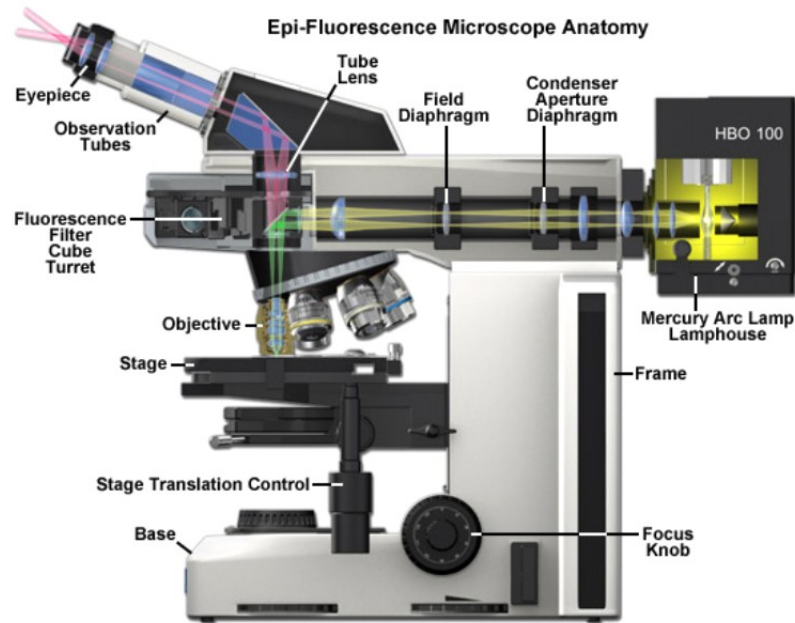
Figure 4.14: Schematic view of the fluorescence microscope Nikon Eclipse 80i [89].

In this work the Millipore's Actin Cytoskeleton and Focal Adhesion Kit (Catalog Number FAK100) is used. This is a very sensitive immunocytochemical tool that contains fluorescent-labeled Phalloidin to map the local orientation of actin filaments and a monoclonal antibody to Vinculin that is very specific for the staining of focal contacts in cells. The kit also contains DAPI (4',6-diamidin-2-phenylindole) for the fluorescent labeling of the nuclei. In details, in the images reported in this thesis, the actin cytoskeleton will appears in red while the nucleus in blue. In reality the yellow labeling of the focal adhesion is not used in our images.

Chapter 5

Set-Up Development and Calibration

In order to work with cells and the biological environment, sterility condition and protocol must be respect. The first challenge of this work was to design a set-up that, at the same time, respect these condition and allow to perform electrical measurements during the cell growth. The main constrains to be respected are biocompatibility and statistical significance. Moreover in this chapter are discussed all the operation that have been implemented to validate the set-up ready for the monitoring of cell tissue. In this calibration are included the MTT assay, the sterilisation protocol, the device characterization and a description of a custom software to perform the data analysis. All the measurements presented in this chapter are performed using a *complete cell buffer* (described in Section 4.3.1) in order to keep as much as possible the same experimental conditions of the cell growth.

5.1 Development and Realization of TE-OECT

First of all the biocompatibility, all the set-up element, that are in contact with the biological environment, must not be cytotoxic. To ensure this the first step is to choose suitable materials to the intent. In particular the multiwell and the O-rings are the two elements which directly contact the biological system. The first is the structure in which there are the wells that contain the electrolyte (that is also the cell buffer); the second is a seal that ensure the confinement of the biological environment. The chosen materials are the Polyether ether ketone (also called PEEK) for the multiwell and the silicone for the O-rings. Another focus concerns the cellular respiration. To proliferate the cells require a mix of O_2 and CO_2, then the cover of our set-up have to respect a constrain too. This must be realized to not hermetically seal the multiwell in order to make possible the air flux and allow the cellular respiration. Another important aspect concerns the electrical connections, these can indeed produce cytotoxic effect. The electrical part of the set-up must be placed outside of the O-rings, indeed it must be able to work in

physiological condition. To satisfy these requests, the base of the set-up is projected and realized as a PCB; this choice ensures greater protection of electrical paths and less space footprint. This set-up is named *Tissue engineering-Organic ElectroChemical Transistor* or TE-OECT (that is shown in Figure 5.1) and is composed of three part: the PCB base, the multiwell PEEK and the plexiglass cover. The three part of the TE-OECT are held together by eight screws, screwed in the PEEK. In the next two Section the three part of the TE-OECT are analyzed in detail.
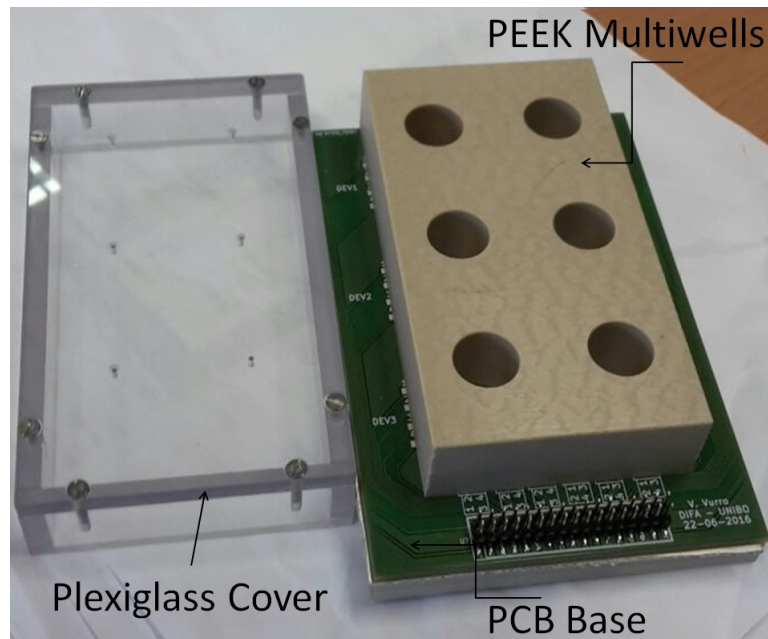
Figure 5.1: Image of the assembled TE-OECT.

5.1.1   PCB and Electronic circuit

The base is projected with a free software suite for electronic design automation (EDA) named *KiCad* [90]. To develop a project in this software there are two step, the design of a schematic for electronic circuits (designed by *Eeschema*) and then its conversion to PCB design (realized by *Pcbnew*). For each component are associated two models, one used in the Eeschema (a block function diagram) and one used in Pcbnew (called footprint). The Block function diagram is a schematic representation of the component, it contains all the information concerns its pins (such as input or output pins). The footprint instead is the physical appearance of the component, it contains information about the dimension and the position of the pins. Eeschema is schematic capture software distributed as part of KiCad, it is an integrated application where it is possible to draw and connect the circuit component. This level hasn't complex limits and is an interface

focused on productivity, in the schematic all the connection are automatically verified by the Electrical Rules Check (ECR). The ECR check for output pin conflicts, missing drivers and unconnected pins. It is instead possible to deign a custom block diagram and export the ended circuit in Pcbnew. Pcbnew is a printed circuit board software that work in association with Eeschema. Pcbnew read the schematic produced by Eeschema then find and placed all the footprints associated to the components of the circuit. The user have to set all design rules (like the distance between tho tracks or their size) and connect the components. Pcbnew provides a designe rules check (DRC) which prevents track and pad clearance as well as preventing wrong connections; the DRC continuosly run guiding the user to connect the right pins and to respect the design rules. In this program it is possible to generate up to 31 layers of copper, 14 technical layers (silk screen, solder mask, component adhesive, solder paste and edge cuts) plus 4 auxiliary layers (drawings and comments). It is possible to design custom footprint and export 3D-view of the circuit and gerber files, used to built the designed layout.

The first step, for the purpose of this work, is the designed of the component OECT. This component must reproduce the glass substrate dimensions and provides the electrical connections. Moreover in the footprint a hole has to be placed, this will be used to take the optical transmission imaging. The Figure 5.2 shows the block diagram and the footprint of the OECT.
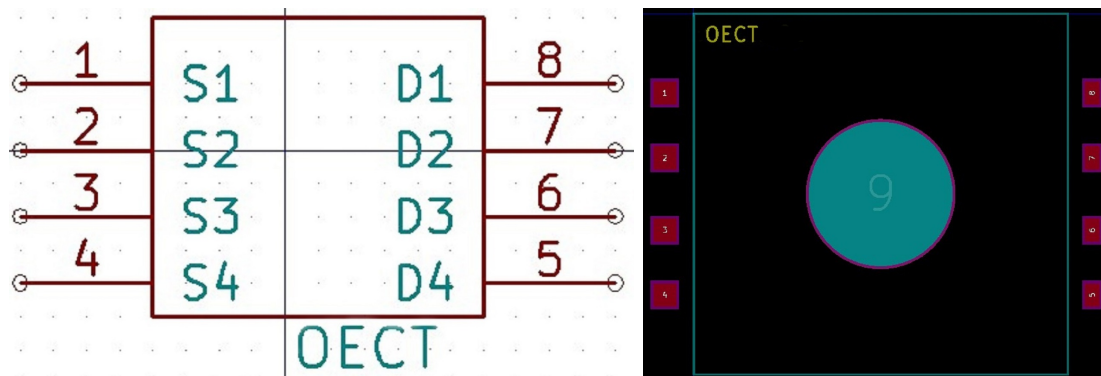
Figure 5.2: On the left the custom block diagram and on the right the custom footprint of the component OECT.

Another custom component is a simple hole, located in eight specific positions, used as a through hole for the screw. When the custom components are done the schematic and then the layout are designed, the layout is shown in Figure 5.3. The pin header are placed in bottom part of the PCB while in the upper part two connection are placed in order to insert a ground plane directly underneath the PCB. This detail is added in order to reduce as much as possible the noise because the electrical measures will work with small amplitude signals. The prototype is realized by a fast prototyping company [91]. In Figure 5.4 it is shown the PCB board and the ground plane, this is obtained by

a copper tape. This choice is made to keep the thickness of the base as small as possible not to limit the optical measurements.
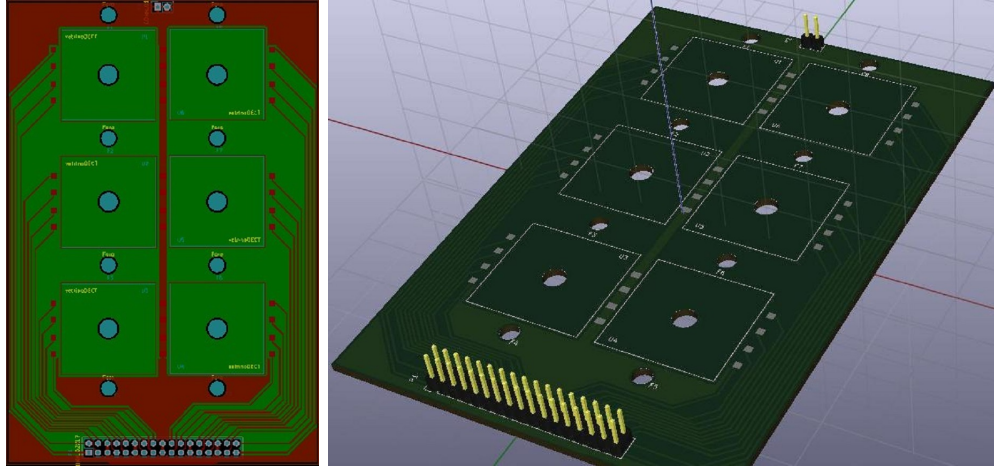
Figure 5.3: Ended layout of the PCB board and its 3D view.
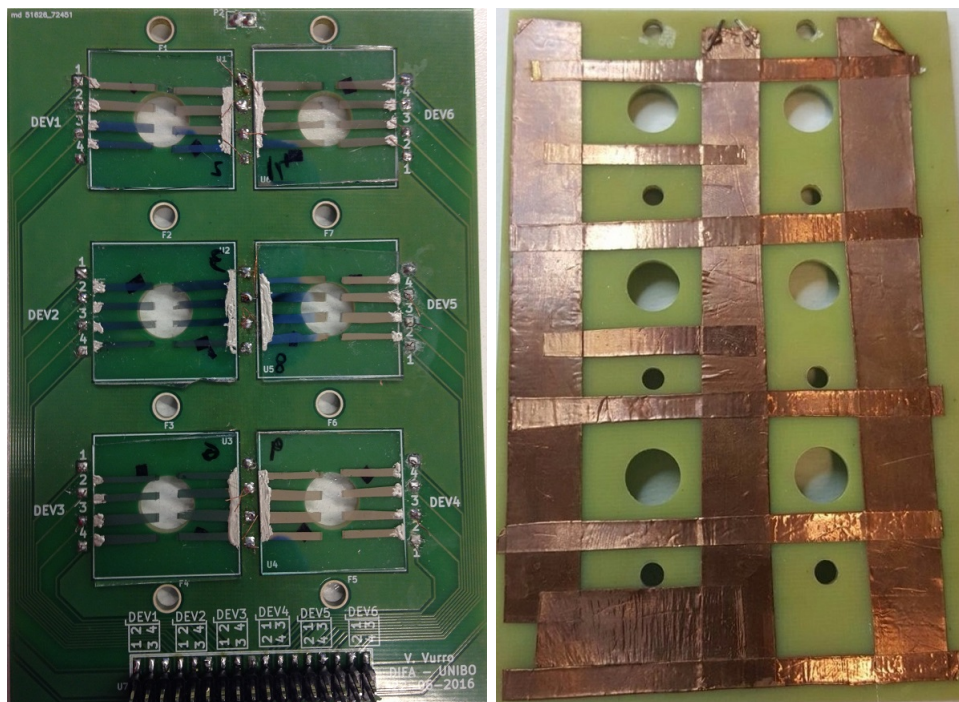
Figure 5.4: The realized PCB base. On the left the front side of the PCB with six OECT assembled on it. On the right the rear side with the ground plane obtained with the copper tape.

The connections between the PCB and the OECT are made by a copper wire. The wire is solder to the appropriate pitch on the PCB and is connected to the electrodes (drain or source) by silver paste. Furthermore to make more solid the contact a silicon drop is applied over the silver paste.

5.1.2 Well, Cover and Electrodes

As previously said, the multiwell is made of PEEK, a biocompatible termoplastic organic polymer, this is very easy to work because of its physical-mechanical characteristics. The PEEK board is $110 \times 60 \times 20$ mm and there are 14 holes in it. Six holes are the wells , these have a cylinder shaped of diameter equal to 14.5 mm. Each single well is able to contain 3.3 ml of liquid in order to use a correct quantity of cell medium. The remaining eight hole are threaded in order to provide an anchor to the screws. An important role of this closing mechanism is the compression of the O-rings, this ensure the proper isolation of the biological environment (in the well) from the electrical connections.

Each gate electrode is obtained by a gold wire. The length of the wire is 120 mm and the diameter is equal to 0.508 mm. 75 mm of this wire are coiled and this part is immersed in the electrolyte. It is possible to consider the surface area in solution equal to 120 mm^2. This condition ensure a high ratio between gate and channel areas in order to focus the potential drop on the electrolyte-channel interface. Each single gate electrode is placed in the apposite 1 mm diameter hole to ensure the correct channel-gate distance. The cover is realize in plexiglass to allow the optical images. The Figure 5.5 shows the cover and the PEEK multiwell do disassembled yet.

5.2 Data Analysis Software

The data acquired by the Source Meter (see Section 4.2.1) is treated by a custom Matlab program. This program consist of four blocks, the first imports the data (*ReadFile* function), the second manipulates the data (*PartialPulseIsolation* function), the third does some graphical comparisons (*Pulse5* and *GaphicComparison* functions) and the last performs an exponential fit (*Fitting* function).

The acquisition program save a file ".dat" which is read by the function *ReadFile*. The drain current and the relative time is saved in two vector, a plot of this quantities was previously showed in Figure 4.8. In this work the selected figure of merit is the decay time τ_i, extracted by fitting a single transient response (see Section 4.2.1). To make the extraction the first step is the treatment of the signal by the function *PartialPulseIsolation*. This function first of all converts the $I(t)$ into mA, then cuts the portion of the signals containing the spike (because it is attributed to the application of the gate potential and it has a length of approximately 0.01s) and isolates each single transient response. Furthermore the function calculate the absolute value of the current. More-
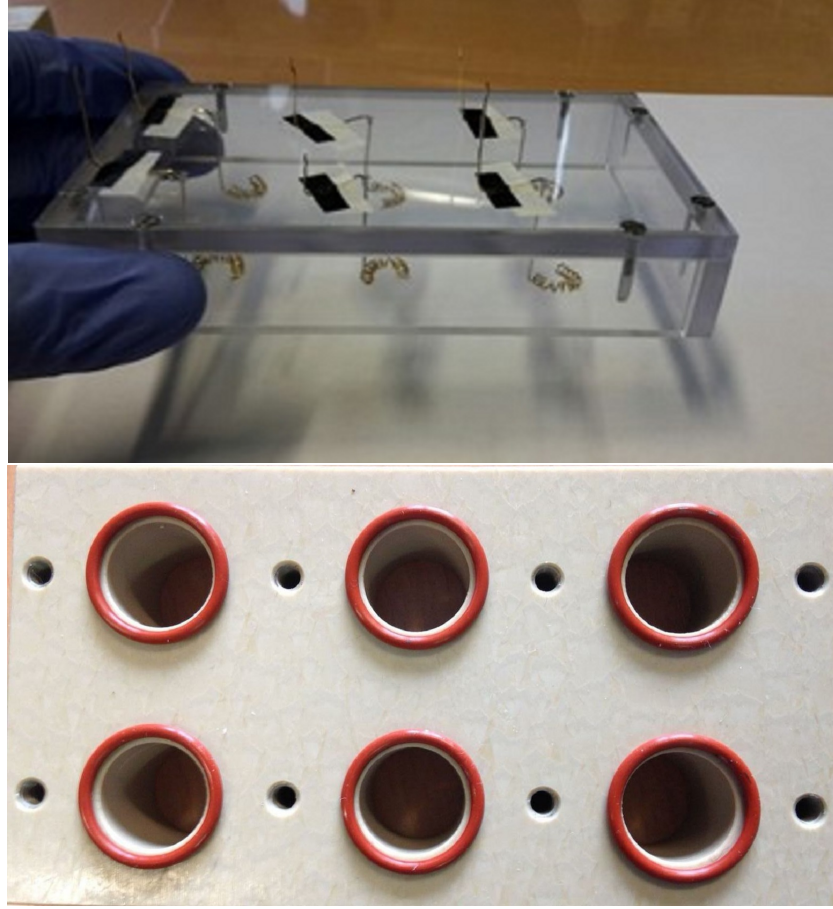
Figure 5.5: On the top an image of the six gate electrode assembled on the Cover and on the bottom the PEEK well and the six red silicon O-Rings.

over the function is able to normalized the isolated pulse in order to allow a comparison between pulse with different current variation. The Figure 5.6 shows the result of this operation.

The third block of the program uses the *PartialPulseIsolation* function to isolate the five response of the same $I(t)$ in the *5Pulse* function. The *GaphicComparison* instead uses the *ReadFile* and the *PartialPulseIsolation* functions sequentially to compare graphically the same pulse of different files. The last function, the *Fitting* functions, perform a fit to a bi-exponential equation (Equation 5.1)

$$I_d = \alpha_0 \cdot \left[1 - e^{\frac{-(t-t_0^0)}{\tau_i^0}} \right] + \alpha_1 \cdot \left[1 - e^{\frac{-(t-t_0^1)}{\tau_i^1}} \right] \tag{5.1}$$

Where the figure of merit used in the work are the characteristic time τ_i^0 and τ_i^1.
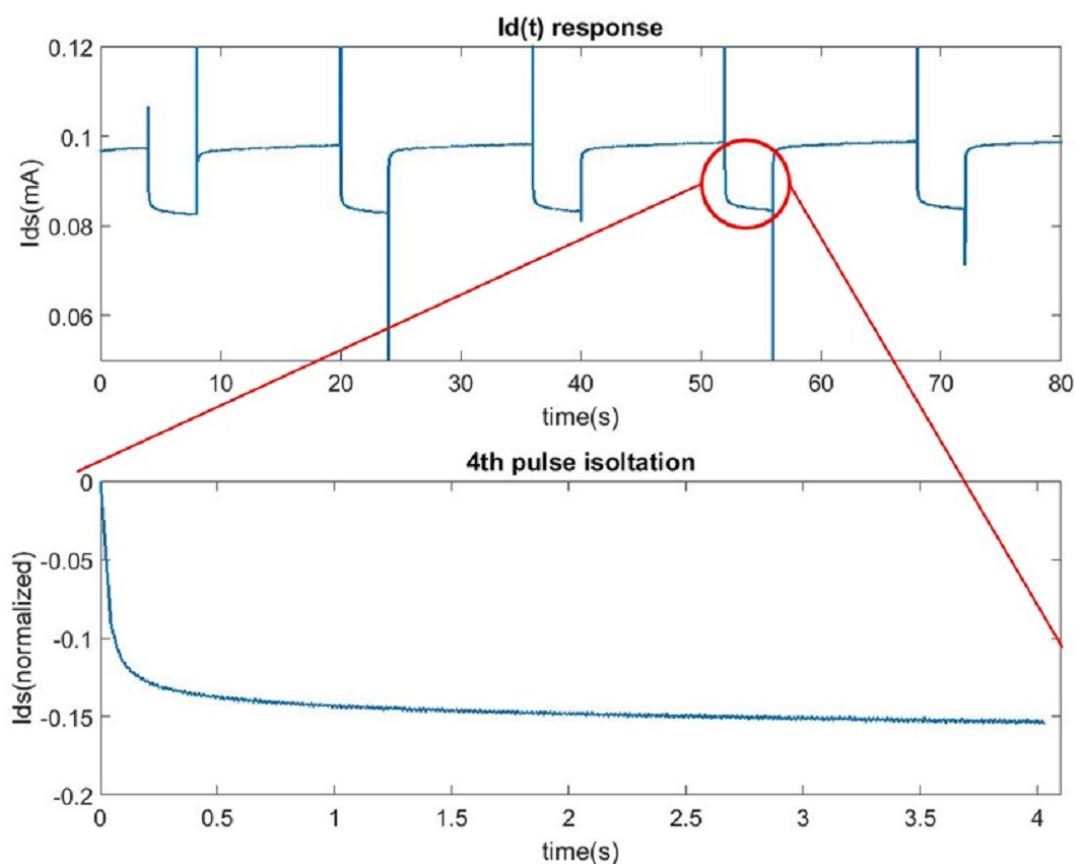
Figure 5.6: Example of a pulse isolation process performed by the function.

The Figure 5.7 show a fit obtain with this program. All the errors on the response time τ_i^0 and τ_i^1 are calculated as the standard deviation of two possible way. The first is the standard deviation on the 5 pulse of a single measurement and the second is the standard deviation between different channel. The value of the first error is equal to the 3 % while the value of the second error is equal to the 5 % of the quantity. In all the graph show in the following Sections the error is fixed as the 5 % of the value.

5.2.1 Physical Interpretation of the Fit

The response time theoretically should follow an exponential behaviour while in this work a bi-exponential fit is used, as just explained. In Figure 5.8 are shown the response of the devices fabricated with the previous batch in DMEM and in *Phosphate-buffered saline* (or PBS). It is possible to observe that the drain current reaches the saturation both in PBS and DMEM in lower time and this response time can be fitted with a exponential trend.
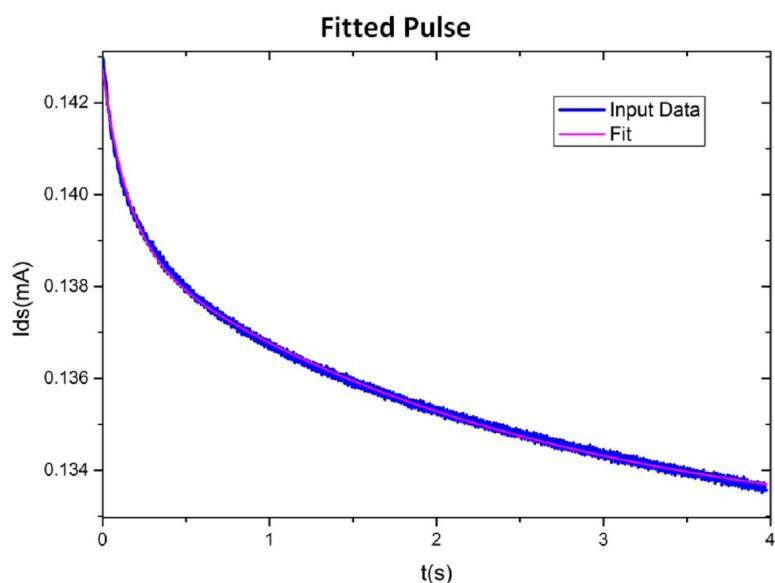
Figure 5.7: Single pulse fitted with the custom Matlab program.

This two exponential response time are obtained with the same fabrication process and the same geometry, therefore this different relaxation can be attributed to a different composition of the new batch of PEDOT:PSS. Lastly it is possible to attribute the difference in the response of the device to batch to batch reproducibility of the polymer and it is possible to state that the bi-exponential trend is not caused from the cell growth. Despite this different behaviour, the extracted parameter, as reported in literature [84] [86], are sensitive to cell layer changes.
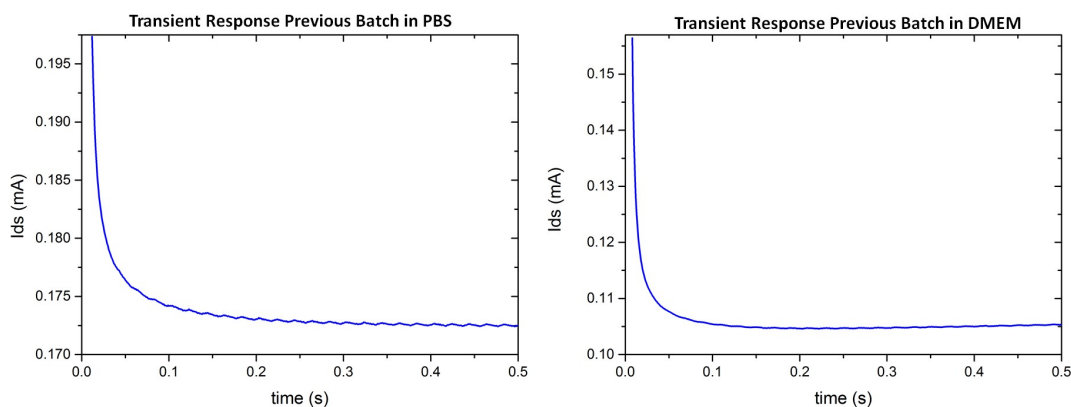
Figure 5.8: Faster response of OECT in PBS and in DMEM with previous batch of PEDO:PSS.

5.3 OECT Characterization

The first phase of the set-up calibration is the characterization of the device with the TE-OECT. To characterize the OECT two quantities are measured, the electronic time τ_e and the ionic time τ_i. The two parameter are measured as explain in Section 3.4.

5.3.1 Electronic Time

To measure the Electronic Time the source meter is set to deliver a constant gate current (I_g). This measurement is described by the Equation 3.12 and it is performed several times with different values of I_g. The Figure 5.9 shows the acquire signal.
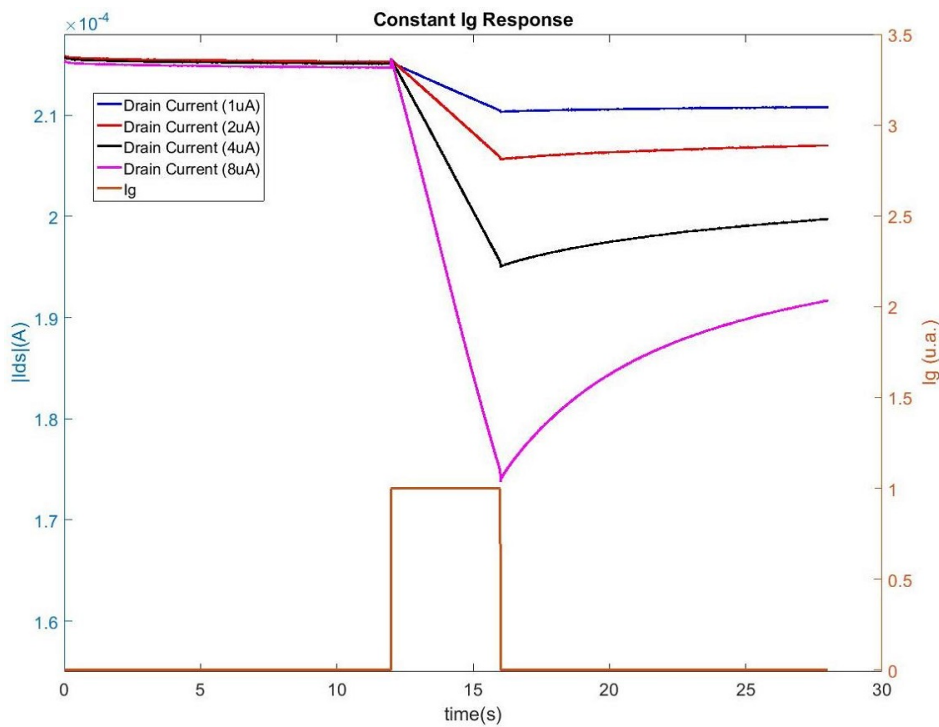
Figure 5.9: Measurement of I_d under a constant application of gate current plotted and analyzed with the Matlab custom program. The different drain current are determined by the left y axis (in cyan) while the gate current is referred to the orange y axis (on the right). All the measurements are performed with $V_d = 0.1\ V$

The central part of the signal is the linear response of the I_d and it can be fit with a linear function to obtain the electronic time τ_e. The Table 5.1 summarizes the obtained value. This results are consistent with the values presented in bibliography [77]. Indeed in their work Bernards and Malliaras evaluate a τ_e value equal to 0.5 s.

$I_g(\mu A)$	$\tau_e(s)$
$1\mu A$	0.371 ± 0.003
$2\mu A$	0.370 ± 0.003
$4\mu A$	0.38 ± 0.04
$8\mu A$	0.42 ± 0.04

Table 5.1: Electronic Time extracted by the constant I_g measurement. The τ_e values and the errors are calculated from four measurement performed with the same I_g.

5.3.2   Ionic Time

Because the ionic time is the figure of merit chosen to evaluate the cell growth, the starting value τ_i of our device is measured by two different techniques. This choice is made to ensure the relevance of the selected parameter after the formation of the cell layer. The first technique is the impedance measurement (described in Section 4.2.2), the τ_i is calculated as the equivalent circuit (remembering that $\tau_i = 1/RC$). The second is the transient response (Section 4.2.1) and the subsequent extraction of the ionic time via fitting. The Figure 5.10 shows the impedance measurement and the equivalent circuit obtained by the fit. The equivalent circuit of the interface channel-electrolyte is fitted as a contact resistance and two parallel of a resistance and a capacitance. The second is the equivalent of the interface channel-electrolyte while the first is the interface of everything is not channel, like the exposed gold electrode. Because the impedance measurement is performed connecting all the four channel of one OECT the values shown in the Figure must be corrected. The resistances values are 4 times greater while the capacitances are 4 times lower.

The transient response is elaborate as explained in Section 5.2. The obtained value is summarize in Table 5.2.

	Impedance Measurement	Transient Measurement
$\tau_i(s)$	3.021	2.207

Table 5.2: Ionic Time τ_i obtained by the two different methods.

5.4   Sterilization Techniques

To work in biological environment the sterility is mandatory. Since the cell buffer is particularly nutrious, it i easy that bacteria and microorganisms contaminate the culture. The described set-up is not disposable so it must be sterilised before each use. The OECT must be sterilised too so in this Section the influence of sterilisation on the device performance is studied. Three different type of sterilisation are considered:
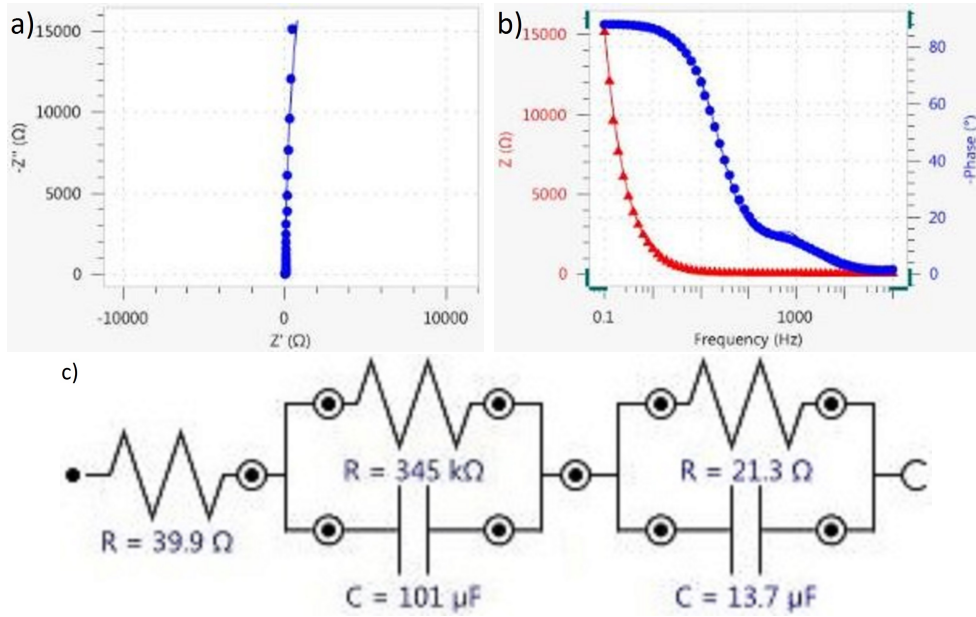
Figure 5.10: a) the Nynquist plot and (b) the Bode plot of the impedance measure of the device. (c) The equivalent circuit obtained by the fit.

30 *minutes* under UV light, $100\,\mu l$ of *EtOH* (70% *EtOH* and 30% H_2O) and a dry cycle of 20 *minutes* in autoclave. The effect of sterilisation is studied by two methods: measuring the change of the channel resistance and the change of the characteristic time. The Table 5.3 summarizes the obtained result.

	$\Delta R(\Omega)$	$\Delta\tau_i^0(s)$	$\Delta\tau_i^1(ms)$
EtOH	254.8 ± 65.2	0.1 ± 0.2	31 ± 58
UV	91.7 ± 18.7	0.1 ± 0.1	32 ± 43
Autoclave	304 ± 41.5		

Table 5.3: Parameters changes due to the three types of sterilisation.

The sterilisation process, used in the following experiments, is chosen after different observation. First of all the EtOH sterilisation produce delamination and detachment of the PEDOT:PSS channel from the glass. This is showed in the resistance value change. The autoclave process is a recent discovery (November 2016 [92]). To increase the confidence level of this process further experiments are planned in order to be sure the channel is not damaged in the process. Although the change in the transient time τ_i^0 and τ_i^1 are comparable with the EtOH and UV process, the smaller increase of the resistance value makes the UV process preferable. In fact lower is resistance values, bigger is the current change and a great current variation is easy to detect. Moreover in

the UV process it is possible to sterilised all devices and all the parts of the TE-OECT at the same time. The UV enlightenment is the process used in the following experiments.

5.5   Cell Viability Assay

The last test concerns the cell viability, it is important to understand if the TE-OECT is comparable to the commonly used commercial multiwell. Cell viability is determined by the MTT assay (see Section 4.3.2) used on a fibroblasts cell-line (NIH-3T3) growth in common multiwell and in TE-OECT. The comparison is made between a 24 multiwell, the TE-OECT assembled with laboratory glass and the TE-OECT assembled with the device. Unlike what is said in the Section 4.3.2 the 96 multiwell is replaced with a 24 multiwell in order to have a comparison between wells with same geometrical dimensions.

The multiwell is used as a reference for cell viability, the average value of absorbance for the multiwell is equal to 1.18. It is possible to fix equal to 100 % the average value of absorbance in the multiwell. The absorbance average value obtained from the TE-OECT assembled with glass is equal to 1.12, it is possible to obtain its percentage value equal to 94.97 % and the absorbance average value obtained from the TE-OECT assembled with OECT is equal to 0.96, it is possible to obtain its percentage value equal to 81.54 %. Generally a value higher than 60 % indicates a good viability of the cells while a value higher than 80 % returns an excellent cell viability in the set-up. The Figure 5.11 shows this excellent result. The error on the average value is obtained as the standard deviation.
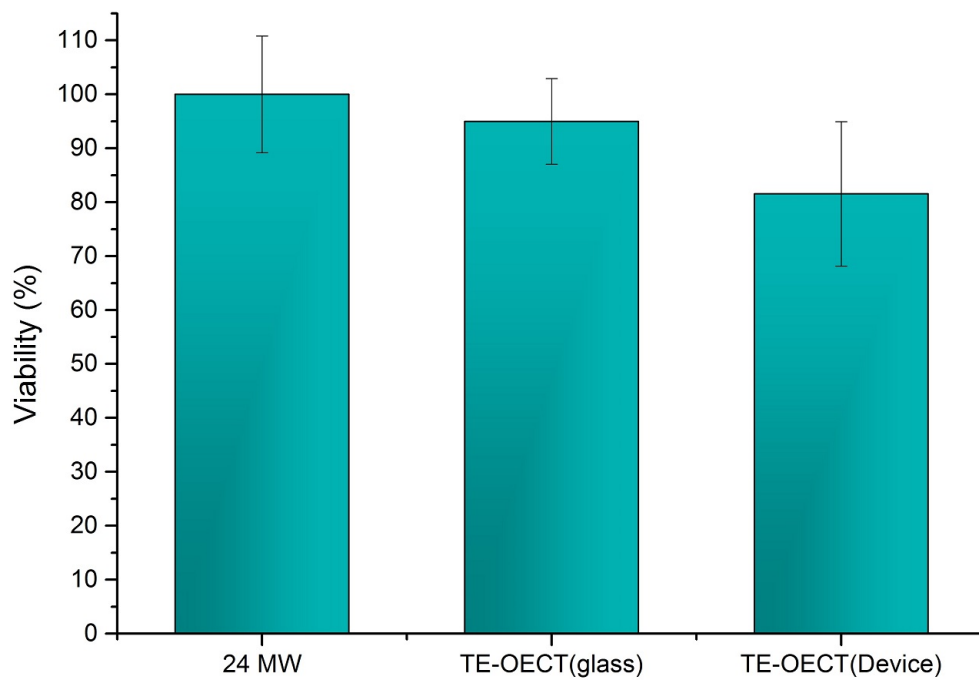
Figure 5.11: Histogram of the studied viability of the cell with its error.

Chapter 6

Cell Layer Monitoring

Images, analyzes and measurements of cellular tissues are performed at the laboratories, supervised by Francesco Valle, of the research group *Nanotechnology of Multifunctional Materials* (NMM) directed by Massimo Cavallini. This is a group of Bologna *CNR* (Consiglio Nazionale delle Ricerche) and in particular of the *Institute for the study of nanstructured materials* (ISMN). A great support to this work is given by the researcher Marianna Barbarinaldo, who is the supervisor for all the biological analysis. As previously said (Section 4.3.1), the cell lines used in this work are the *HeLa* and the *NIH-3T3* (Section 2.2). The HeLa cell line is chosen due to its great resistance and its easy of growth, this line is perfect to evaluate the technical feasibility of the experimental tests. The first two Section of this chapter focus on the measured performed on the two used cell-lines while the third Section develop a comparison between the figure of merit (response time of OECT) extracted from the electrical measure.

6.1 HeLa Cells on TE-OECT

The level of HeLa coverage is evaluated, optically and electrically, in four time, before the seeding (0 *h*), four hours (4 *h*), twelve hours (12 *h*) and twenty-four hours (24 *h*) after the seeding. The electrical measure, performed at 0 *h*, is used as reference for evaluate the change in the transient time of the OECT and it is performed after the calibration process. The TE-OECT is used as explained in Figure 6.1, five well are seeded with the same cell concentration equal to 40.000 $Cells/cm^2$. The sixth well (the device 3) is leaved without cells to monitor the potential degradation of OECTs. The Figure 6.2 shows the images acquired by the optical microscope throughout the cell growth.

This images are provided on the device 4 and prove the simultaneous electrical and optical acquisition. It is possible to observe that 4 hours after the seeding the cell are still rounded, this means that they are not yet adherent to the substrate. After 24 hours the cell shape is changed as well as their number. It is possible to observe empty areas which
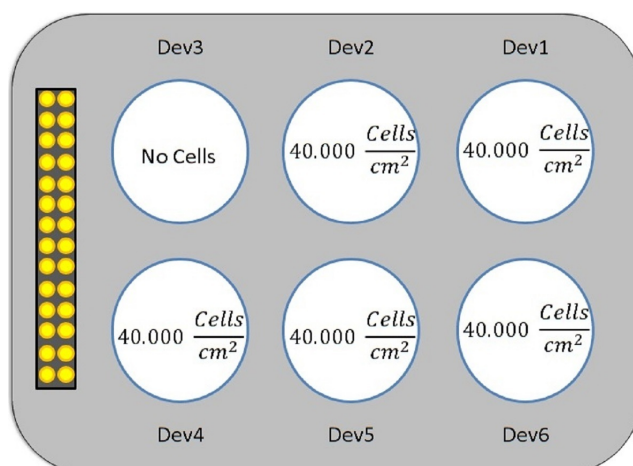
Figure 6.1: Schematic diagram of the HeLa seeding performed on the TE-OECT.
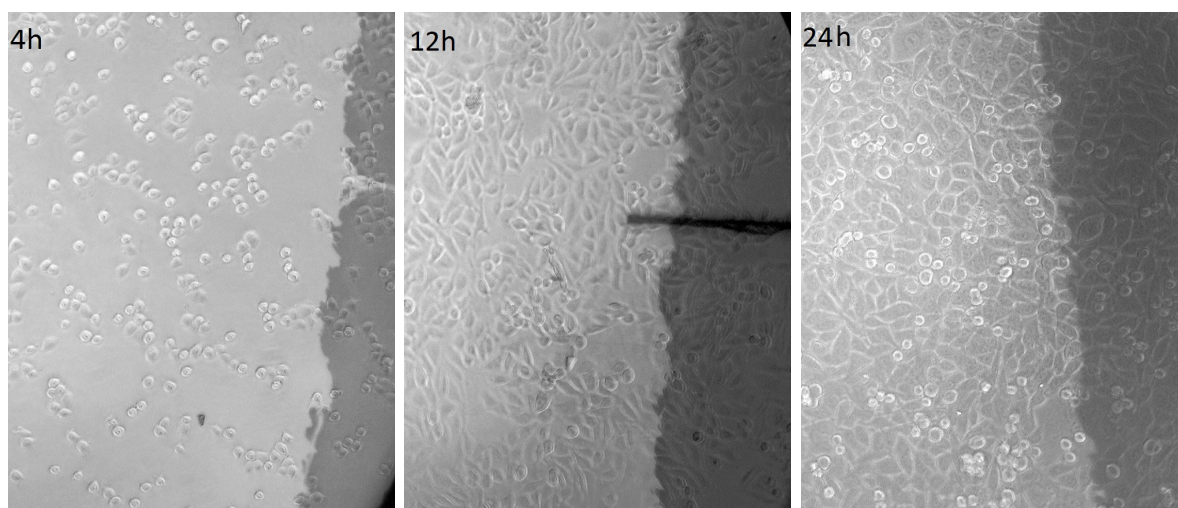
Figure 6.2: Images of HeLa cells growing on the device 4 at different incubation times (4h on the left, 12h on the center and 24h on the right) after seeding. The images are taken with the optical microscope with a 20X magnification.

outline that the confluence is not reached. Lastly after 48 hours the confluence is reached and it is possible to observe some round-shaped cells which probably are detaching due to the contact inhibition. The observed area is the PEDOT:PSS channel close the Cr/Au electrode in dark grey. Moreover the device 4 and 6 are used to acquire fluorescence images after the cells have reached the convergence. This fluorescence images are shown in Figure 6.3. The three remaining devices (1, 2 and 5) are used to monitoring the layer detachment.
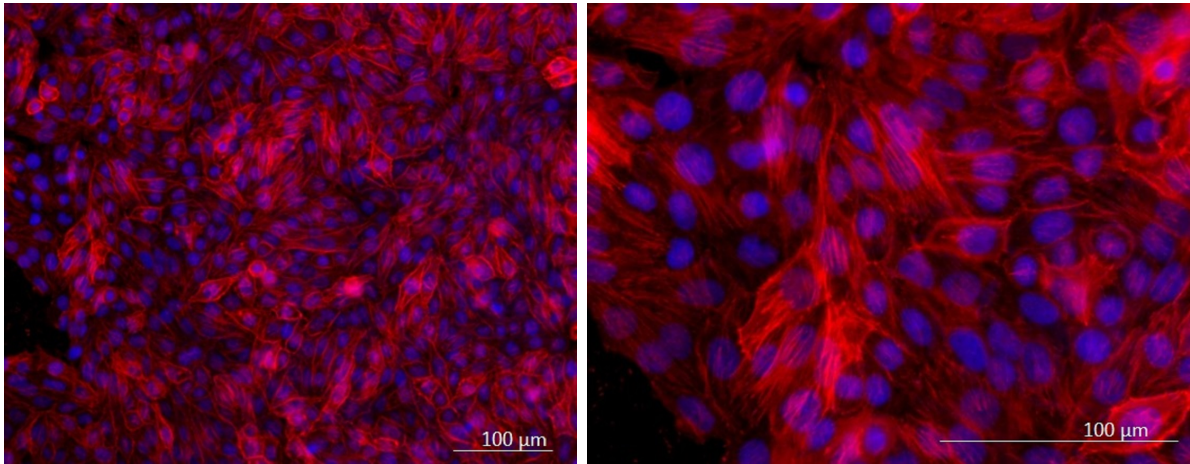
Figure 6.3: Fluorescence images of HeLa cells. As previously discussed in Section 4.3.3 it is possible to see the nuclei in blue and the actin filaments in red. The cells show no signs of suffering despite they are grown in the device. The images are taken with the fluorescence microscope with a 20X (on the left) and 40X (on the right) magnification.

6.1.1 Electrical Monitoring of Layer Forming

The electrical transient response, acquired as explained in Section 4.2.1, are shown in Figure 6.4. The Figure shows the fourth pulse of the measurement acquired at different time after seeding, indeed it shows a comparison between the device 3 in Figure 6.4.a (monitoring without cell growth) and the device 1 in Figure 6.4.b. In this Figure the characteristic time seems to increase in different measurements moments, this can be observed in the different trend of the percentage variation of the drain current in Figure 6.4.b. Comparing for example the blue and the green lines, is easy to observe that the decay is changing during the cell growth.

To emphasize this change the transient time are extracted in agreement with Section 5.2. Figure 6.5 is the graphic of the trend of the response time τ_i^0 and τ_i^1, it is possible to see easily the expected trend which confirms the previous observation (Figure 6.4).

6.1.2 Electrical Monitoring of Detachment

The second step is the evaluation of cell detachment, this effect is obtained due to the Trypsin-EDTA (Section 2.4).

The Trypsin is used on device 1, 2 and 5, it is $5X$ diluted in DMEM instead of in physiological solution. This choice is made to keep the same electrolyte and do not change the condition of the electrical measurement because, as discussed in Chapter 3, the number of ions determine the OECT response. The effectiveness of the enzyme diluted in DMEM was previously tested. It is observed that also in this condition the

a)

b)
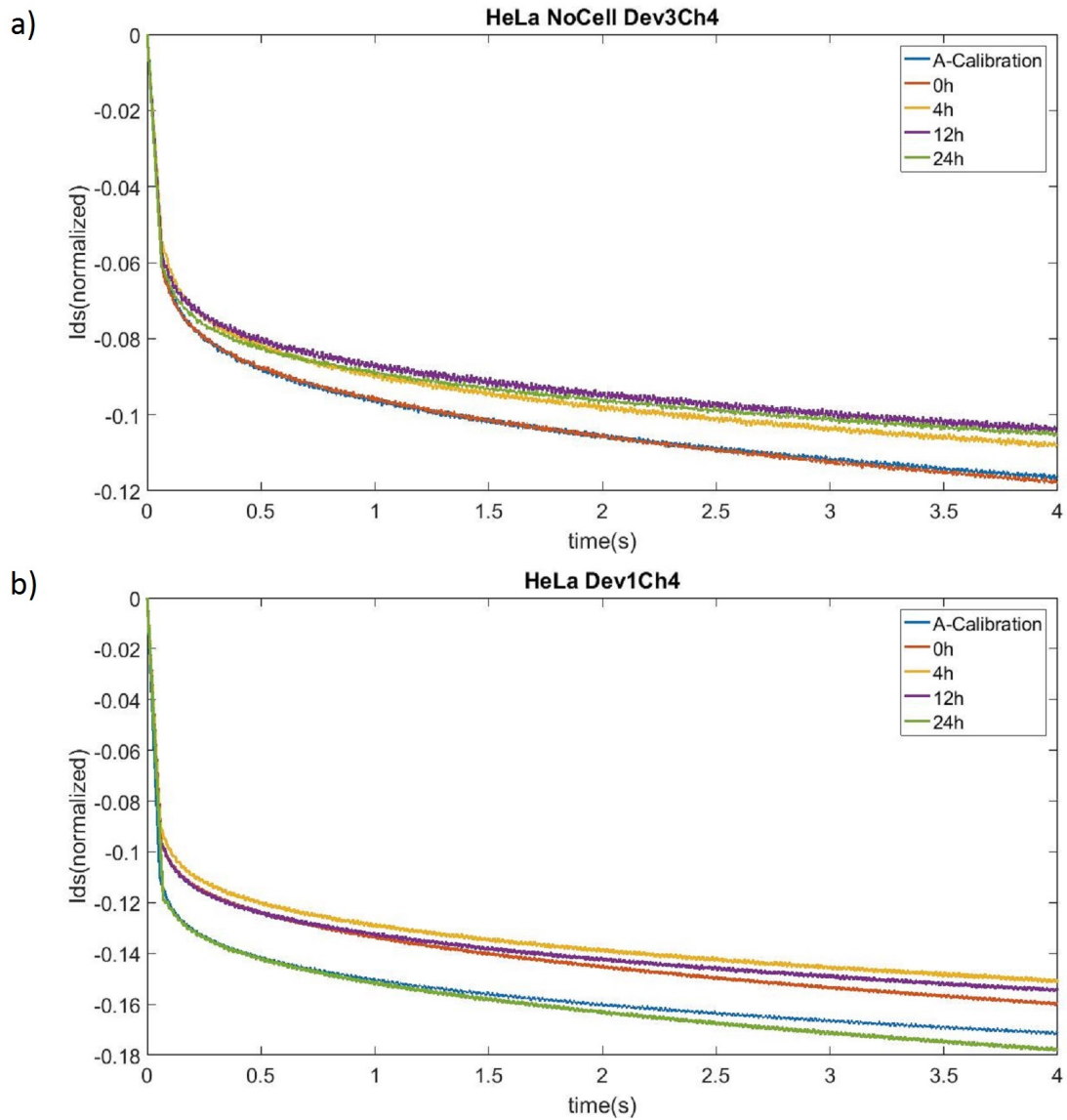
Figure 6.4: Transient response of two different device in HeLa culture. (a) The graphic shows the response of the device 3 (no cell). It is possible to observe the percentage change of the response time. The decay time is comparable at different time. (b) The graphic is the response of device 1. In this case the characteristic time seems to increase in time.

enzyme acts, but longer times are request to obtain a complete detachment (10 minutes instead the 5 minutes suggested by the protocol). All the measurement are performed in the incubator to keep the physiological condition, this allow the Trypsin to act in the best condition.
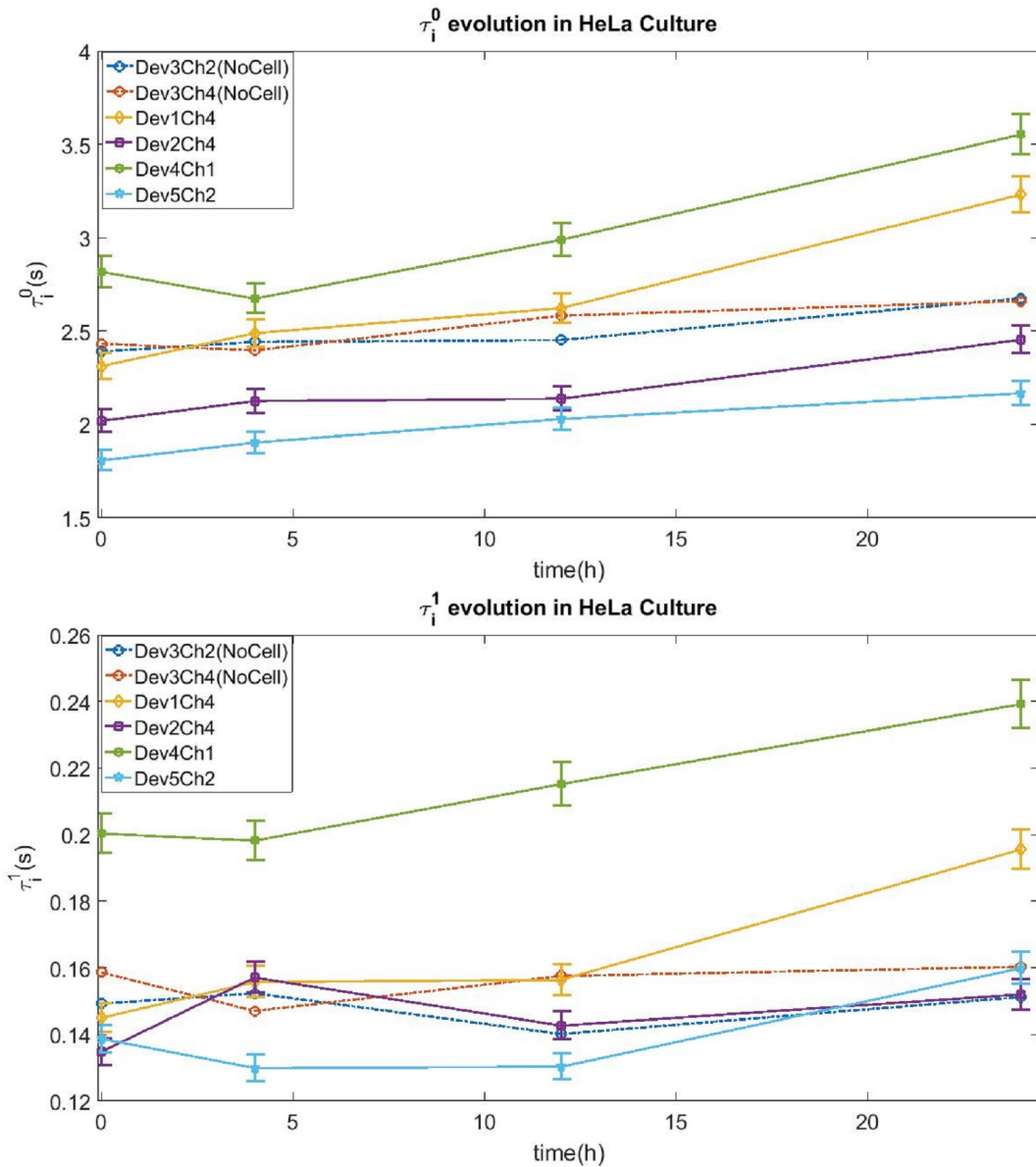
Figure 6.5: Evolution of response time τ_i^0 and τ_i^1 as function of hours after seeding in HeLa culture. The two dashed lines are the devices with no cell. The error bar is obtained as the absolute error, equal to the 5% as explained in Section 5.2.

To electrically evaluate this effect two kind of measurement are performed, the first is the analysis of the transient response before the treatment and 10 minutes after the addition of the Trypsin. This measurement is used evaluate the change of the response time after the complete detachment of the cell coverage. The results of this measurement

are summarize in Table 6.1. All of them outline a decrease of the response time as expected.

Device	$\Delta\tau_i^0(s)$	$\Delta\tau_i^1(ms)$
Dev3Ch2 (No Cell)	0.178 ± 0.005	7.8 ± 0.2
Dev3Ch4 (No Cell)	0.157 ± 0.005	10.8 ± 0.3
Dev1Ch1	0.45 ± 0.01	27.8 ± 0.8
Dev1Ch4	0.51 ± 0.02	31.1 ± 0.9
Dev2Ch4	0.71 ± 0.02	29.9 ± 0.9
Dev5Ch2	0.41 ± 0.01	76 ± 2

Table 6.1: Changes of the transient time in HeLa culture after the Trypsin treatment. All the devices decrease the response time.

The second measurement is a quick reply of a single pulse and it is called *Live Tripsyn*. The idea of this measurement is to monitoring the change of the transient time during all the 10 minutes throughout which the Trypsin is acting. This evaluation is show in the Figure 6.7.

Optically the devices are observed before and after the 10 minutes to be sure of the detachment of the layer. Figure 6.6 shows a channel of the device 2 before and after the Trypsin treatment.
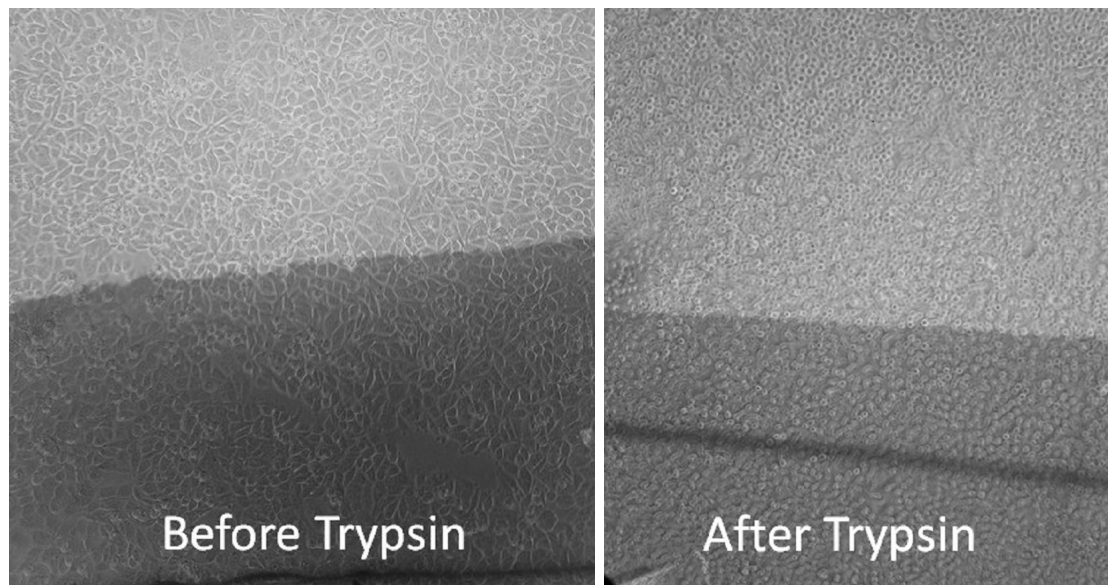
Figure 6.6: Effect of Trypsin-EDTA on HeLa. On the left a channel of the device 2 before the Trypsin treatment and on the right the same channel after the detachment. The rounded shape of the cells is indicative of the detachment. The images are taken with the optical microscope with a 20X magnification.
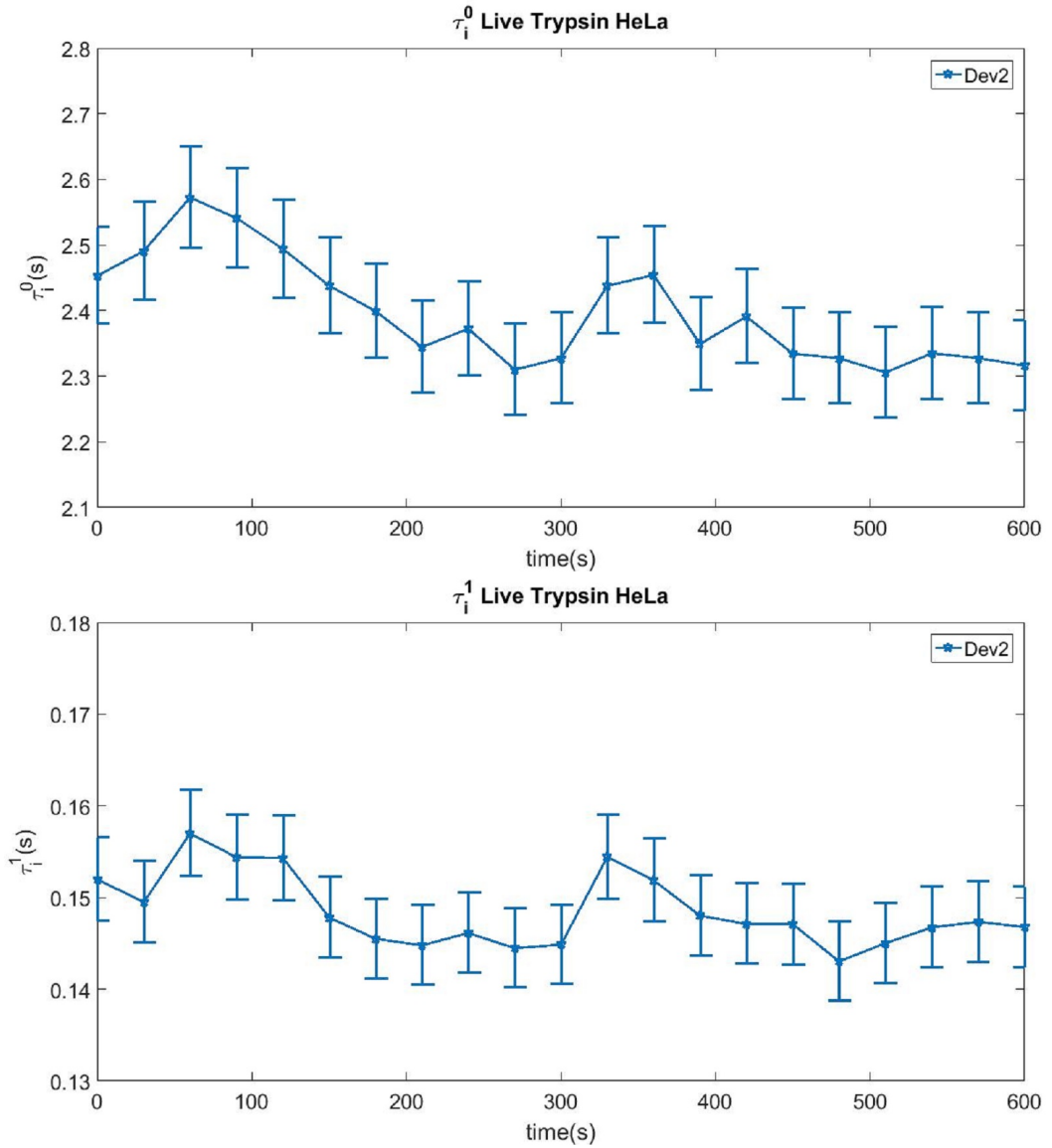
Figure 6.7: Evolution of response time τ_i^0 and τ_i^1 in HeLa culture as function of time after the adding of Trypsin. The error bar is obtained as the absolute error, equal to the 5% as explained in Section 5.2.

6.2 NIH-3T3 Cells on TE-OECT

Cell growth and detachment are repeated with a second cell line, the NIH-3T3. Also in this case the optical and electrical measurements are performed simultaneously but a greater number of points are electrical acquired. This choice is done to increase the confidence about the response time changes. A measurement is take at 0 (before the seeding), 4, 5 hours after seeding; then four points are taken between 24 and 29 hours after seeding and three points between 50 and 54 hours. The TE-OECT is composed as shown in Figure 6.8. All the wells are seeded with a concentration of 35.000 $Cells/cm^2$, the concentration is decreased, compared to HeLa, because the NIH-3T3 are bigger. Three devices (device 1, 2 and 3) are used to take fluorescence images while the remaining three are treated with Trypsin after the achievement of the confluence.
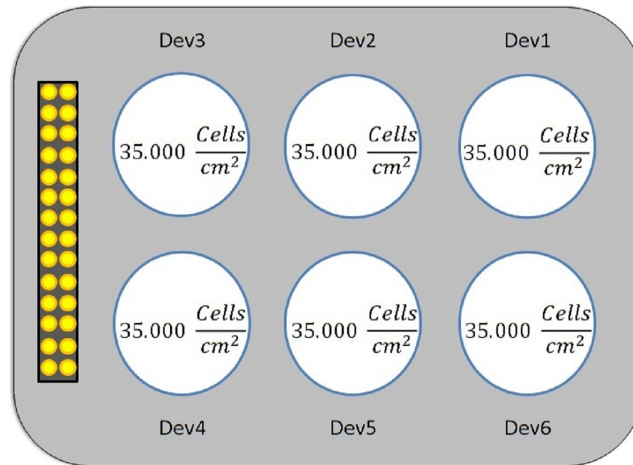
Figure 6.8: Schematic diagram of the NIH-3T3 seeding performed on the TE-OECT.

The image shows in Figure 6.9 are acquired throughout the cell growth while the Figure 6.10 shows the fluorescence images of NIH-3T3 grown on the device 2. It is possible to observe that 4 hours after the seeding most of the cell are still rounded, this means that they are not yet adherent to the substrate. Instead some cells are already taking their final form that is an elongated shape directed towards neighboring cells. After 24 hours the cell shape is changed as well as their number. It is possible to observe empty areas which outline that the confluence is not reached. Lastly after 48 hours the confluence is almost reached and no round-shaped cells, detaching due to the contact inhibition, are visible. The observed area is the PEDOT:PSS channel close the Cr/Au electrode in dark grey.
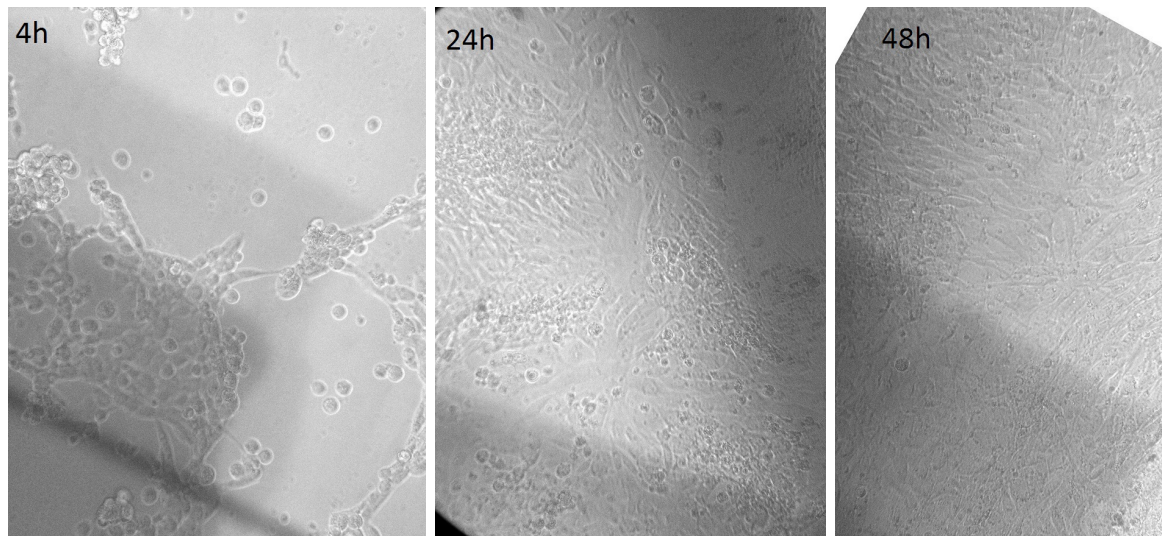
Figure 6.9: Images of NIH-3T3 cells growing on the device 4 at different incubation times (4h on the left, 12h on the center and 24h on the right) after seeding. after seeding. The images are taken with the optical microscope with a 20X magnification.
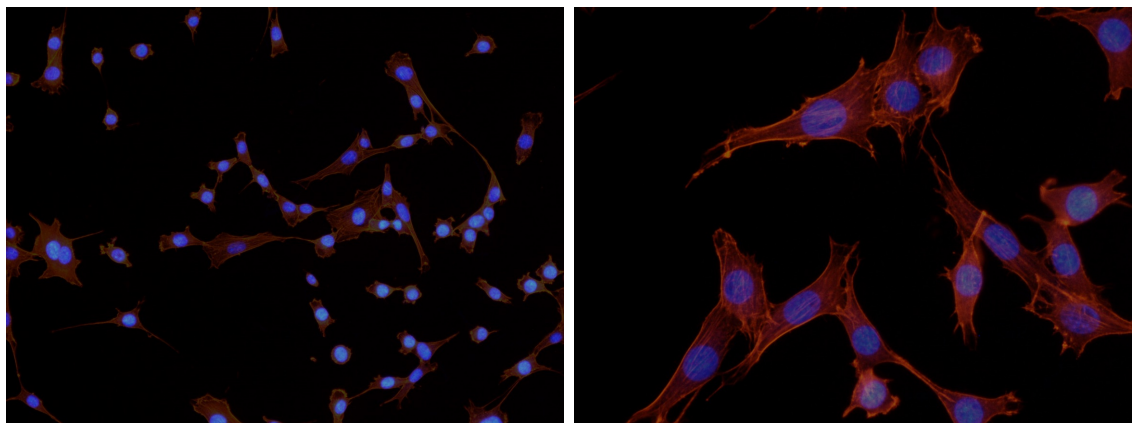
Figure 6.10: Fluorescence images of NIH-3T3 cells. The images are taken with the fluorescence microscope with a 20X (on the left) and 40X (on the right) magnification.

6.2.1   Electrical Monitoring of Layer Forming

Following the same consideration of the Section 6.1.1 the layer forming is monitored. As expected the NIH-3T3 reproductive rate is slower than the HeLa so the growth time is extended up to 50 hours. The changes of the transient time are reported in the graphs in Figure 6.12. As expected the response time increase with the increasing of the cell covering. Another important observation concerns the measurements performed several

minutes from each other. A high reproducibility of this measurement is expected because, lasting the cell cycle 24 hours, no changes of the biological system are expected. The Figure 6.11 shows 5 points acquired between 24 and 30 hours after seeding. Optically it is possible to observe that the cell growth is not influenced by the electrical measurement and electrically the devices do not show deterioration in its electrical performance.
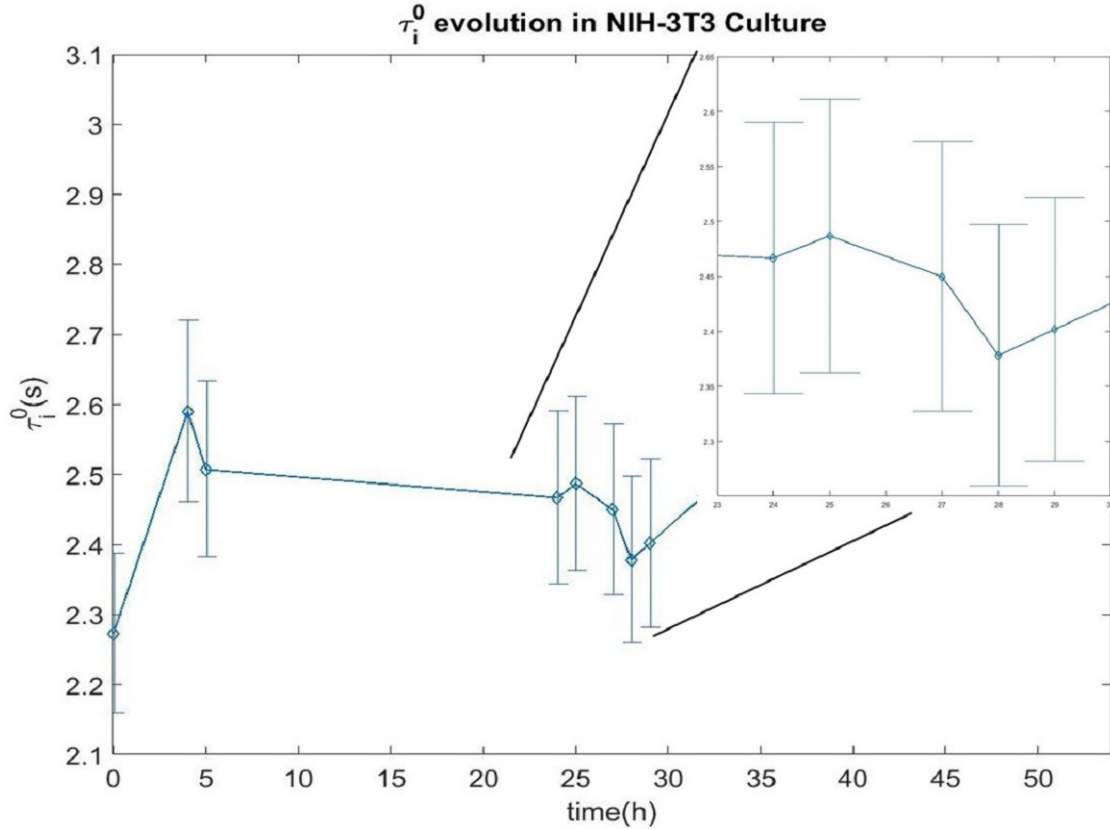
Figure 6.11: High reproducibility of the measured observed in 5 close temporal moments. The error bar is obtained as the absolute error, equal to the 5% as explained in Section 5.2.

In the Figure it is possible to observe a theoretically anomalous trend of the channel 1 and 3 of the device 6. The unexpected decreasing observed between 4 and 24 hours is due to a detachment of a piece of cell layer in the medium exchange operation. But confirming the good cell viability the growth and the increasing of the response time resumes with the expected trend.

6.2.2 Electrical Monitoring of Detachment

The detachment of the NIH-3T3 is monitored as explained in Section 6.1.2. A faster detachment process is expected compare to that seen for the HeLa. The process is
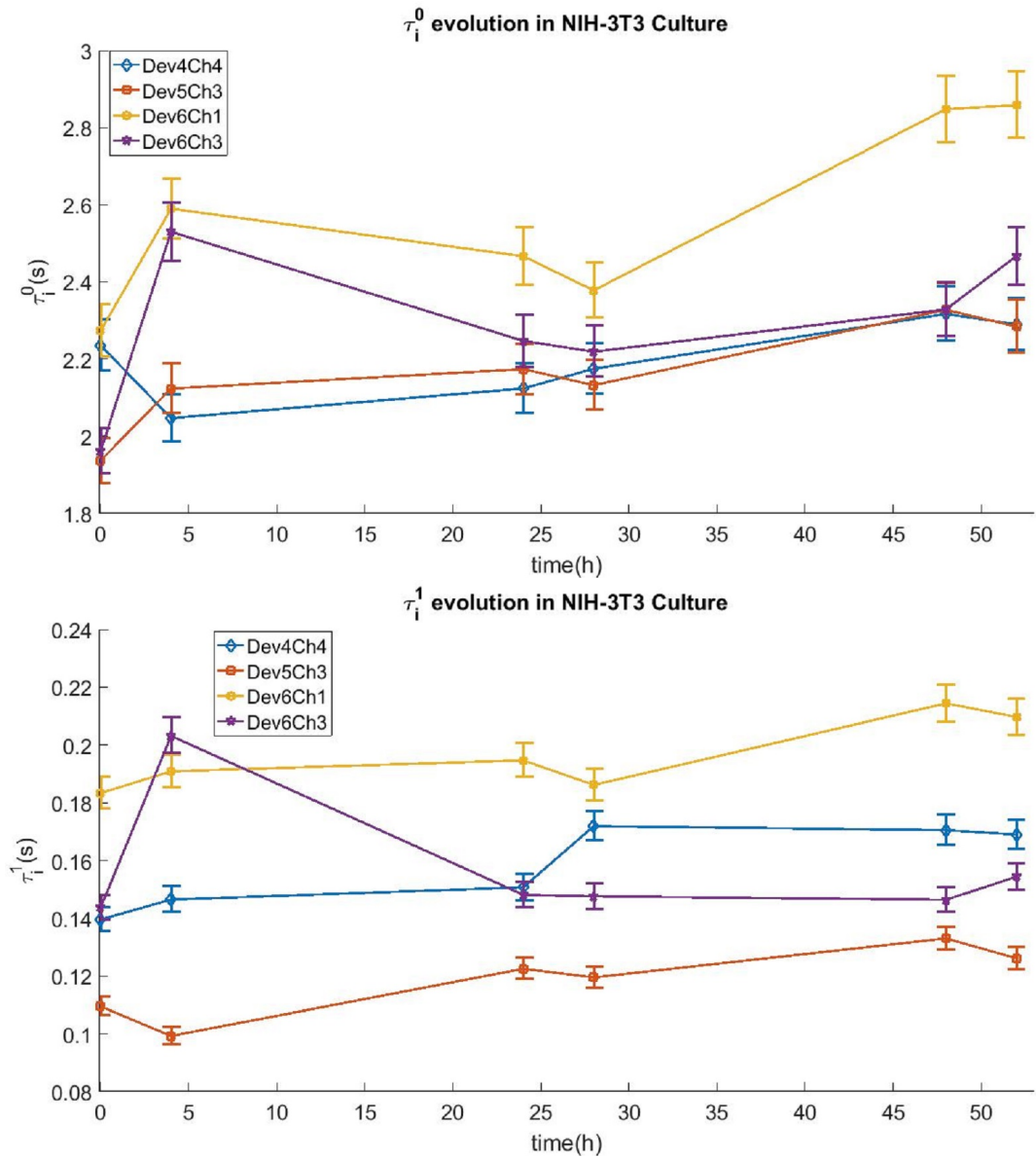
Figure 6.12: Evolution of response time τ_i^0 and τ_i^1 as function of hours after seeding in NIH-3T3 culture. The error bar is obtained as the absolute error, equal to the 5% as explained in Section 5.2.

faster because the Trypsin cuts the Focal Adhesion with the substrate (see Section 2.1 and Figure 2.1) and fibroblasts express more Focal Adhesion than the HeLa. For this reason the Trypsin concentration is decreased to 1X to be sure to observe the detachment otherwise too fast. Despite the Trypsin concentration in DMEM is lower, the complete detachment process is lasted about 3 minutes. The monitoring of detachment is lasted

10 minutes performing the same measures explained in Section 6.1.2. The Table 6.2 summarizes the change of the transient time after the Trypsin treatment and Figure 6.14 shows the *Live Trypsin* measurement performed on the device 6. Figure 6.13 shows the device 4 before and after the detachment. As expected all the τ values decrease with time and reaches values that, taking into account the degradation of the PEDOT:PSS, are comparable with the initial values.

Device	$\Delta\tau_i^0(s)$	$\Delta\tau_i^1(ms)$
Dev6Ch4	0.271 ± 0.008	13.3 ± 0.4
Dev4Ch1	0.50 ± 0.02	20.5 ± 0.6
Dev4Ch2	0.38 ± 0.01	13.9 ± 0.4
Dev4Ch3	0.271 ± 0.008	38 ± 1

Table 6.2: Changes of the transient time in NIH-3T3 culture after the Trypsin treatment. All the devices decrease the response time.
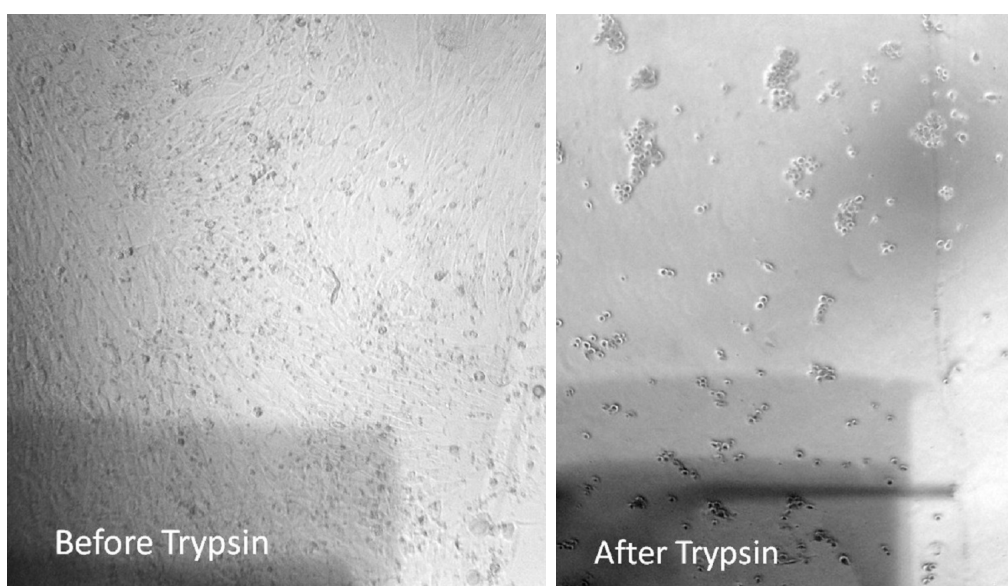
Figure 6.13: Effect of Trypsin-EDTA on NIH-3T3. On the left a channel of the device 2 before the Trypsin treatment and on the right the same channel after the detachment. The rounded shape of the cells is indicative of the detachment. The images are taken with the optical microscope with a 20X magnification.
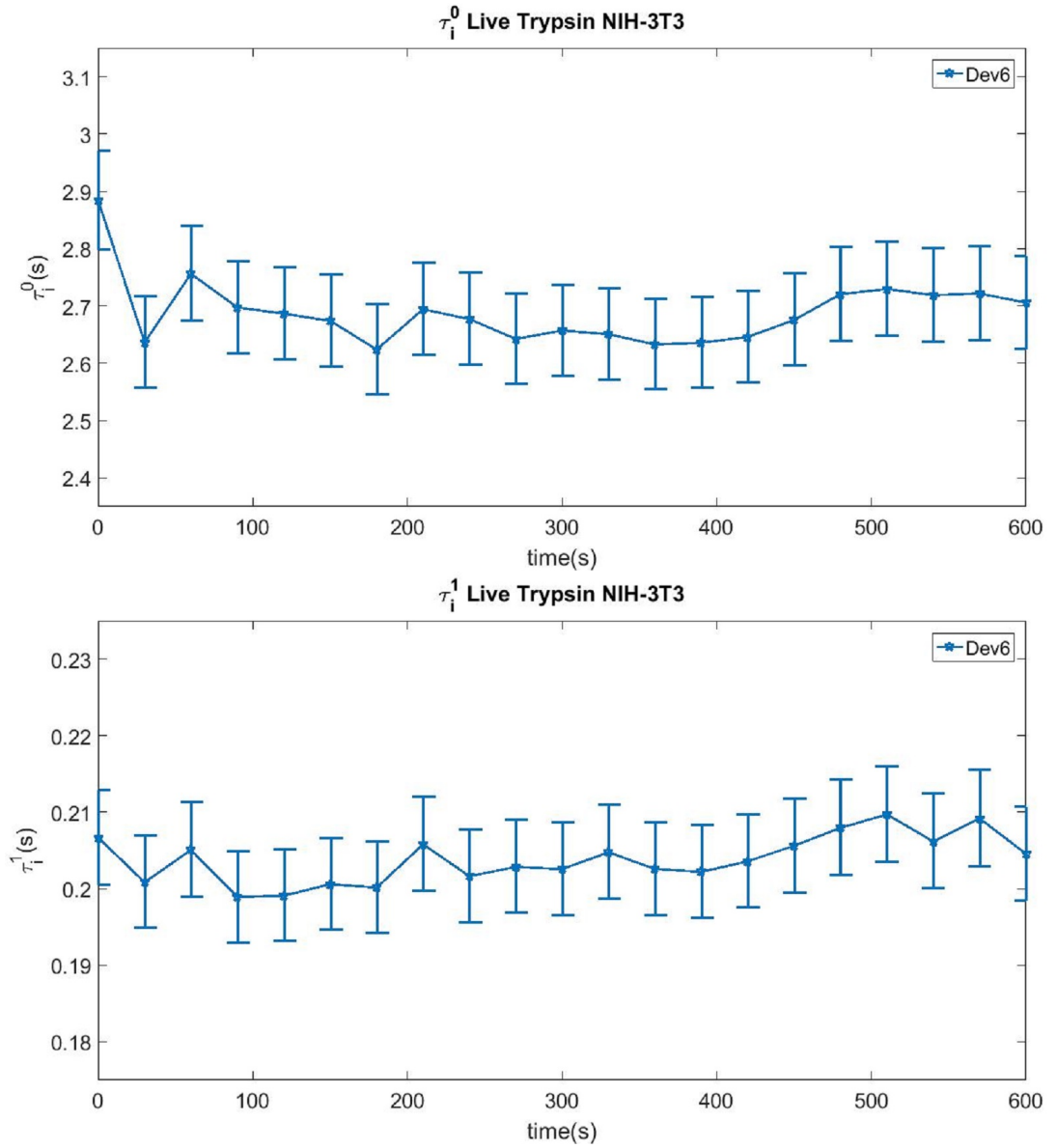
Figure 6.14: Evolution of response time τ_i^0 and τ_i^1 in NIH-3T3 culture as function of time after the adding of Trypsin. The error bar is obtained as the absolute error, equal to the $5\,\%$ as explained in Section 5.2.

6.3 Interpretation and Comparison

First of all it is important to make a consideration about extracted response timeτ_i^0 and τ_i^1. Because the values of τ_i^0 changes with the cell growth, it is possible to correlate this parameter with it. The trend of τ_i^0 are consistent with the observation by optical microscope in the growing and detaching monitoring for both cell-lines. This interpretation is confirmed by the comparison between device with and without cells. Both in growth and detachment monitoring the variations of the τ_i^0 are consistent with the 5 % which is the absolute error.

Observing the changes of τ_i^1, it is possible to obtain a different conclusion. Despite this parameter seems to change during the cell growth, there is no significant changes in the *Live Trypsin* measurements. It is possible to correlate this parameter with a PEDOT:PSS degradation which is visible on a long time scale (in accordance with [84]), thus explaining its variation in growth measurements and the absence of significant changes in the *Live Trypsin* measurement.

From Figure 6.5 and 6.12 it is possible to evaluate the changes of τ_i^0. In both cell-lines the lower changes of this transient time is about $0.35\,s$ while the same parameter, in a device monitored without cell, shows a change lower than $0.2\,s$.

The differences in the response time variation make consistent the assumption on the real monitoring of the cover forming. This change is in accordance with the work of Ramuz *et al.* [87] in which the covering is monitored with the transconductance while is in contrast with their previously work [84] in which the HeLa covering don't produce τ variation (as it is previously described in Section 3.5).

Another observation concerns the possible deterioration of the PEDOT:PSS channel by the action of Trypsin. Observing the values reported in Table 6.1, it is possible to correlate this change with the error, excluding an interaction between Trypsin and PEDO:PSS. Moreover a *Live Trypsin* measurement is performed on a device without cell. The Figure 6.15 shows a comparison between the *Live Trypsin* on the device without cell and the *Live Trypsin* on the two cell-lines. It possible to observe that the τ_i^0 variations is equal to $0.1\,s$ and it is consistent with the 5 % absolute error. The theory about the τ_i^1 changes is confirmed also in this measurement, indeed is not possible to observe significant variation in the measurement performed on cell detachment compared to the no cell measurement.

The second evaluation is performed on the detachment of cell layer. This evaluation is performed by the Owens research group [84] on a different cell-line, the MDCK-I line-cell. They electrically measure a complete detachment with 1X Trypsin concentration in several minutes. As shown in Figure 6.16 this observation is in agreement with the acquired data, in particular with the NIH-3T3 detachment time.

Comparing the two studied covering the detachment time of NIH-3T3 is shorter than of the HeLa as expected. The first is about 3 minutes while the second is about 5 minutes. Also in this measurement is possible to observe that the time response in NIH-3T3 culture do not show a higher variation compared to HeLa culture. In both lines it is

possible to evaluate the beginning of the detachment before the optical analysis, indeed in HeLa culture the detachment can not be optically observed before 5 minutes while the electrical monitoring is able to sens it already during the second minute. It is possible to make the same consideration for the NIH-3T3 line, in this case the electrical monitoring is able to detect it already during the first minute while the optical observation can not be made before 3 minutes.
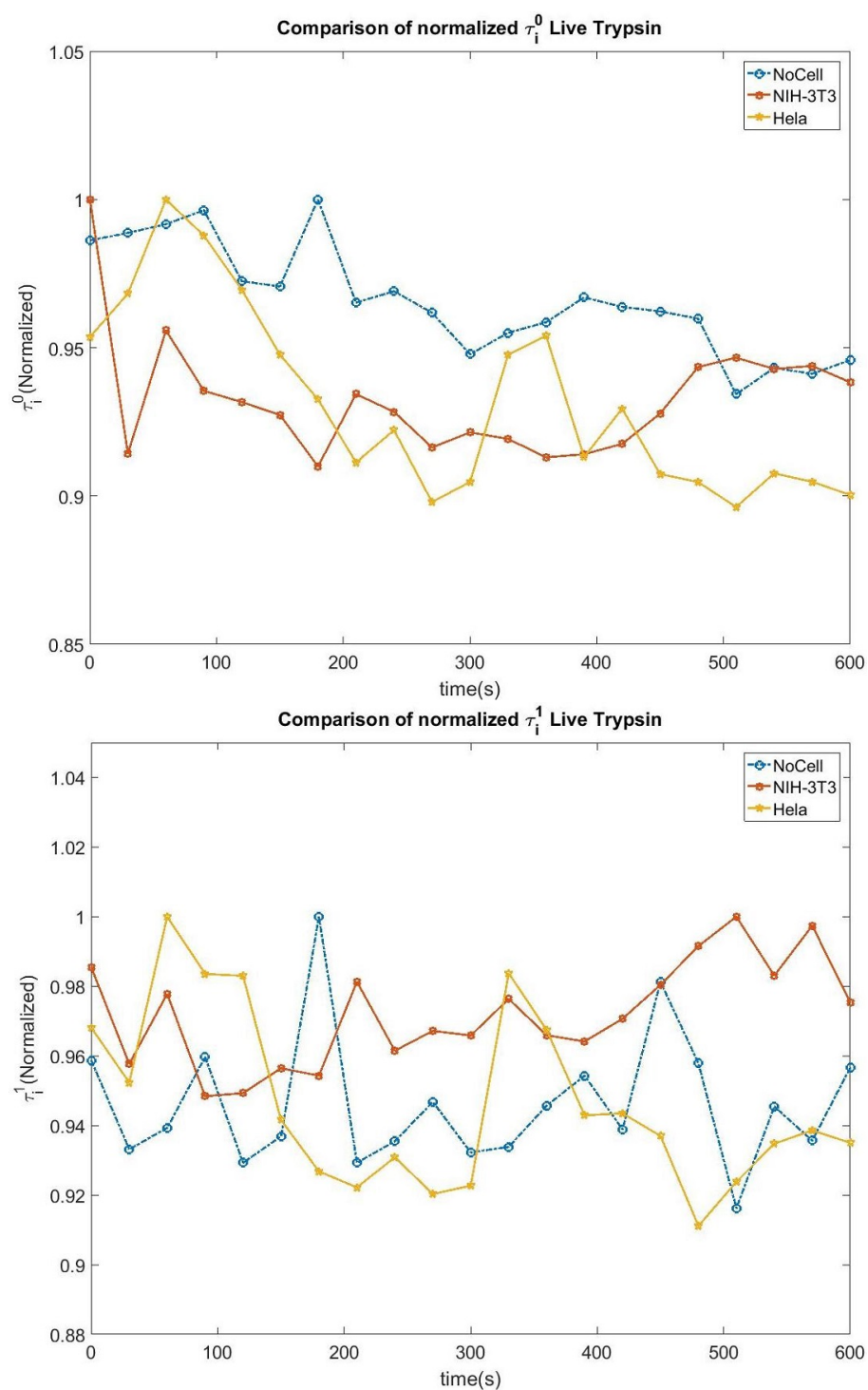
Figure 6.15: The *Live Trypsin* measurement performed on a cell without cell, on the HeLa detachment and on the NIH-3T3 detachment.
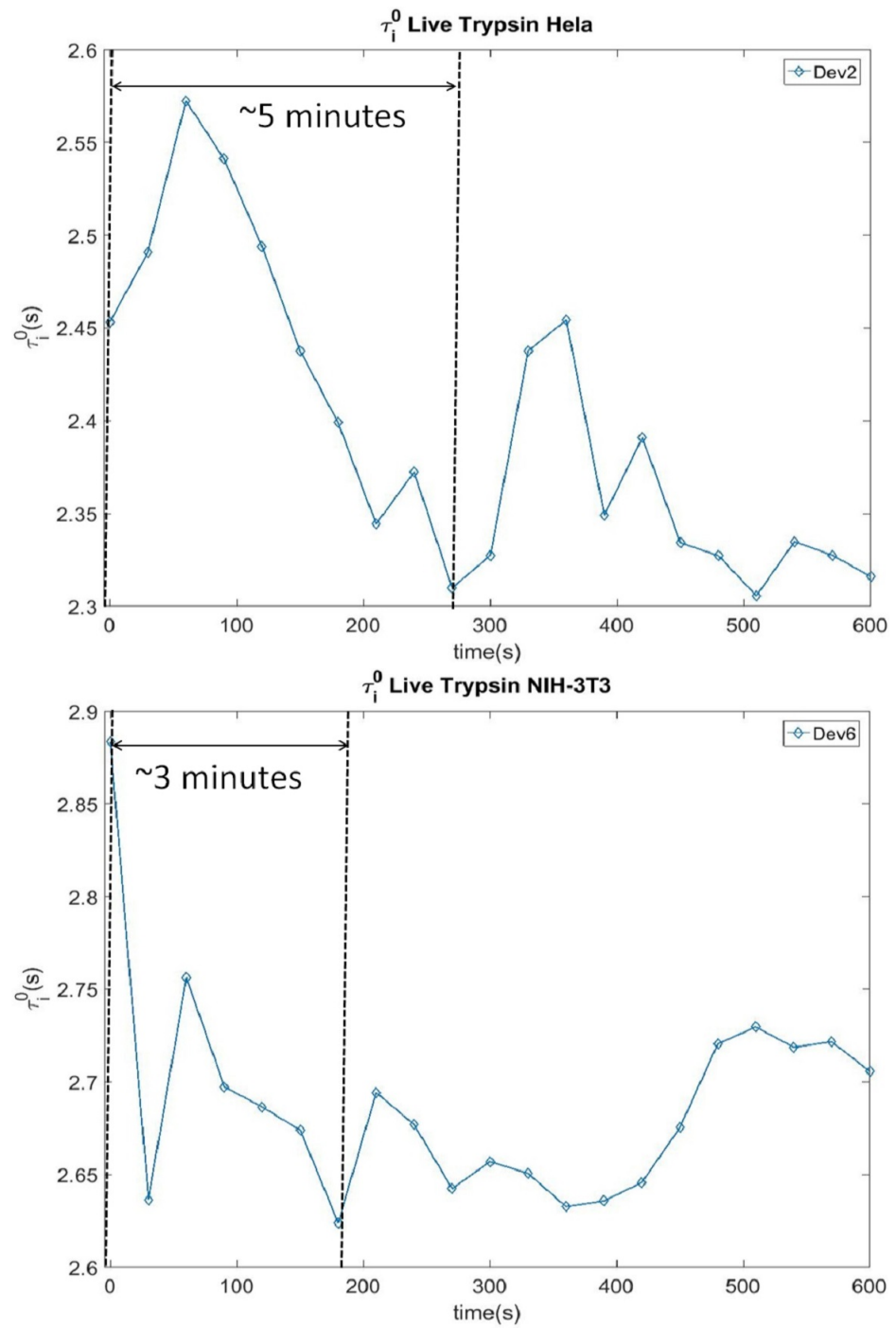
Figure 6.16: A comparison between the detachment time in the the used cell-lines.

Conclusion and Future Work

This work can be insert in the Bioelectronics field in order to realize a compact and sensitive set-up that is able to monitor the formation and the detachment of cell covering and barrier. The sensing element of the set-up is the OECT that is a transistor realized with a PEDOT:PSS channel and gold electrode immersed in an electrolyte. This device has the ability to transduce ionic into electronic signals and vice versa and, thanks to its biocompatibility, allows to bridge the gap between organic system and electronic worlds. The formation of the cell layer has to be performed inside an incubator in order to maintain the physiological conditions. This measurement became possible with the development of the experimental set-up TE-OECT. This is realized satisfying the constrains on the sterility, the dimensions and the biocompatibility. Moreover a custom software, developed in Matlab, is realised to analyzed the acquired measurements.

The TE-OECT is tested with two different lines (HeLa and NIH-3T3). A high viability has been demonstrated ($> 80\,\%$) for NIH-3T3 cells growth directly over the device demonstrating the biocompatibility of the TE-OECT.

Observing the results it is possible to say that:

- The extracted parameter τ_i^0 increase during the cell growth;

- The response time τ_i^0 decrease after the detachment of the cells.

The experiments confirms the hypothesis about the screening effect of the cell layer. The studied coverage decreases the ionic current flowing from the gate electrode into the polymer channel. This effect is visible in the increase of the response time τ_i^0 and this variations validate the idea of using the OECT to monitor the layer forming. Moreover a statistical repetition of this experiments can be used to create a match between the confluence level and the response time τ_i^0 in order to obtain an evaluation method of the confluence which is independent from the optical subjective measurements.

A great advantage of this method is the possibility to evaluate the integrity of the cell layer in physiological condition (controlled temperature, CO_2 and humidity) without the need to bring the samples under the microscope, such a method can be used for the evaluation of the action of pathogens in particular condition. Moreover the electrical evaluation represents an simple method to live monitor the cells detachment that otherwise can be observed only with complex and expensive set-up.

Although the used cell-lines are barrier forming, the experimental results are satisfying despite the difficulty of assessing cell layer that do not form Tight junctions.

The results presented in this thesis can be used as starting point for other evaluations. First of all it would be possible to monitor other cell-lines, such as Caco-2 or MDCK, which form Tight junctions in order to investigate the barrier properties.

Another future work concerns the test of different detachment or toxic agent. Assess the sensitivity of this methos to different toxic agents allows to count it as an alternative in the field of toxicology.

Lastly a further improvement of the TE-OECT would be the fabrication of a multiplexing circuit and a new version of the custom program which allow the automatic measurement of all the 24 channel of the set-up continuously during all the days of monitoring. Currently a first test of multiplexing measurements on 4 channel and a first project of the multiplexing circuit for all the 24 channel is realized.

List of Figures

List of Tables

Bibliography

[1] G. Malliaras and R. Friend - *An Organic Electronics Primer* - Phys. Today. (2005, 58(5), 53)

[2] M.Berggren and A.Richter-Dahlfors - *Organic Bioelectronics* - Adv. Mater. (2007, 19, 3201-3213)

[3] R.M.Owens and G.Malliaras - *Organic Electronics at the Interface with Biology* - MRS Bulletin (2010, 35, 449-456)

[4] G.Malliaras - *Organic bioelectronics: A new era for organic electronics* - Biochim. Biophys. Acta (2013, 1830, 4286-4287)

[5] J. Rivany, R.M.Owens and G.Malliaras - *The Rise of Bioelectronics* - Chem. Mater. (2014, 26, 679-685)

[6] F. Scholz - *Electroanalytical Methods - Guide to Experiments and Applications* - Springer (2010)

[7] T. Simon, E.O. Gabrielsson, K. Tybrandt and M. Berggren - *Organic Bioelectronics: Bridging the Signaling Gap between Biology and Technology* - Chem. Rev. (2016, 116, 13009-13041)

[8] S.K. Vashist and J.H.T. Luong - *Recent advances in electrochemical biosensing shemes using graphene and graphene-based nanocomposites* - Anal Chim. Acta (2015, 84, 519-550)

[9] J.Q. Liu *et al.* - *Moleculary engineered rgaphene surfaces for sensing applications: a review* - Anal. Chim. Acta (2015, 859, 1-19)

[10] N. Yang *et al.* - *Carbon nanotube based biosensors* - Sens Actuators (2015, B, 207, 960-715)

[11] A. Saha, J. Chengmin and A.A. Matri - emphCarbon nanotube networks on different platforms - Carbon (2014, 79,1-18)

[12] X. Duan and C.M. Lieder - *Nanoscience and the nano-bioelectronics frontier* - Nano Research (2015, 8(1), 1-22)

[13] S.Krishnamoothy - *Nanostructured Sensor for biomedical applications a current perspective* - Curr. Opin. Biotechnol. (2015, 34, 118-124)

[14] H. Shirakawa *et al.* - *Synthesis of electrically conducting organic polymers: halogen derivatives of polyacetylene, $(CH)_X$* - Chem. Soc.Chem.Commun. (1977, pages 578-580)

[15] C.K. Chiang *et al.* - *Electrical conductivity in doped polyacetylene* - Phys.Rev.Lett. (1977, 39, 1098)

[16] Nobelprize.org Nobel Media AD 2014. The Nobel Prize in Chemistry 2000. *http://www.nobelprize.org/nobel_prizes/chemistry/laureates/2000*

[17] A.J. Heeger - *Semiconducting and Metallic Polymers: The Fourth Generation of Polymeric Materials (Nobel Lecture)* - Angew. Chem. Int. Ed. (2001, 40, 2591-2611)

[18] A. Elschner, S. Kirchmeyer, W. Lovenich, U. Merker e K. Reuter - *PEDOT: Principles and Applications of an Intrisically Conductive Polymer* - CRC Press (2010)

[19] R. Hoffman, C. Janiak end C. Kollmar - *A Chemical Approach to the Orbitals of Organic Polymer* - Macromolecules (1991, 24(13), 3725-3746)

[20] J.H. Davies - *The Physics of Low-dimensional Semiconductors* - Cambridge University Press (2009)

[21] B.E. Kohler and I.D.W. Samuel - *Experimental detemination of conjugation lengths in long polyene chains* - J. Chem. Phys (1995, 103(14), 624-6252)

[22] R.E. Peierls - *Quantum Theory of Solids* - Oxford University Press (2001)

[23] M. Grundamm - *The Physics of Semiconduction - An Introduction Including Device and Nanophysics* - Springer (2006)

[24] G. Inzelt - *Conducting Polymers: A New Era in Electrochemistry* - Springer (2012)

[25] A.J. Heeger, S. Kivelson, J.R. Schreieffer and W.-P. Su - *Solitons in conducting polymers* - Reviews on Modern Phys. (1988, 60, 781)

[26] S. Kivelson - *Electron Hopping Conduction in the Soliton Model of Polyacetylene* - Phys. Rev. Lett. (1981 77(1-4), 65-79)

[27] Y. Wang - *Research progress on a novel conductive polymer-poly(3,4-ethylenedioxythiophene) (PEDOT)* - J. Phys. Conf. Ser. (2009, 152, 012023)

[28] D. Mecerreyes *et al.* - *A simplified all-polymer flexible electrochromic device* - Electrochim. Acta (2004, 49(21), 3555-3559)

[29] R. Kiebooms *et al.* - *Thermal and electromagnetic behaviour of doped poly(3,4-ethylenedioxythiophene) film* - J. Phys. Chem. B (1997, 101(51), 11037)

[30] Q.Pei, G. Zuccarello, M. Ahskog and O. Inganäs - *Electrochromic and highly stable poly(3,4-ethylenedioxythiophene) switches between opaque blue-black and transparent sky blue* - Polymer (1994, 35(7), 1347)

[31] G. Heywang and F. Jonas - *Poly(alkylenedioxythiophene)s new, very stable conducting polymers* - Adv. Mater (1992, 4(2), 116-118)

[32] J. Ouyang *et al.* - *On the mechanism of conductivity enhancement in poly(3,4-thylenedioxythiophene):poly(styrene sulfonate) film through solvent treatment* - Polymer (2004, 45, 8443-8450)

[33] S. Kirchmeyer and K. Reuter - *Scientific importance, properties and growing application of poly(3,4-thylenedioxythiophene)* - J. Mater. Chem (2005, 15(21), 2077-2088)

[34] O. Yaghmazadeh *et al.* - *Optimization of organic electrochemical transistor for sensor application* - J. Polym. Sci. Part B Polym. Phys. (2011, 49(1), 34-39)

[35] F.C. Krebs - *Fabrication and processing of polymer sola cells: A review of printing and coating techniques* - Solar Energy Mater. and Solar Cells (2009, 93(4), 394-412)

[36] Manifacturer: H.C. Starck Clevios GmbH, Leverkusen, Germany, www.clevios.com

[37] L. Giraudet *et al.* - *Spin-coated conductive polymer film resistivity measurement using TLM method* - Synth. Met. (2006, 156, 838-842)

[38] P.M. Brosenberger and D.S. Weiss - *Organic Photoreceptors for Imaging System* - New York: Marcel Dekker (1993)

[39] A.N. Aleshin, S.R. Williams and A.J. Heeger - *Transport properties of poly(3,4-ethylenedioxythiophene)/poly(styrenesulfonate)* Synth. Met. (2001, 94(2), 173-177)

[40] N.F. Mott and E.A. Davis - *Electronic Process in Non-Crystalline Materials* - Oxford Press (2012)

[41] J.Y. Kim *et al.* - *Enhancement of electrical conductivity of poly(3,4-ethylenedioxythiophene)/poly(styrenesulfonate) by a change of solvent* - Synth. Met (2002, 126(2-3), 311-316)

[42] A.N. Nardes, R.A.J. Janssen and M. Kemerink - *A Morphological Model for the Solvente-Enhanced Conductivity of PEDOT:PSS Thin Films* - Adv. Funct. Mater. (2008, 18(5), 865-871)

[43] L.Zuppiroli *et al.* - *Hopping in disorder conducting polymers* - Phys. Rev. (1994, B50, 5196)

[44] A.G. MacDiarmid and A.J. Epstein - *The concept of secondary doping as applied to polyaniline* - Synth. Met. (1994, 65(2-3, 103-106)

[45] B.D. Martin *et al.* - *Hydroxylated secondary dopants for surface resistance enhancement in transparent poly(3,4-ethylenedioxythiophene)-poly(styrenesulfonate) thin films* - Synth. Met. (2004, 142(1), 187-193)

[46] A. Elschner and W. Lövenich - *Solution of PEDOT for transparent conductive application* - MRS Bull. (2011, 36(10), 794-798)

[47] X. Crispin *et al.* - *The Origin of the High Conductivity of Poly(3,4-ethylenedioxythiophene)-Poly(styrenesulfonate) (PEDOT-PSS) Plastic Electrodes* - Chem. Mater (2006, 18(18), 4354-4360)

[48] S. Zhang *et al.* - *Solvent-induced changes in PEDOT:PSS films for organic electrochemical transistor* - APL Mater. (2015, 3(1), 014911)

[49] B.Friedel *et al.* - *Effect of Layer Thickness and Annealing of PEDOT:PSS Layers in Organic Photodetectors* - Macromolecules (2009, 42, 6741-6747)

[50] L. Shen, C.R. Weber, D.R. raleigh, D. Yu and J.R. Turner - *Tight Junction Pore and Leak Pathways: A Dynamic Duo* - Annu. Rev. Physiol (2011, 73, 283-309)

[51] T.S. Thomasen *et al.* - *Synthesis and deposition of basement membrane proteins by brain capillary endothelial cells in a primary murine model of the blood-brain barrier* - J. Neurochem (2017, 140, 741-754)

[52] N.J. Abbot *et al.* - emphAtrocyte-endothelial interactions at the blood-brain barrier - Nat. Rev. Neuroscience (2006, 7, 41-53)

[53] - S.Guerit and S. Liebner - *Blood-Brain Barrier Breakdown Determines Differential Therapeutic Outcome in Genetically Diverse Forms of Medulloblastoma* - Cancel Cell (2016, 29, 427-429)

[54] S.A. Tria, L.H. Jimson, A. Hama, M. Bongo, R.M. Owens - *Validation of the organic electrochemical transistor for in vivo toxicology* - Biochim. Biophys. Acta (2012, 1830, 4381-4390)

[55] A. Hartsock and W.J. Nelson - *Adherens and Tight Junctions: Structure, Function and Connections to the Actin Cytoskeleton* - Biochim. Biophys. Acta (2008, 1778(3), 660-669)

[56] A.S. Fanning, C.M. Van Itallie, J.M. Anderson - *Zonula occludens-1 and -2 regulate apical cell structure and the zonula adherens cytoskeleton in polarized epithelia* - Mol. Biol. Cell (2012, 23(4), 577-590)

[57] M. Furuse *et al.* - *Occludinn: A Novel Integral Membrane Protein Localizing at Tight Junction* - J. Cell Biolo. (1993, 123, 1777-1788)

[58] O.R. Colegio *et al.* - *Claudins create charge-selective channels in the paracellular pathway between epithelial cells* - Am. J. Physiol. Cell Physiol. (2002, 283(1), 142-147)

[59] https://www.lgcstandards-atcc.org/Products/All/CCL-2.aspx

[60] https://www.lgcstandards-atcc.org/Products/All/CRL-1573.aspx

[61] https://www.lgcstandards-atcc.org/Products/All/CRL-1658.aspx

[62] https://www.lgcstandards-atcc.org/Products/All/CRL-2935.aspx

[63] https://www.lgcstandards-atcc.org/Products/All/HTB-37.aspx

[64] https://www.corning.com/worldwide/en/products/life-sciences/products/permeable-supports/transwell-snapwell-netwell-falcon-permeable-supports.html

[65] B. Srinivasan *et al.* - *TEER measurement techniques for in vitro barrier model system* - J. Lab. Autom (2015, 20(2), 107-126) ,

[66] R. Rao, R.D. Baker and S.S. Baker - *Inhibition of Oxidant-Induced Barrier Disruption and Protein Tyrosine Phosphorylation in Cac0-2 Cell Monolayers by Epidermal Growth Factor* - Biochem. Pharmacol. (1999, 15;57(6), 685-695)

[67] T.Y. Ma, D. Nguyen, V. Bui, H. Nguyen and N. Hoa - *Ethanol modulation of intestinal epithelial tight junction barrier* - Am. J. Physiol. Gastrointest. Liver Physiol. (1999)

[68] S. Tria, L.H. Jimson, A. Hama, M. Bongo and R.M. Owens - *Sensing of EGTA Mediated Barrier Tissue Disruption with Organic Transistor* - Biosensor (2013, 3(1), 44-57)

[69] H.S. White, S.P. Kittlesen and M.S. Wrighton - *Chemical derivatization of an array of three gold microelectrodes with polypyrrole: fabrication of a molecule-based transistor* - J. Am. Chem. Soc. (1984, 106(18), 5375-5377)

[70] D.Khodagholy *et al.* - *High transconductance organic electrochemical transistor* - Nat.Commun. (2013, 4, 2133)

[71] C.D. Dimitrakopoulos and P.R.L. Malenfant - *Organic Thin Film Transistors for Large Area Electronics* - Adv. Mater (2002,)

[72] P. Ling *et al.* - *The Application of Organic Electrochemical Transistor in Cell-Based Biosensor* - Adv.Mater (2010, 22, 3655-3660)

[73] C. Liao *et al.* - *Flexible Organic Electronics in Biology: Materials and Devices* - Adv. Mater. (2014, 27, 7493-7527)

[74] A.G. MacDiarmid *et al.* - *The concept of "doping" of conducting polymers: The role of reduction potentials (and discussion)* - Philos. Trans. R. Soc. A Math. Phys. Eng. Sci. (1985, 314, 3-15)

[75] D. Nilsson, N. Robinson, M. Berggren, E. Forchheimer - *Electrochemical Logic Circuits* - Adv. Mater. (2005, 17(3), 353-358)

[76] J.T Friedlein *et al.* - *Microsecond Response in Organic Electrochemical Transistor: Exceeding the Ionic Speed Limit* - Adv. Mater (2016, 28, 8398-8404)

[77] D.A. Bernars and G.G. Malliaras - *Steady-State and Transient Behaviour of Organic Electrochemical Transistor* - Adv. Func. Mater. (2007, 17, 3538-3544)

[78] A.J. Bard and L.R. Faulkner - *Electrochemical Methods: Fundamentals and Applications* - Wiley (2001)

[79] G.A. Snook, P. Kao and A.S. Best - *Conducting-polymer-based supercapacitor devices and electrodes* - J. Power Source (2011, 196(1), 1-12)

[80] F. Lin and M.C. Lonergan - *Gate electrode process in anelectrolyte-gated transistor: Non-Faradaically versus Faradaically coupled conductivity modulation of a polyacetylene ionomer* - Appl. Phys. Lett. (2006, 88(13), 133507)

[81] J. Rivnay *et al.* - *High-performance transistor for bioelectronics through tuning of channel thickness* - Sci. Adv (2015, 1, 1400251)

[82] Y. Zhang *et al.* - *A Surface-Charge Study on Cellular-Uptake Behavior of F3-Peptide-Conjugated Iron Oxide Nanopaticles* - Small (2009, 5(17), 1990-1996)

[83] L.H. Jimison *et al.* - *Measurement of Barrier Tissue Integrity with an Organic Electrochemical Transistor* - Adv. Mater. (2012, 24, 5919-5923)

[84] S.A. Tria *et al.* - *Dynamic Monitoring of Salmonella typhimurium Infection of Polarized Epithelia Using Organic Transistor* - Adv. Healtcare Mater. (2014, 3, 1053-1060)

[85] M. Ramuz *et al.* - *Combined Optical and Electronic Sensing of Epithelial Cells Using Planar Organic Transistor* - Adv. Mater. (2014, 26, 7083-7090)

[86] M. Ramuz *et al.* - *Optimization of a Planar All-Polymer Transistor for Characterization of Barrier Tissue* - Chem. Phys. Chem. (2015, 16, 1210-1216)

[87] M. Ramuz, A. Hama, J. Rivnay, P. Leleux and R.M. Owens - *Monitoring of cell layer coverage and differentiation with organic electrochemical transistor* - J. Mater. Chem (2015, 3, 5971-5977)

[88] http://jacobsschool.ucsd.edu/cosmos/2016.html

[89] https://www.microscopyu.com/techniques/fluorescence/introduction-to-fluorescence-microscopy

[90] http://kicad-pcb.org/

[91] http://www.mdsrl.it/

[92] I. Uguz *el at.* - *Autoclave Sterilization of PEDOT:PSS Electrophysiology Devices* - Adv. Healthcare Mater. (2016, 5, 3094-3098)

[93] http://www.ecochemie.nl/Products/Echem/Software/Nova.html

Acknowledgements

First of all i want to thank my supervisor, Prof. Beatrice Fraboni, for her availability and her leadership at the crucial moments of the work; not least for positivity in approach the research and its uncertainty.

I am grateful to my co-supervisor, Dr. Marta Tessarolo, for the attention put into the details and for the continuous incentive during all phases of this thesis. In addition I want to thank her for the always open and friendly confrontation in working and personal topic.

Moreover I express my thanks to all the research group Dr. Tobias Cramer, Dr. Filippo Maria Giorgi, Dr. Maria Calienni, Dr. Laura Brasicò and Dr. Andrea Ciavatti.

I want to thank Massimiliano Cavallini director of the research group *Nanotechnology of Multifunctional Materials* (NMM) and Francesco Valle supervisor of the biolab for his constant supervision and to the researcher Denis Gentili. Another big thanks goes to Marianna Barbarinaldo for her infinite availability, her patience and her guidance for all biological phases of this work.

I want to give sincere thanks to my lab colleagues Francesco Decataldo and Dario Cavedale for all the time, the music and the laughter that turned the work into fun. In particular i want to thank Francesco for the constant teamwork in all the moments of this thesis.

This goal would not have been possible *with a little help of my "physics" friend* Goffredo, Adriano, Valerio, Emilio, Simone, Alessandra, Elena e Lucianna.

Equally I am grateful to the friends of a lifetime Michele, Giuseppe, Silvio, Andrea e Francesco. Despite the distance that separates us, they never let me think *I wish you were here*.

I have a thought for the Pietralata's friend and to all the times in Bologna passed to think how to *save tonight*.

I am grateful to Vittoria for her optimism and her radiant personality. Maybe I am *thinking out loud* but I hope to have her always by my side and I want to express her *all my loving*.

Lastly i want to give sincere thanks to all my family, from the grandparents to the uncles and my cousins. In particular to the new Gallego-Vurro family and to my parents who always believed in me and have always supported me.